RNA Analysis of Liquid Biopsies for Cancer Diagnosis

By

Xin Zhou

Submitted to the graduate degree program in Department of Chemistry and the Graduate Faculty of the University of Kansas in partial fulfillment of the requirements for the degree of Doctor of Philosophy.

_____

Chair: Dr. Yong Zeng

_____

Dr. Cindy L. Berrie

_____

Dr. Susan Lunte

_____

Dr. Timothy Jackson

_____

Dr. Bo Luo

Date Defended: June 16th, 2020

The dissertation committee for Xin Zhou certifies that this is
the approved version of the following dissertation:

RNA Analysis of Liquid Biopsies for Cancer Diagnosis

_____

Chair: Dr. Yong Zeng

Date Defended: June 16th, 2020

Abstract

Early diagnosis of cancer is critical to improving the first 5-year survival rate of patients. However, tissue biopsy, as the gold standard for cancer diagnosis, is invasive and costly, thus not ideal for cancer early screening. Imaging-based methods are noninvasive but lack sensitivity to capture small size tumors at early stages. Liquid biopsies, i.e., circulating tumor DNAs, circulating tumor cells and exosomes in body fluids, are emerging as a promising paradigm for developing sensitive and specific molecular biomarkers for screening and early detection of cancer in a non-invasive manner.

Circulating microRNAs (miRNAs) and exosomal messenger RNAs (mRNAs) in the bloodstream have been implicated in tumor initiation, progression, and metastasis. Therefore they have been intensively investigated to develop cancer biomarkers for liquid biopsy tests. Real-time reverse transcription polymerase chain reaction (RT-qPCR), as the gold-standard method for quantitative measurement of miRNA and mRNA, is highly sensitive and robust, but labor-intensive and expensive. Microfluidics is a technology that can manipulate microliters to picoliters of fluids and integrate function modules for multiple laboratory operations in a single device. My research projects took advantage of microfluidic technology to developed methods for the detection of miRNAs and mRNAs that are low cost, robust, sensitive, and automatic. In project 1, we designed a microfluidic device that employed the Duplex-Specific-Nuclease Signal Amplification (DSNSA) for miRNA detection. In Project 2, we developed an exosomal mRNAs quantitation method that combined on-chip exosome

enrichment and lysis with droplet digital PCR. In Project 3, we developed a microfluidic alternating-pull-push active digitization method for sample-loss-free digital PCR, which served for Project 4— to develop a microfluidic exosomal mRNA absolute quantitation approach that integrated beads capture, on-chip lysis, and on-chip one-step digital RT-PCR. Our work facilitated the quantitative analysis of miRNA and exosomal mRNA in cancer diagnosis. Moreover, we envision that our work is adaptable in further broader RNA quantitation requests, such as detection of lncRNA, in board biological and clinical applications.

Acknowledgment

I would like to express my sincere gratitude to my supervisor, Dr. Yong Zeng, for his unlimited help and support. I feel extremely lucky to be under his mentorship. I almost gave up on my academic dream in my second year, and it was he who saved me and helped me go back on track. His encouragement, patience, and guidance always give me the power to overcome those frustrations that lays on my Ph.D. career. He is very supportive whenever I meet troubles in research or life. It is my fortune to be his student.

I would like to acknowledge all my committee members Dr. Susan Lunte, Dr. Cindy Berrie, Dr. Timothy Jackson, and Dr. Bo Luo, for their time and suggestions.

I greatly thank all the members of Zeng Group for their help and assistance. I would like to thank Dr. Peng Zhang for his suggestions and training, Dr. Yang Yang for sharing his experience in lab work and job seeking, Gopi Chandran Ravichandran, Yaohua Zhang, Dr. Yutao Li, Dr. He Yan and Dr. Shibo Cheng for their aids.

I would like to express my appreciation to my beloved wife Sijin Ren. You are the sunshine of my life. I could not make it this far without your understanding, trust, and love. I would like to thank my lovely son Rui Zhou, who always greatly helps me relax from the anxiety and stress from work. Last but not least, I am grateful to my parents Zhiling Liang and Weiping Zhou for all their love and supports.

Outline

List of Figures

List of Table

Chapter 1. Introduction

Liquid biopsy for cancer diagnosis

Cancer, also known as malignant tumor, is a group of heterogeneous diseases due to abnormal cell growth. As the second leading cause of death in the United State, cancer has already been one of the major public health problems.[1] Predicted by the American Cancer Society, approximately 1.8 million new cancer cases and 0.6 million deaths will occur in 2020. To our knowledge, patients who are diagnosed with cancer in the early stage have a higher 5-year survival rate due to better response to treatment. Thus, early-stage cancer diagnosis becomes extremely critical.

The gold standard of cancer diagnosis is the tissue biopsy, which is enabled by retrieving a small piece of tissue from the tumor for pathological examination. However, this method is invasive and sometimes requiring surgeries. It is painful and not practical for patients to get multiple biopsies on the primary tumor and metastases due to tumor heterogeneity. In some cases, the tumor is not even accessible for a tissue biopsy test.[2] Thus this approach cannot be utilized for screening and longitudinal monitoring of cancer. Besides the tissue biopsy, imaging-based method, such as ultrasound,[3-5] computed tomography (CT) scan,[6-8] positron emission tomography (PET) scan,[9-11] magnetic resonance imaging (MRI),[12, 13] also play important roles in cancer diagnosis. Although these methods are not as invasive as the tissue biopsy is, small size tumors are not able to be found due to the limited resolution of the imaging-based methods. In addition, the radiation exposure to the patients during the imaging test also needs to be considered deliberately.[14-16] Therefore, there is an urgent need of a noninvasive and sensitive cancer screening method.

Liquid biopsy is emerging as a promising noninvasive cancer diagnosis approach by analyzing microliters to milliliters of blood samples, including detection of circulating tumor DNAs (ctDNAs), circulating tumor cells (CTCs), exosomes, etc. The cancer biomarkers for a test can be CtDNAs are 180 to 200 base pairs in length cell-free DNAs (cfDNAs) derived from tumor cells, bearing tumor-specific sequence mutations.[17] Their expression level is related to tumor burden, cancer stage, cellular turnover, and response to therapy.[18] CTCs are exfoliated cells derived from primary tumors, existing in blood circulation.[19] Although the CTCs are rare in the bloodstream, usually 1 -10 CTCs per ml of blood,[20] they can provide critical information of cancer progression.[21, 22] Exosomes are 30 – 150 nm in size extracellular vesicles that are secreted by cells and play an important role in intercellular communications.[23] Unlike CTCs which are low abundant in blood, exosomes show a relatively higher concentration in blood (10^9 – 10^{12} exosomes per ml).[24, 25] The cargo carried by tumor-derived exosomes, such as proteins, miRNA, mRNA, are cancer biomarkers that are closely related to the cancer progression.[26] Overall, the liquid biopsy is a promising noninvasive cancer diagnostic approach for cancer screening and longitudinal monitoring.

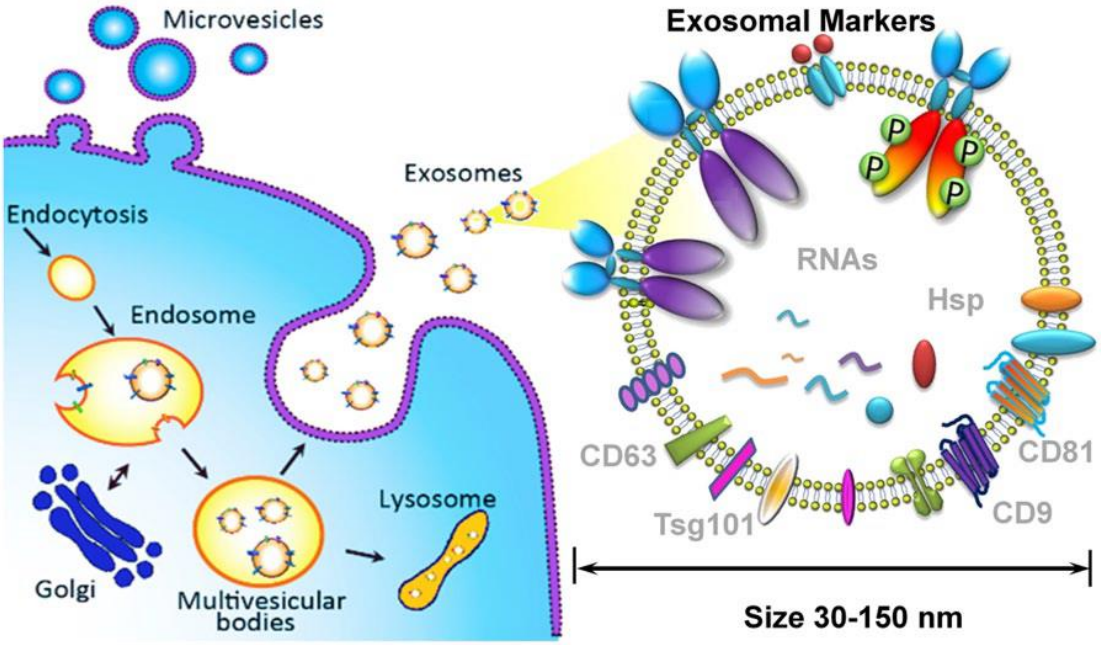

Figure 1-1. Exosome biogenesis, properties, and molecular composition (reprinted with permission).[27]

Tumor-derived exosomes

Exosomes are produced via cell's recycling endosomal pathway.[28] Although they were previously considered as waste products of cells,[29] they have been found playing a significant role in intercellular communication.[23] Tumor-derived exosomes are deeply involved in immune response suppression, tumor progression, angiogenesis, and metastasis.[30-32] Moreover, exosomes are carrying components from the original cell, including proteins, lipids, and ribonucleic acids (miRNA, mRNA, etc.),[28, 33, 34] as illustrated in Figure 1-1. Therefore, exosomes are believed to be promising biomarkers for cancer.

Due to their small size, it is challenging to isolate exosomes out of body fluids. Several approaches are available to address this problem, such as ultracentrifugation,[35, 36] ultrafiltration,[37, 38] size exclusion chromatography,[37-39] polymer-based precipitation,[40, 41] and immunoaffinity capture,[42, 43] etc., and most of these exosome

isolation methods are commercially available. Ultracentrifugation is the most commonly used method for exosome isolation. By spinning the sample in an ultra-high spin rate (100,000× g), the exosomes can be pelleted and then collected. This method is able to process a large volume of sample, but the yield and the purity are relatively low. In addition, long processing time and expensive instruments are required for this method. Ultrafiltration is enabled by employing nanomembranes or filters to isolate the exosomes out of the sample. The sample processing time is relatively short (~2 hours), and it is able to process multiple samples simultaneously, but the body of exosome could be damaged and sample loss always happens during the filtration and thus cause a low recovery rate. The size exclusion chromatography also separates exosomes by size. This method advantages in high purity with minimum sample loss. However, the sample volume is limited for each separation. Also, exosomes are diluted after the separation. The polymer-based precipitation method isolates exosomes by changing the solubility of exosome in the presence of superhydrophilic polymers. The precipitate of exosome can be pelleted and collected with a low spin rate by centrifuge. This method enjoys a high yield of exosomes without the requirement of complicated operations, but the purity is relatively low. The immunoaffinity capture method, as illustrated in Figure 1-2, isolates exosome by taking advantage of antibodies to target the antigens on the surface of exosomes, e.g. tetraspanin family proteins, such as CD81, CD63, CD9, or biomarkers, such as EpCAM. This approach is highly selective and holding great promise for the enriched exosome. However, it is limited by the availability and the affinity of the antibodies. Overall, these methods all have their superiorities and defects, and the choice should be deliberated picked based on the requirement of the downstream analysis for best results.

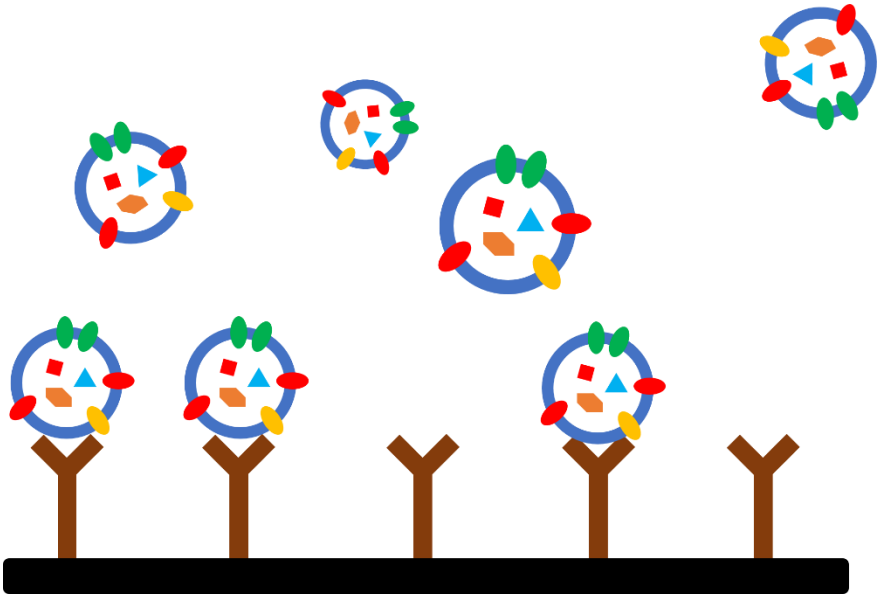

Figure 1-2. Exosome isolation based on immunoaffinity capture

Circulating microRNAs (miRNA) and messenger RNAs (mRNAs) as tumor biomarkers

RNAs can be classified as coding RNAs, such as mRNAs, and non-coding RNAs, such as miRNAs. Both mRNAs and miRNAs are promising cancer biomarkers that can be utilized in liquid biopsy tests.

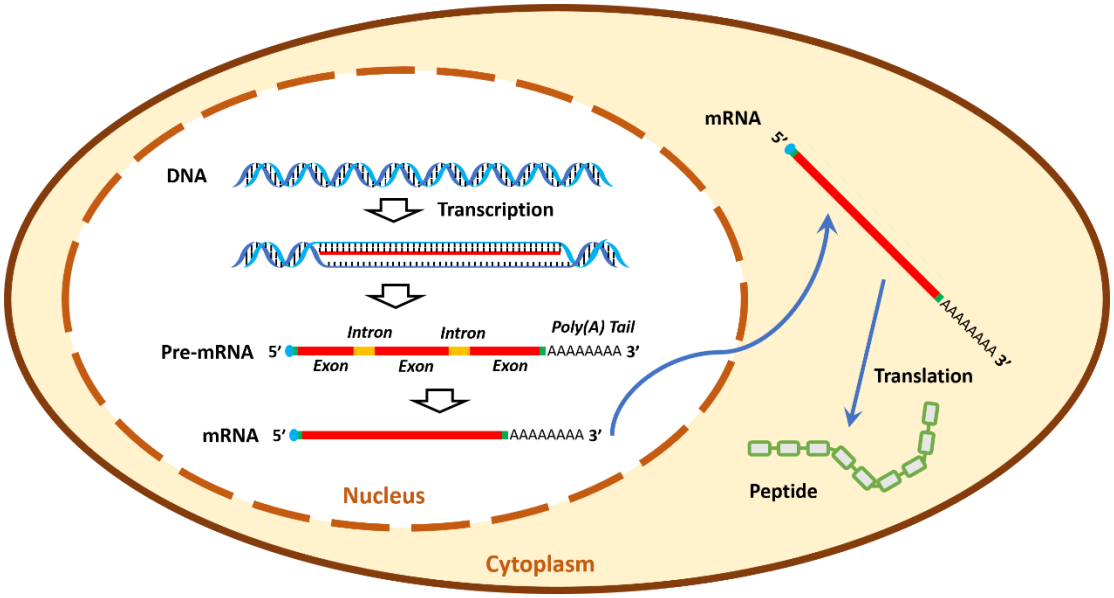

Figure 1-3. Schematic of messenger RNA processing

Biogenesis of mRNAs and their association with cancer

Messenger RNAs (mRNAs) are single-strand RNA that functions in protein synthesis, which undergoes several steps termed messenger RNA processing.[44] As illustrated in Figure 1-3, precursor mRNAs are firstly synthesized by the transcription of DNAs. The intron is then removed from the precursor mRNA via RNA splicing, forming the mature mRNAs which only consist of exons. Subsequently, the mature mRNAs are read by ribosome according to the codons on each exon, thus the proteins are synthesized via translation. mRNAs are found closely correlated to cancer. In cancer cells, dysregulation of mRNA translation is very common, leading to the phenotypic hallmarks of cancer and neoplastic transformation.[45-47] In addition, mutation of mRNAs occurs frequently in cancer. For example, EWS-FLI1 fusion transcript is a mutation observed in Ewing Sarcoma, as a result of a chromosomal translocation;[48] BCR-ABL fusion transcript is a mutation that is specific to leukemia;[49] MSH2 and MLH1 mRNAs are mutations that found in hereditary non-polyposis colon cancer syndrome.[50]

Moreover, the expression level of mRNAs is also correlated with cancer. E.g. the P53 mRNA was observed to be overexpressed in colorectal cancer.[51] More importantly, tumor-associated mRNAs were found not only within cancer cells but also in the bloodstream,[52] correlated with colorectal cancer,[53] breast cancer,[54] lung cancer,[55] oral cancer,[56] thyroid cancer,[57] malignant melanoma,[52] etc. The circulating mRNAs are encapsulated and protected by exosomes,[58, 59] thus avoiding being degraded in the overexpressed-RNase environment in the blood of cancer patients.[60] These characteristics of mRNAs make them promising biomarkers for cancer diagnosis via liquid biopsy.

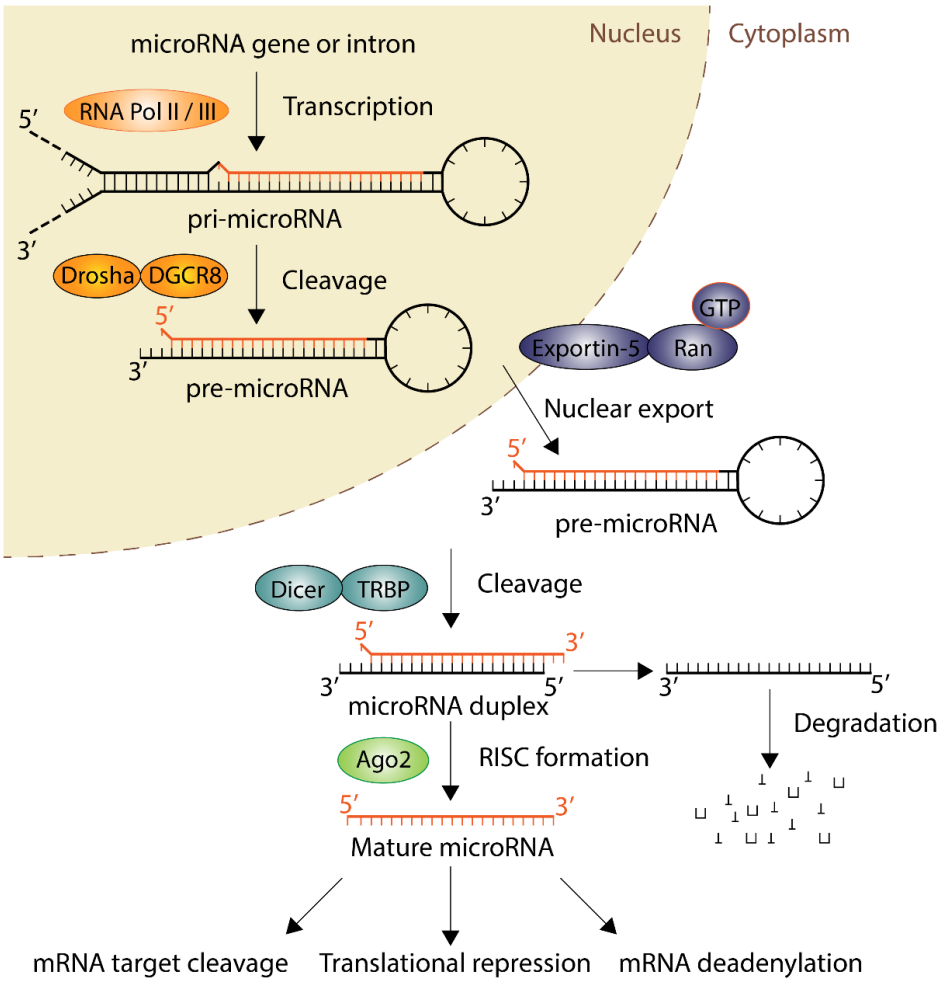

Figure 1-4. miRNA Biogenesis Pathway (reprinted with permission).[61]

Biogenesis of miRNAs and their association with cancer

MicroRNAs (miRNAs) are 20-22 nucleotides non-coding RNAs that function in gene regulation.[62] As shown in Figure 1-4, miRNAs are synthesized from primary miRNAs (pri-miRNAs) which is encoded in the nucleus via transcription of the introns of the protein-coding gene. The pri-miRNAs are then cleaved by endonucleases (DROSHA and DGCR8) to form the precursor miRNAs (pre-miRNAs), which have a hairpin loop structure. The pre-miRNAs were then transferred from the nucleus to the cytoplasm, and the hairpin loop structure are also cleaved, forming the mature miRNAs, which are then bound to proteins to form the RNA-induced silencing complex (RISC).[63] The RISC targets mRNAs that have a sequence complementary or partially complementary to the miRNA.[64, 65] miRNAs play a critical role in controlling cellular functions, such as cell differentiation, proliferation, and apoptosis.[66, 67] Tumor-associated miRNAs are also detectable in the bloodstream, protected by either exosomes or the protein of the RISC.[68] The expression level of the circulating tumor-derived miRNAs can either be up-regulated or down-regulated depending on different cancer types and stages.[69] Thus, circulating miRNA in the bloodstream can be powerful tools via liquid biopsy for cancer diagnosis, cancer staging, and prognosis.

Conventional methods for mRNA and miRNA detection

The detection of mRNAs or miRNAs in the blood is challenging due to low abundance, and there are several methods commercially available. Quantitative reverse transcription polymerase chain reaction (RT-qPCR), also known as real-time RT-PCR, is the gold standard for mRNA or miRNA detection.[70, 71] The RT-qPCR is an exponential amplification method with superior sensitivity and specificity. It consists of a reverse transcription (RT) step and a polymerase chain (PCR) reaction step. The

RT step converts the mRNA or miRNA into complementary DNA (cDNA) in the presence of Reverse Transcriptase and Reverse transcription primers. The specific primer, random primer, or oligo-dT primer are for mRNAs, and the stem-loop primer is for miRNAs. The specific primer is designed specifically for the RNA analyte with a complementary sequence, and it only reverse transcribes the RNA analyte among the total RNA to cDNA, avoiding the potential non-specific amplification that might happen in the downstream qPCR and holding great promise for specificity. The random primer is a mixture of primers with distinct sequences that can reverse transcribe all RNAs containing binding sites for any of the primers, ensuring the high yield of cDNA. The oligo-dT primer is a single strand of multiple deoxythymine (dT) that only reverse-transcribes the mRNAs by the targeting poly(A) tail, thus balancing the specificity and the availability of multiple mRNAs profiling of the downstream qPCR. The stem-loop primer is designed for miRNAs with its stem-loop structure to efficiently lengthen the cDNA to fit the requirement of the downstream qPCR.[72]

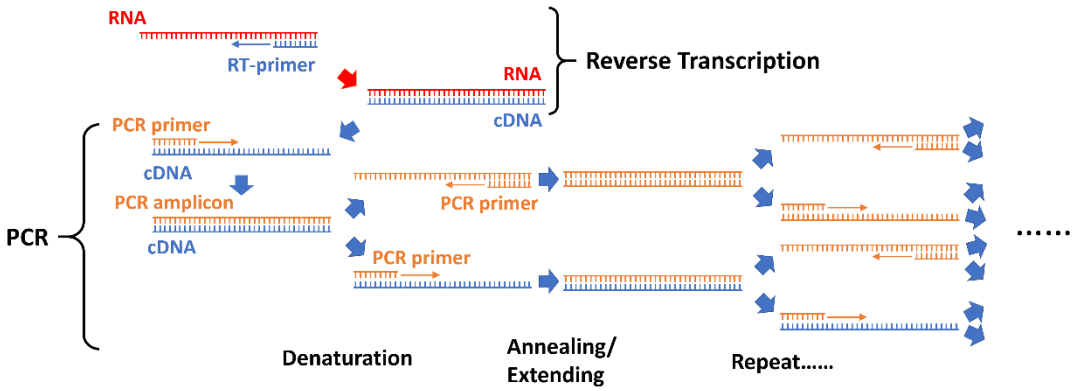

Figure 1-5. Principle of Standard RT-PCR

The qPCR is similar to the conventional PCR: it requires a forward primer and a reverse primer to specifically and exponentially amplify the template cDNA in the

presence of DNA polymerase and dNTPs via denaturation and annealing / extending cycles, as demonstrated in Figure 1-5. However, qPCR detects the RNA analyte through the fluorescence intensity of the reaction solution in real-time.

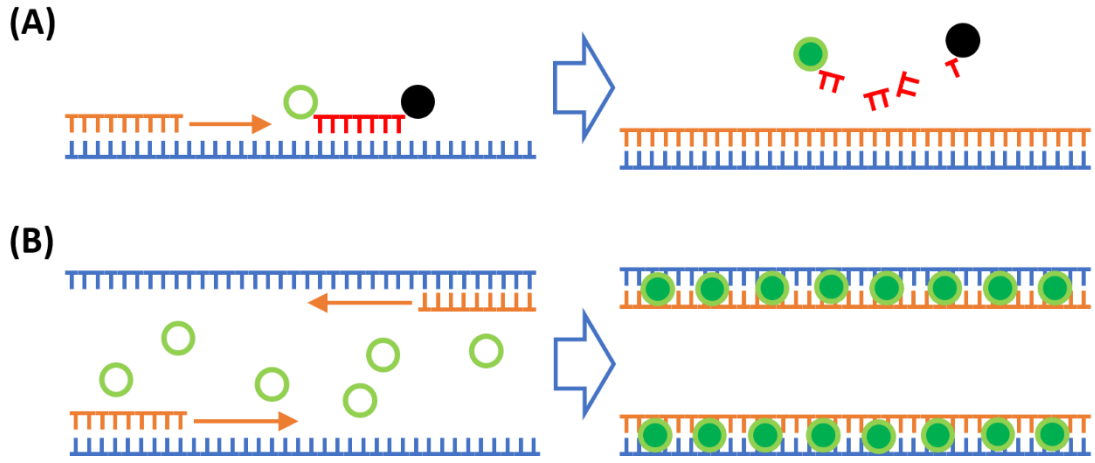

Figure 1-6. Schematic illustration of signal generation in qPCR by (A) FRET Probe and (B) Intercalating Dye.

The most commonly used molecule probes for fluorescence signal generation are Fluorescence resonance energy transfer (FRET) probe and intercalating dye. As shown in Figure 1-6(A), the FRET probe is a single-strand DNA (ssDNA) with a fluorophore at its 5' end and a quencher at its 3' end. The sequence of the FRET probe is complementary to a selected region in the middle of the cDNA template. Thus, when the DNA polymerase passes along the template during chain extending, it cleaves the ssDNA part of the FRET probe and releases the fluorophore from the quencher, generating fluorescence signal. As depicted in Figure 1-6(B), Intercalating dyes, such as SYBR green or EvaGreen, are fluorescent dyes that only generate fluorescence signal when inserted in double-strand DNA (dsDNA). Real-time fluorescence signal intensity can be monitored via a charge-coupled device (CCD) or photodetectors. Once the fluorescence signal intensity of a reaction system reaches the threshold during the

reaction, the current cycle number would be recorded for analyte concentration calculation. Although the RT-qPCR is sensitive enough in most of the cases, it requires reference or standards for quantitative measurement.

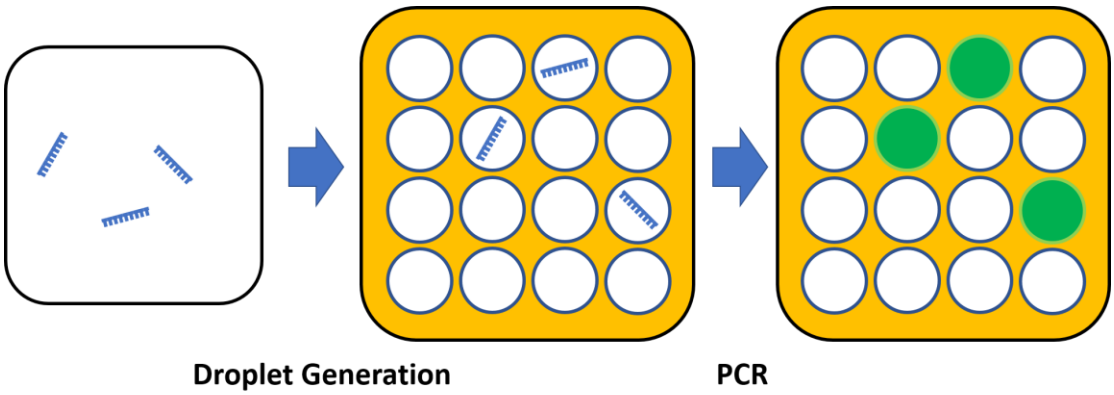

Figure 1-7. Schematic illustration of droplet digital PCR.

Droplet digital PCR (ddPCR) is another commercially available approach that can be relied on for miRNA and mRNA quantitation.[73, 74] The ddPCR is an absolute quantitation method that does not need a calibration curve. Just like RT-qPCR, the ddPCR also requires an RT step and a PCR step in the presence of FRET probe or intercalating dye. However, as shown in Figure 1-7, the reaction system is packed into more than ten thousand of droplets that immerse in oil phase prior to the PCR reaction, and each droplet only contains one or two cDNA molecules according to the Poisson Statistic when the concentration of cDNA template is low, thus single-molecule measurement can be achieved. More importantly, as the template is dispensed into droplets, its concentration becomes much higher in droplets than that in bulk solution, thus the ddPCR reveals higher toleration to PCR inhibitors than the qPCR does. Also, instead of monitoring the fluorescence signal intensity of the bulk reaction system during the PCR, each droplet will be measured for fluorescence after all the PCR has

been completed. A threshold of fluorescence signal intensity is set to differentiate the positive droplets and the negative droplets. The concentration of the cDNA can be calculated by employing Poisson distribution on the ratio of positive droplet amount to total droplet number. Although these PCR-based RNA quantitative methods are sensitive, reliable, and robust, they require an RNA extraction process and expensive instruments, making it tedious and not cost-effective.

Another option for mRNAs or miRNAs profiling RNA microarray,[75, 76] which is a high-throughput method based on DNA-RNA hybridization. In this approach, capture probe ssDNAs, which are complementary to a region of the target RNAs, are modified in different capture zones on the surface of a microarray chip. The sample solution is introduced into the chip and then incubated to let different RNAs be captured in distinct zones according to their sequences. Once the RNAs are captured, fluorophore-labeled ssDNA detection probes are introduced to bind with another region of the target RNAs. Thus, different target RNAs can be profiled by detecting the fluorescence signal in each capture zones, respectively. Although the RNA microarray method is high-throughput and easy to operate, it usually requires overnight incubation, and its sensitivity is relatively low, which may lead to false-negative results.

RNA sequencing is also a high-throughput RNA profiling method that is commercially available.[77] This method is based on the Next-generation sequencing (NGS), which is a combination of the technology of microarray, PCR, and Sanger sequencing. During this approach, RNAs are reverse transcribed into cDNAs, which are then fragmented to <500 nucleotides in length and linked to two different adapter ssDNAs at 5’ end and 3’ end. After the library construction, the sample is introduced and captured on the Flowcell chip, in which the primer ssDNAs complementary to the adapters are modified on the surface of each lane. After the capture, PCR-based bridge

amplification is performed to generate clusters, because the sequencing is based on fluorophore labeling, which is way much easier to be detected in a DNA cluster than that in a single strand. The sequencing is based on Sequencing by Synthesis, which is performed by the PCR reaction with the reversible dye-terminator dNTPs. Fluorescent images are taken for later data analysis after each dNTP is immobilized on the amplicon, and after the image is recorded, the dye and the terminator are removed and the system will go for next read. This method is able to achieve millions to billions of reads per run, with 300-600 bases per read, at an accuracy higher than 99.9 %. Also, it does not require knowing the sequence of the interested RNA prior to the test. However, compared to RT-qPCR and RT-ddPCR, its sensitivity is relatively low. Moreover, RNA sequencing-based quantitative measurement can be affected by the bias occurring during the library construction and the sequence alignment.[78]

Microfluidic technology on mRNA and miRNA detection

Microfluidics and lab-on-a-chip

Microfluidics is a technique to manipulate and process a small quantity (μL to pL) of fluid, miniaturized the conventional macroscopic laboratory operations in wet labs into microscopic processing in microchips, thus also known as Lab-on-a-chip. It is capable to integrate multiple laboratory operations, such as sampling,[79] sample preparation,[80] mixing,[81] isolation,[82, 83] detection,[84] etc., within a single micro-device. Benefiting from the capability of handling a small amount of fluids, it enjoys a number of advantages in comparison with traditional off-chip approaches, including higher sensitivity, lower cost, lower risk of sample contamination, and less reagent consumption. In addition, microfluidic devices are automatable, which can greatly

improve the robustness and reliability of assays, and also reduce the tedious labor-intensive operations. The applications of microfluidic technology have been broadly carried out in numerous fields, including organics synthesis,[85] nanomaterial synthesis,[86, 87] disease diagnosis,[88-90] gene expression analysis,[91, 92] protein profiling,[93] single-cell analysis,[94] cell manipulation,[95] screens of drug discovery,[96] etc.

Microfluidic devices are usually made of silicon, glass, or polymers,[97] among which polymers are more preferred nowadays because they are relatively cheaper and easier to fabricate. Polymers that commonly used for microfluidic device fabrications include polydimethylsiloxane (PDMS), polymethyl methacrylate (PMMA), polycarbonate, polyamide, etc. Among them, PDMS is favorable for the application of laboratory research.[98] It is a biocompatible material that is inert, non-toxic, non-flammable, and easy to cast. It is optically clear, thus enabling the convenient signal readout for fluorescence-based and chemiluminescence-based assays. Its porous structure is gas permeable, which is important for the application of cell culture[99] and allowing for dead-end filling.[100] In addition, this material is soft and elastic, which is the foundation of the valves and pumps built-in.[101, 102] These characteristics of PDMS make it suitable for application in a verity of fields, such as diagnostics, microbiology, etc.

Valves, on-chip pump and dead-end filling in PDMS microfluidic devices

The capability of manipulating and processing of small volume of fluid in microfluidic devices is enabled by the built-in functional components. Valves are one of the most critical units for fluidic manipulation in microfluidic devices.[103] The most commonly used valves in PDMS devices can be classified as Actuate-to-Close (AtC)

valve and Actuate-to-Open (AtO) valve. AtC valves are normally open valves that controlled by the air pressure within the control channel in the pneumatic layer.

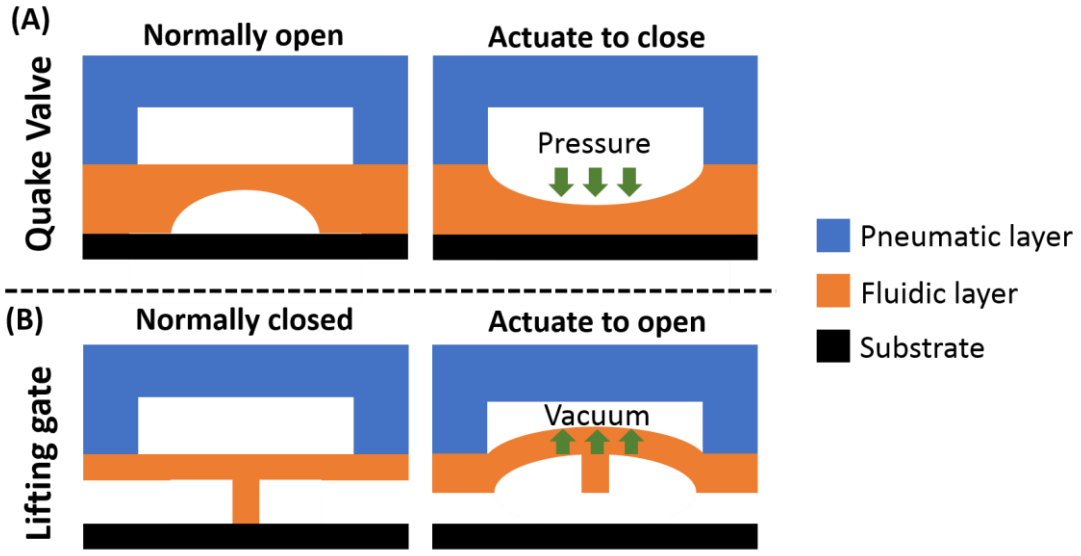

Figure 1-8. Schematic illustration of (A)Quake valve and (B)Lifting gate valve.

The most widely used AtC valve is the Quake valve as demonstrated in Figure 1-8(A), which was reported by Quake Group in 2000.[102] Although this type of valves is easy to be integrated into soft lithography design, it requires precise and continuous pressure control to prevent leakage, and the cross-section of the fluidic channel must be curved in order to achieve a good seal. AtO valves are normally closed valves that actuated by the vacuum in the pneumatic channel. The most frequently used AtO valve is the "lifting gate" valve as shown in Figure 1-8(B), which was introduced by the Kenis group.[101, 104] This type of valve is easier to fabricate because it does not require a specific shape of the fluidic channel's cross-section. Also, chips equipped with AcO valves are easier to transport, since all the valves remain closed without any connection to the external pump. However, the AcO valves suffer from relatively low product quality, since they can be occasionally permanently closed due to the treatment of

UV/ozone or oxygen plasma.

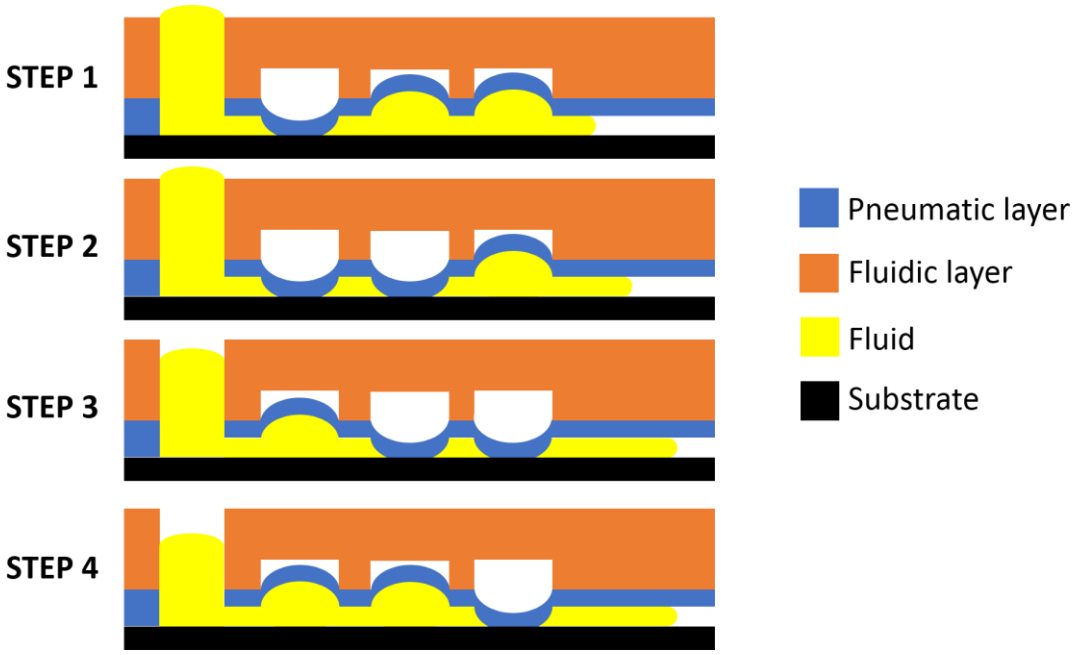

Figure 1-9. Schematic illustration of the working principle of the three-microvalve pump

Although the sample flow in a microfluidic device can be driven by external pumps, such as syringe pumps or peristaltic pumps, the dead volume of tubing can cause issues when only a small volume of sample is supplied. In this case, the utilization of the on-chip pump is extremely necessary. Based on the on-chip microvalve mentioned above, the three-valve-based micropump was designed to address this problem.[102, 105] As shown in Figure 1-9, three tandem microvalves are pumped periodically, thus dragging and pushing the fluid forward along the channel. Besides, the sample solution can also be introduced into PDMS chips by dead-end filling, which is based on the gas permeability of PDMS due to its porous structure.[100] As demonstrated in Figure 1-10, when a vacuum is applied in the pneumatic channel, the air in the fluidic channel penetrates the PDMS to the pneumatic channel, resulting in a drop of air pressure in the fluidic channel, thus pulling in the sample solution by suction.

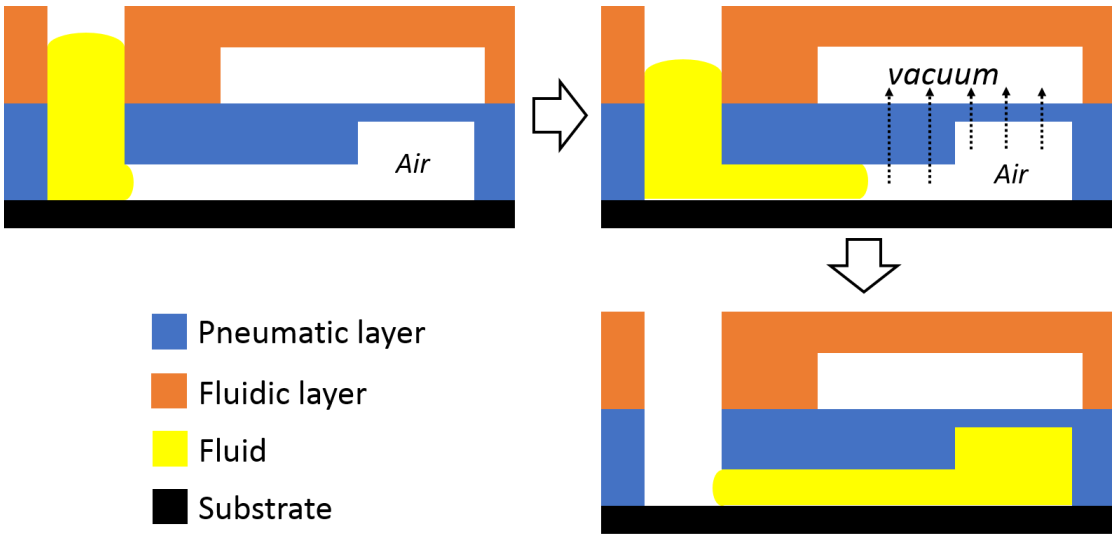

Figure 1-10. Schematic illustration of the working principle of the dead-end filling.

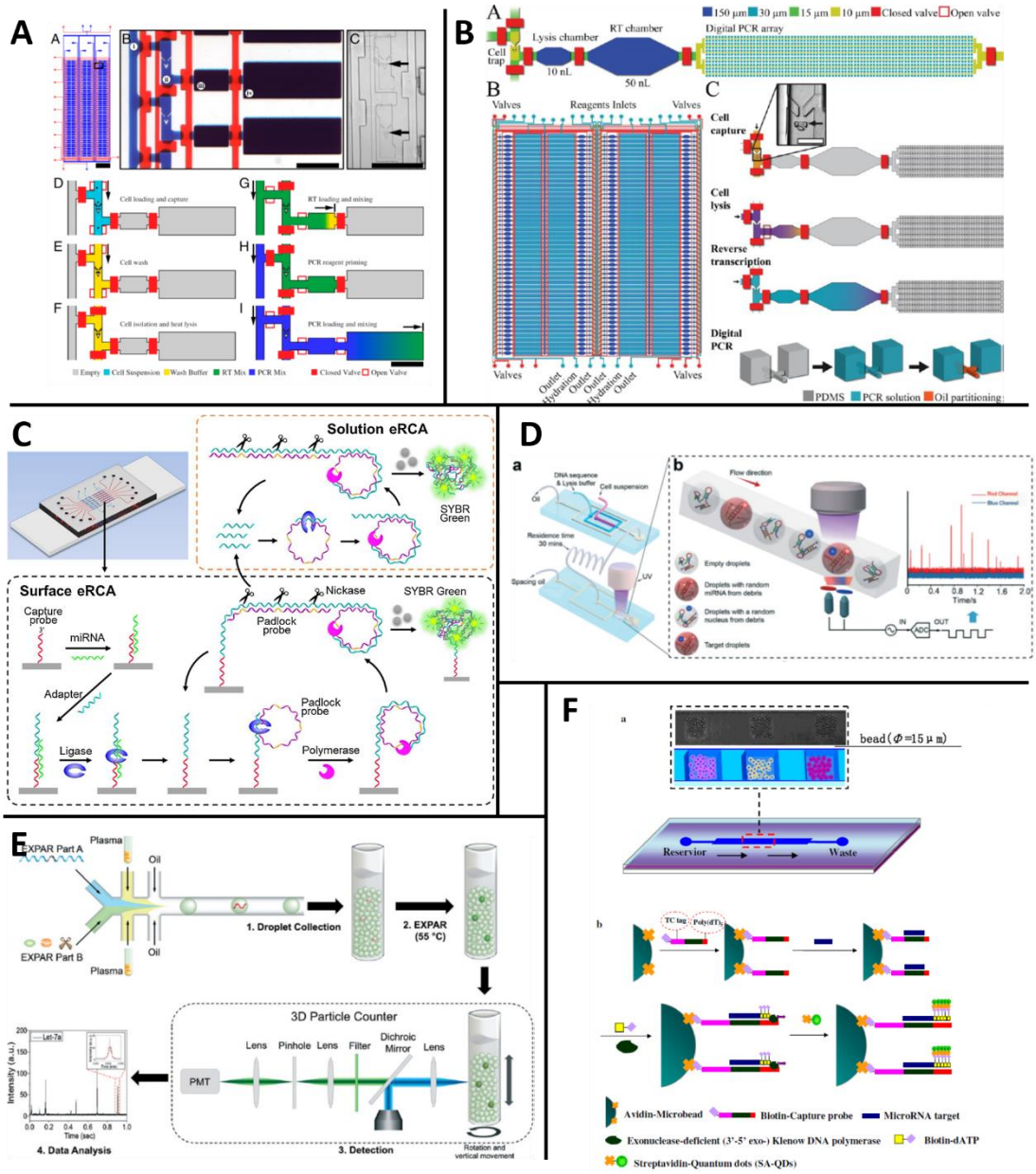

Figure 1-11. Microfluidic devices for miRNA quantitation. (A) An integrated device for single-cell miRNA and mRNA quantitation based on RT-qPCR.[106] (B) An integrated chip for single-cell miRNA and mRNA absolute quantitation based on digital RT-PCR.[107] (C) A microfluidic device for exosomal miRNA detection based on dual-phase eRCA.[108] (D) A microfluidic device for single-cell miRNA detection.[109] (E) An integrated comprehensive droplet digital detection system for directly miRNA quantitation in plasma.[110] (F) A microfluidic bead-based enzymatic amplification for miRNA detection.[111] (reprinted with permission).

Quantitative RNA measurement on microfluidic platforms

A variety of RNA detection methods have been developed on microfluidic

platforms. For the on-chip detection of miRNAs, a number of microfluidic methods have been reported. Some of them were developed leveraging RT-PCR due to its high sensitivity, specificity, and robustness. For example, White et al. designed a microfluidic device for single-cell miRNA and mRNA profiling.[106] As shown in Figure 1-11A, their chip integrated cell trapping, lysis, reverse transcription, and quantitative PCR (qPCR) modules all-in-one device, capable of simultaneously processing 300 parallel single-cell RT-qPCR assays. With this device, they successfully measured the expression of miR-16 and GAPDH mRNA in K562 cells with over 3,300 single-cell experiments, and also investigated the coregulation of miR-145 and OCT4 in single cells. Moreover, years later, they altered the device by replacing the qPCR module with digital PCR (dPCR) module in order to achieve absolute quantitation of miRNA and mRNA at a single cell level,[107] as shown in Figure 1-11B. Their dPCR device achieved high-throughput with the capability to simultaneously measure 200 cells. This approach was applied to measure the expression of miR-16, GAPDH mRNA, and BCR-ABL transcript in K562 cells. In addition, quantitation of single-nucleotide RNA editing of EEF2K in single K562 cells was accomplished with their device. The application of their fully integrated devices demonstrated the ability of high-throughput miRNA and mRNA profiling at the single-cell level. Although on-chip RT-qPCR enjoys high sensitivity and robustness, the complicated thermal cycling process requires expensive instrumentation. To overcome this problem, many microfluidics methods employing isothermal amplification methods were developed. For instance, Cao et al. designed a microfluidic device for exosomal miRNA detection based on dual-phase exponential roll cycling amplification (eRCA).[108] As shown in Figure 1-11C, the target RNA was first captured on the surface of the microfluidic channel via hybridization with ssDNA capture probe, and then detected based eRCA reaction. Their method obtained a limit-

of-detection <10 zeptomoles of let-7a. This on-chip eRCA approach was utilized for the quantitation of let-7a and miR-21 in total RNA, whole cell lysate, and tumor-derived exosome samples, respectively. Their approach revealed the ability to be utilized in the applications of miRNA profiling in complex biological materials. Guo et al. developed a microfluidic device for miRNA detection at single cell level.[109] As shown in Figure 1-11D, their chip was able to process 300-500 cells per minute by encapsulating cells into droplets and then performing lysis and hybridization chain reaction (HCR) for miRNA quantitation. As a proof-of-concept, the expression of miR-21 in MCF-7, MDA-MB-231, and MCF-10a was measured with their method. This ultrahigh-throughput approach fitted the requirement of rapid biomedical identification. Zhang et al. developed an integrated comprehensive droplet digital detection (IC 3D) system for directly miRNA quantitation in plasma samples.[110] As shown in Figure 1-11E, in their method, the plasma sample was first mixed with reaction buffer and then encapsulated in droplets, which were then collected in a tube where exponential amplification reaction (EXPAR) was carried out for target miRNA detection. A dynamic range from 10 to 10000 copies/ml of let-7a was obtained with their approach. The expression of let-7a in 3 colon cancer patient blood samples and 3 healthy control was analyzed with the IC-3D chip and validated with RT-qPCR. This method enabled rapid miRNA analysis directly in plasma samples with high-throughput and robustness. Zhang et al. reported a microfluidic bead-based enzymatic amplification for miRNA detection.[111] As shown in Figure 1-11F, target miRNA was captured by probe-conjugated microbeads which were trapped inside the microwells, and then labeled with multiple biotin-tags by Exonuclease-deficient (3'-5' exo-) Klenow DNA polymerase with Biotin-dATP, on which streptavidin-labeled quantum dots were attached for signal generation. This method obtained a limit-of-detection of 0.1 pM miR-29a, and further

investigation was carried out by detecting miR-29a spiked in total RNA extracted from A549 cells. This approach enabled miRNA quantitation with the advantages of high specificity, remarkable sensitivity, little sample consumption, and low cost. It is noted that most of the miRNA quantitation approaches on microfluidic platforms are capable to directly process crude biological or clinical samples, such as cell lysate,[108, 112] human serum,[113] without the need of sample preparation, and meanwhile achieving good sensitivity with small sample usage and low cost.

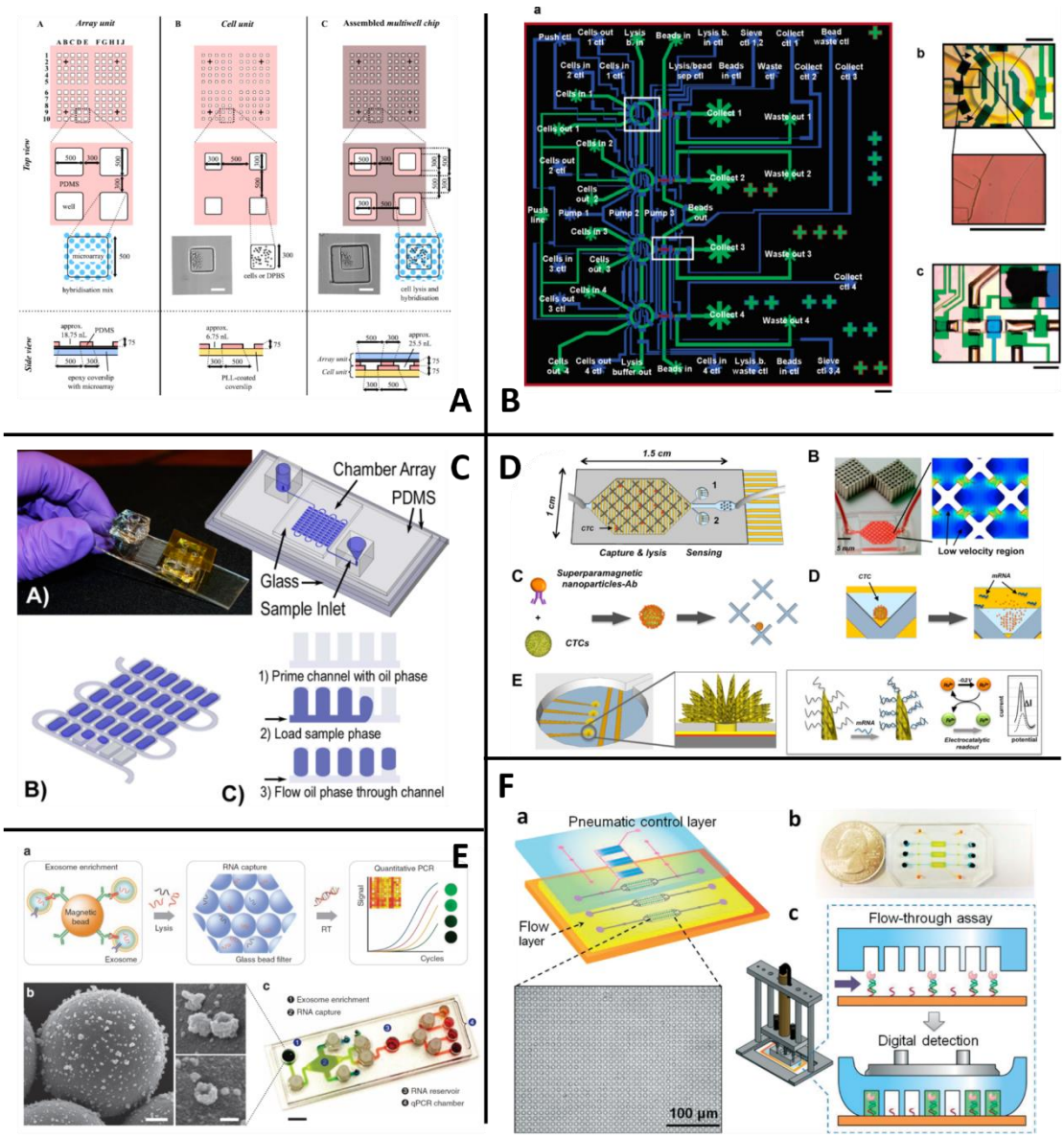

Figure 1-12. Microfluidic devices for mRNA quantitation. (A) A microfluidic multiwell chip for enzyme-free detection of mRNA from few cells.[114] (B) A highly integrated microfluidic system for single-cell mRNA detection.[115] (C) A self-digitization (SD) chip for quantitation of mRNA for single-cell analysis.[116] (D) A microfluidic device for CTCs isolation and mRNA profiling.[117] (https://pubs.acs.org/doi/abs/10.1021/ac5035924, further permissions related to the material excerpted should be directed to the ACS) (E) A microfluidic immuno-magnetic exosome RNA (iMER) platform for exosomal mRNA profiling.[118] (F) An integrated microfluidic digital analysis chip for ultrasensitive quantification of tumor mRNAs in extracellular vesicles.[119] (reprinted with permission)

For the on-chip detection of mRNAs, several approaches have been developed

besides White et al.'s single-cell RT-qPCR chip and RT-dPCR chip that were mentioned above.[106, 107] Haider et al. reported a microfluidic one-step cell lysis, target labeling and hybridization approach,[114] with the capability to simultaneously target 6 different mRNAs in 96 samples, as shown in Figure 1-12A. In each microwell, trapped cells were lysed and thus releasing the target mRNA, which was then captured by ssDNA capture probe and labeled with fluorescent ssDNA detection probe. Six genes in Panc-1 cells were studied with their method as a proof-of-concept. This method was high throughput but lack of sensitivity for low abundant mRNA detection. Marcus et al. developed a highly integrated microfluidic system for single-cell mRNA detection,[115] as shown in Figure 1-12B. Their device implemented cell capture, cell lysis, RNA purification, cDNA synthesis, cDNA purification. After the on-chip sample processing, the cDNA was collected at the output and analyzed by conventional qPCR. This method was high throughout and automatic on the sample processing step, but the final detection still required off-chip conventional qPCR. Thompson et al. reported the self-digitization (SD) chip for quantitation of mRNA for single-cell analysis, which was enabled by on-chip one-step digital RT-PCR,[116] as shown in Figure 1-12C. Their device was utilized to measure the expression of BCR-ABL fusion gene in K562 cell. Their approach was capable of absolute quantitation of mRNA, but an off-chip sample preparation was still required before loading the sample onto their chip. Mohamadi et al. designed a microfluidic device that implemented CTC capture and mRNA detection.[117] As shown in Figure 1-12D, magnetic nanoparticle-bounded CTCs were captured and lysed at the capture zone, and the released target mRNA was captured and detected on nanostructured electrode sensor. A detection limit of 2 CTCs per mL of whole blood was obtained. The approach achieved rapid CTC capture with corresponding mRNA analysis, but only part of the released mRNA could be captured

on the NMEs surface, resulting in a decrease of sensitivity. Although many on-chip mRNA quantitation methods have been reported, there are only a few on-chip assays developed for the detection of exosomal mRNAs to our best knowledge. Shao et al. reported a microfluidic immuno-magnetic exosome RNA (iMER) platform for exosomal mRNA profiling.[118] As shown in Figure 1-12E, their device integrated magnetic-bead-based exosome enrichment, on-chip RNA isolation, and on-chip RT-qPCR in a single device. MGMT and APNG mRNAs in exosomes derived from glioblastoma multiforme were analyzed with their device. This highly integrated chip achieved convenient exosomal mRNA quantitation in an on-chip workstream, but this device required fully manual operations due to the built-in torque-activated valves. Zhang et al. introduced an integrated microfluidic digital analysis chip for ultrasensitive quantification of tumor mRNAs in extracellular vesicles.[119] As shown in Figure 1-12F, the target mRNA was firstly enriched by ssDNA capture probe at the detection area, and then the digital enzymatic signal amplification was carried out for detection. A limit-of-detection of 20 aM synthetic GAPDH mRNA was obtained with this method. Moreover, EWS-FLI-1 fusion transcript and GAPDH mRNA were quantitatively measured in exosome from CHLA-9 and CHLA-258 cell line with their approach, validated with conventional droplet digital PCR. This method obtained remarkable sensitivity, but it did not integrate the exosome enrichment module. In conclusion, although there are numerous mRNAs analysis methods taking advantage of microfluidic platforms, a fully automatic exosomal mRNA profiling approach that can integrate all the processing steps, including exosome isolation, lysis, and mRNA detection is still lacking.

Chapter Overview

Overview of Chapter 2

Duplex-specific nuclease signal amplification (DSNSA) is a promising microRNA (miRNA) quantification strategy. However, existing DSNSA based miRNA detection methods suffer from costly chemical consumptions and require laborious multi-step sample pretreatment that are prone to sample loss and contamination, including total RNA extraction and enrichment. To address these problems, herein we devised a pneumatically automated microfluidic reactor device that integrates both analyte extraction/enrichment and DSNSA-mediated miRNA detection in one streamlined analysis workflow. Two flow circulation strategies were investigated to optimize the on-chip DSNSA reaction in a bead-packed microreactor. With the optimized protocol, we demonstrated that on-chip detection of miR-21 confers a limit of detection of 1.168 pM (35 amol), while greatly reducing the consumption of DSN enzyme to 0.1 U per assay. Therefore, this microfluidic system provides a useful tool for many applications, including clinical diagnosis.

Overview of Chapter 3

The performance of current microfluidic methods for exosome detection is constrained by boundary conditions and by fundamental limits to microscale mass transfer and to interfacial exosome binding. Here, we show that a microfluidic chip designed with self-assembled 3D herringbone nanopatterns can detect low levels of tumor-associated exosomes in plasma (10 exosomes μL−1, or approximately 200 vesicles per 20-μL spiked sample) that would otherwise be undetectable by standard microfluidic systems for biosensing. The nanopatterns promote microscale mass

transfer, increase surface area and probe density to enhance the efficiency and speed of exosome binding, and permit drainage of the boundary fluid to reduce near-surface hydrodynamic resistance, thus promoting particle–surface interactions for exosome binding. With our approach, a capture efficiency of 76.5 ± 2.6% for exosomes derived from SKOV3 cell line and 80.1 ± 5.0% for exosome derived from OVCAR3 cell line were achieved by measuring the exosomal GAPDH mRNA via droplet digital PCR (ddPCR). The mRNAs of human epidermal growth factor receptor 2 (HER2), epidermal growth factor receptor (EGFR), FRα, CA-125, EpCAM, and CD24 are also measured by using our method and validated via ultracentrifugation with downstream ddPCR. This approach was also employed on clinical plasma samples taken from 10 ovarian cancer patients and 10 non-cancer controls, probing mRNAs of FRα, EpCAM and CD24. The results showed great agreement with the protein quantitation result from the on-chip ELISA. We believe our approach should facilitate the use of liquid biopsies for cancer diagnosis.

Overview of Chapter 4

Digital polymerase chain reaction (dPCR) is a powerful tool for genetic analysis, providing superior sensitivity and accuracy. In many applications that demand minuscule reaction volumes, such as single-cell analysis, efficient and reproducible sample handling and digitization is pivotal to accurate absolute quantification of targets, but remains a significant technical challenge. In Chapter 4, we described a robust and flexible microfluidic alternating-pull-push active digitization (μAPPAD) strategy that confers close to 100% sample digitization efficiency for microwell-based dPCR. Our strategy employs pneumatic valve control to periodically manipulate air pressure inside the chip to greatly facilitate the vacuum-driven partition of solution into microwells,

enabling efficient digitization of a small-volume solution with significantly reduced volume variability. The μAPPAD method was evaluated on both tandem-channel and parallel-channel chips, which achieved a digitization efficiency of 99.5% and 94.6% within 10.5 min and 2 min, respectively. To assess the analytical performance of the μAPPAD chip, we calibrated it for absolution dPCR quantitation of λDNA across a range of concentrations. The results obtained with our chip matched well with the theoretical curve computed from Poisson statistic. Compared to the existing methods for highly efficient sample digitization, not only does our technology greatly reduce the limitations in microwell geometries and channel design, but also benefits from the intrinsic amenability of the pneumatic valve technique with device integration and automation. Thus we envision that the μAPPAD technology provide a scalable and widely adaptable platform to promote the development of advanced lab-on-a-chip systems integrating microscale sample processing with dPCR for a broad scope of applications, such as single cell analysis of tumor heterogeneity and genetic profiling of circulating exosomes directly in clinical samples.

Overview of Chapter 5

Sensitive detection of tumor-derived exosomal mRNAs is of great significance in both clinical cancer diagnosis and biological laboratory study, but challenging due to its low abundance in exosomes. The conventional method, which is the combination of exosome isolation by ultracentrifugation, total RNA extraction and RT-qPCR, is low efficient and time-consuming, and also requires a large volume of samples. To address this problem, in Chapter 5, we introduced a microfluidic device that integrated exosome beads capture, on-chip lysis, μAPPAD sample dispensing and on-chip one-step digital RT-PCR for the detection of tumor-derived exosomal mRNAs. To assess the analytical

performance of the on-chip digital RT-PCR, GAPDH mRNA in total RNA from human skeletal muscle was measured, and the result was validated by standard droplet digital PCR. As a proof-of-concept, the detection of GAPDH mRNA of the exosomes from the MDA-MB-231 cell line was performed by our approach. The preliminary results indicated that we've successfully enabled the on-chip exosomal mRNA detection via our highly integrated microfluidic platform. Further optimization is still required for sensitive quantitative measurement of exosomal mRNAs, and we believe this method can potentially be utilized in the field of clinical diagnostic, such as the diagnosis of Ewing Sarcoma by detecting the EWS-FLI1 fusion gene in tumor-derived exosomes in patients' plasma.

Chapter 2. Microfluidic circulating reactor system for rapid and automated duplex-specific nuclease-mediated microRNA detection

Introduction

MicroRNAs (miRNA) are small non-coding RNAs that regulate gene expression[62] and have been found stable in RNase enriched environments, such as blood, urine, saliva, milk, and cerebrospinal fluid.[120-123] Due to these characteristics, miRNAs are promising biomarkers for a variety of diseases, such as diabetes,[124] Alzheimer's disease,[122, 125] and cancer.[126, 127] However, the detection of miRNAs in body fluid is challenging due to the low abundance of miRNAs.[128] The most commonly used methods to detect miRNAs are RT-qPCR[72, 129, 130] and RNA microarray.[131-133] As the gold standard of miRNA detection, RT-qPCR is highly sensitive with a limit of detection at the level of a few copies per microliter; but it usually requests tedious sample processing to remove inhibitory species and costly instrumentation. RNA microarray is a high throughput method that can analyze multiple targets of miRNAs, but its sensitivity is relatively lower. There is still an urgent need of a low-cost, sensitive and easy-to-use miRNA detection methods for biomedical applications, such as clinical diagnosis.

Recently, duplex-specific nuclease (DSN) has emerged as a new tool to develop simple and robust bioassays for miRNA quantitation because of its unique DNase activity that selectively cleaves double-strand DNA (dsDNA) or the DNA strand in a DNA-RNA hybrid, as opposed to single-strand DNA (ssDNA) or RNAs.[134] Based on this characteristic of the DSN, a number of DSN-mediated signal amplification

(DSNSA) miRNA detection methods have been reported. For instance, an in-solution DSNSA-mediated miRNA detection assay that used a Taqman™ probe tagged with a fluorophore on one end and a quencher on the other end.[135] When hybridized with the target miRNA, the DNA probe is cleaved by DSN to separate the fluorescent dye from the quencher, generating the fluorescence signal. The released the miRNA templates that can be recycled for another cycle of hybridization and DSN cleavage, and this process can be repeated thousands of times, leading to significant amplification in signal to improve the sensitivity of miRNA detection. Similarly, gold-nanoparticle (AuNP) labeled fluorescent ssDNA can also be applied as the capture probe during the DSNSA process.[136] The fluorophore attached to the ssDNA capture probe remained quenched by the surface of the AuNP until the ssDNA hybridized with the target miRNA and was cleaved by DSN. In addition, DSNSA based miRNA assays can also be achieved by immobilizing the fluorescently labeled ssDNA capture probe onto solid surfaces. For instance, magnetic beads-conjugated quantum dot-capped DNA capture probes (QD–CPs) were utilized to capture the target miRNA in a DSNSA-mediated miRNA assay for the purpose of Dengue virus detection.[137] After the DSNSA reaction, the beads carrying un-reacted capture probes were removed and the supernatant is measured to quantify the intensity of released quantum dots. In contrast to standard PCR detection of miRNAs, these DSN-based isothermal methods enable direct detection of RNA fragments without the reverse transcription step, ease the design of specific primer/probes for short miRNA sequences, and negates the need of sophisticated thermal cycling instrument. Therefore, DSNSA is well poised to miRNA sensing because it simplifies the assay development, improves the assay robustness, mitigates the problems of sample degradation and contaminations, and reduces the assay cost. Despite these compelling advantages, the widespread application of DSNSA

methods has been hampered by some practical barriers, such as relatively high cost of DSN and lengthy enzymatic reaction required to afford high sensitivity due to the linear amplification process. To address these limitations, DSNSA has been coupled with other signal amplification mechanisms to enhance the sensitivity and shorten the assay time.[138-140] However, these multi-stage signal amplification methods involve complex reagent composition and assay protocols that need to be carefully optimized, which compromises the simplicity and robustness of DSN-based assays.

Herein, we attempted to exploit the microfluidic principles to develop a simple and rapid DSNSA-mediated miRNA detection system. Microfluidics has been broadly applied to bioanalysis because of its ability to improve detection sensitivity and analysis speed while reducing the consumption of sample and reagents.[141-143] It provides a platform that is capable to integrate multiple functions, such as sampling, sample enrichment and detection all in one device by manipulating nanoliters to femtoliters of fluids in microchannels.[144] To date, many microfluidic platforms have been reported for miRNA detection using various assays, including RT-qPCR,[106] digital PCR,[107] RCA,[108, 145] droplet EXPAR assay,[110] and the hybridization assays coupled with encoded hydrogel particles,[112, 113, 146] enzymatic amplification,[111] laminar flow-assisted dendritic amplification,[147, 148] and electrochemical detection.[149] In addition, most of these microfluidic miRNA methods are capable to process crude samples, such as cell lysate,[108, 112] human serum,[113] without the need of off-chip RNA extraction. Despite the obvious advantages of microfluidics, very limited progress has been reported to date towards leveraging DSN-based miRNA detection. To our best knowledge, there has been only one report on combining microfluidics with DSNSA for miRNAs detection.[150] However, in this approach, the DSNSA assay was conducted in the conventional format and the microfluidic device was employed only as the ionization

source for mass spectrometric analysis of the products of the DSN reaction. In contrast to this method, our system reported here directly adapts the microfluidic reaction and reagent manipulation to promote the performance of DSNSA for miRNA detection.

Our DSNSA-mediated microfluidic miRNA detection system integrates an affinity bead-packed microreactor for on-chip sample enrichment and purification and a pneumatically controlled microchannel circuit for DSNSA based miRNA detection. Using the pneumatically automated microreactor system, we investigated the sample flow rate for the solid-phase miRNA capture, studied DSNSA reaction at the circulating and oscillating-flow-control modes and optimized the assay protocol. As a proof-of-concept, we demonstrated on-chip detection of miR-21 which achieved a limit-of-detection (LOD) of 1.168 pM (35 amol) with ~1.5 h of sample enrichment and 2 h of DSNSA reaction. Moreover, our method only consumes 0.1 U of DSN per assay, which is 1/6 of the amount of DSN needed for a 30 μL volume off-chip DSNSA miRNA assay, thus greatly reducing the cost. Overall, our microfluidic device provides a new method to improve the performance of DSNSA-mediated miRNA assays and thus can be useful for various applications, such as clinical diagnosis and point-of-care testing.[42]

Experimental section

Chemical materials

All synthetic ssDNA and miRNA were purchased from Integrated DNA Technologies (IDT, Coralville, IA, USA). Sequences are listed in Table 2-1, respectively. HiTrap NHS-Activated HP affinity column was obtained from GE Healthcare (Chicago, IL, USA). Duplex-specific nuclease (DSN) is purchased from Evrogen (Moscow, Russia). Magnesium chloride (1 M) (Invitrogen), Ribolock RNase inhibitor (40 U/μL), Bovine Serum Albumin (BSA), 1× Tris-EDTA solution,

diethylpyrocarbonate (DEPC) treated water, Sodium chloride, Tris hydrochloride and Tris-Base were ordered from Thermo Fisher Scientific (Waltham, MA, USA). Tween® 20 and ethanolamine were purchased from Sigma-Aldrich (St. Louis, MO, USA). 1× Phosphate-Buffered Saline (PBS) was obtained from Mediatech, Inc. Sylgard® 184 Silicone Elastomer Kit is bought from Dow Corning Corporation (Midland, MI, USA).

Table 2-1. Sequences of oligonucleotides

Name	**Sequence (5′-3′)**
Capture probe for miR-21	5'-FAM-TCAACATCAGTCTGATAAGCTA-NH_2-3'
hsa-let-7a-5p	5′-UGAGGUAGUAGGUUGUAUAGUU-3′
hsa-miR-21-5p	5′-UAGCUUAUCAGACUGAUGUUGA-3′
hsa-miR-200a-3p	5′-UAACACUGUCUGGUAACGAUGU-3′
hsa-miR-200b-3p	5′-UAAUACUGCCUGGUAAUGAUGA-3′

Agarose bead modification

The fluorescent ssDNA capture probe was immobilized on 34 μm-diameter agarose beads via amine-NHS cross-linkage.[151] 0.1g NHS activated Agarose beads were taken from the HiTrap NHS-Activated HP affinity columns and washed with cold 0.1 M HCl twice, cold water once and cold 1× PBS solution twice. The beads were then immerged into 400 μL 1× PBS solution containing 6.6 μM probe ssDNA, mixing overnight on a rotator at room temperature. 0.5 M ethanolamine was used to block the active site on the beads surface by incubating for 2 hours at room temperature in the next day. The probe coated agarose beads were then washed with 1× PBS solution containing 0.5 M NaCl three times and stored in 1× TE buffer at 4 ºC.

Microchip fabrication

The DSN circulation chip involves a Polydimethylsiloxane (PDMS) pneumatic control layer, a PDMS fluidic layer and a glass substrate. Molds for both of the PDMS

layers were fabricated by using standard photolithography on 4" silicon wafers (P100). The mold for the pneumatic layer was constructed with SU-8 2050 (MicroChem) 100 μm in height. The mold for the fluidic layer underwent a first photolithography process by using SU-8 2025 (MicroChem) in a height of 25 μm for the flow channel, and a second photolithography process by using SU-8 100 (MicroChem) in a height of 70 μm for the bead chamber and the detection window. Both of the molds were treated with a gas phase silanization with Trichloro(1H,1H,2H,2H-perfluorooctyl)silane (Sigma Aldrich, St. Louis, MO, USA).

Standard soft lithography was used for fabricating the pneumatic control layer and the fluidic layer. 40.5 g mixture of Sylgard® 184 at 8:1 (base : curing agent) weight ratio was poured onto the mold and incubated at 65 ºC for 2 hours. Once PDMS was cured on the mold, it was peeled off and cut into pieces. 1 mm diameter holes were punched as the inlet of each pneumatic control channel. 6 g mixture of Sylgard® 184 at a 15:1 (base : curing agent) weight ratio was spanned on the fluidic layer mold at 500 rpm for 30 sec and 800 rpm for 30 sec, followed with 2 hours incubation at 65 ºC for 2 hours. The pneumatic control layer and the fluidic layer were treated with UV-ozone, then aligned and assembled manually. The assembled double-layer PDMS chip was incubated at 80 ºC overnight for permanent bonding. After tearing the double layer chip off from the mold, a 2 mm diameter puncher was used to punch holes for inlets and outlets of each flow channel. The glass subtract was treated with piranha solution for 15 min before assembled with the double layer PDMS slab. UV-ozone was used to form permanent bonding between the glass slide and the PDMS slab. All flow channels were blocked with 0.1% BSA for at least 2 hours. The chip was then stored at 4 ºC until usage.

Off-Chip DSNSA assay for off-chip optimization

The DSNSA assay was optimized in 0.5 ml reaction tubes before integrated in chip. For the final optimum condition, 3 μL stock fluorescent ssDNA capture probe conjugated agarose beads were taken and washed with 50mM Tris buffer (pH 8.0). The supernatant was then replaced by 29 μL working solution (50 mM Tris buffer containing 10 mM $MgCl_2$, 0.8 U/μL RNase inhibitor, 0.02 U/μL DSN, pH 8.0). 1 μL miRNA was added to the solution as the analyte. The final reaction volume was 30 μL. The reaction tube was then rotated for 2 hours at 40 ºC in an incubator (Benchmark Scientific, NJ, USA). After the reaction, the fluorescence intensity of the supernatant was measure by Biotek Crytation 5 imaging reader (Biotek, VT, USA).

On-Chip DSNSA assay

Before the assay, all the chip channels were washed with DEPC-treated water, and then the probe conjugated agarose beads were filled into the bead chamber by gravity. The solution in each channel was replaced by the capture buffer (1× TE buffer containing 350mM NaCl and 0.05% (w/v) Tween®20).[146] Right before the capture, the chip was placed on a hotplate at 95 ºC for 5 min and then cooled down to 0 ºC on ice. The on-chip pumping then started to pump the buffer flowing through the beads. During the capture process, at room temperature, 30 μL of sample solution was pumping through the bead chamber at room temperature by using the on-chip 4-step pumping with a flow rate at 0.34 μL/min, followed with 5μL capture buffer. Once the capture process was done, the on-chip pumping was stopped. For the DSNSA reaction, the buffer in all the channels was replaced with ice-cold working solution (50 mM Tris buffer containing 10 mM $MgCl_2$, 0.8 U/μL RNase inhibitor, 0.02 U/μL DSN, pH 8.0) by flushing each channel with 5 μL working solution. All the pneumatic valves were

then closed, and the on-chip pumping was engaged to make the Agarose beads oscillate inside the bead chamber to enhance the mixing efficiency. The chip was placed at a 40 ºC incubator for 2 hours for the DSNSA reaction. After the reaction was finished, the fluorescence intensity of the detection chamber was tested using a fluorescence microscope. The image was analyzed using ImageJ (NIH).

RT-qPCR

Reverse transcription was done by using TaqMan™ MicroRNA Reverse Transcription Kit (Applied Biosystem, Foster City, CA, USA). The operation followed the manufacturer's protocol with a slight change. Briefly, each 30 μL reverse transcription reaction mix consists of 0.3μL 100 mM dNTPs, 2 μL 50 U/μL MultiScribe™ Reverse Transcriptase, 3 μL 10× Reverse Transcription Buffer, 0.38 μL 20 U/μL RNase inhibitor, 16.32 μL RNase free water, 6 μL 5× RT primer and 2 μL RNA sample. The Reverse transcription mix was incubated at 16 ºC for 30 min, 42 ºC for 30 min, 85 ºC for 5 min and ended at 4 ºC. qPCR was done by using TaqMan® MicroRNA assay (Applied Biosystem, Foster City, CA, USA) on Mastercycler epgradient S (Eppendorf). Each 20 μL PCR mix consists of 1 μL 20× TaqMan MicroRNA Assay, 1.33 μL RT reaction product, 10 μL TaqMan 2× Universal PCR Master Mix (No AmpErase UNG) and 7.67 μL Nuclease-free water. The PCR mix was incubated at 95 ºC for 10 min, 40 cycles of 95 ºC denature for 15 sec and 60 ºC anneal/extend for 60 sec. For testing the biological sample, 1 mg/mL Breast Adenocarcinoma (MCF-7) total RNA (Invitrogen, Carlsbad, CA, USA) was diluted to 1 ng/uL and 10 ng/uL with nuclease-free water, and then analyzed by using the RT-qPCR protocol described above. The result was compared with the data from the On-Chip DSNSA assay.

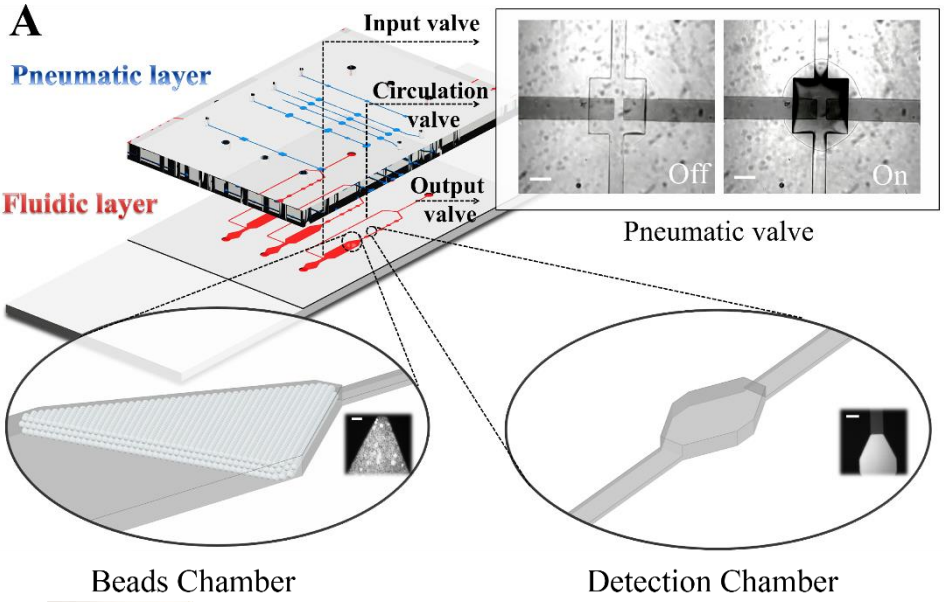
A
Input valve
Pneumatic layer
Circulation valve
Output valve
Fluidic layer
Off
On
Pneumatic valve
Beads Chamber
Detection Chamber

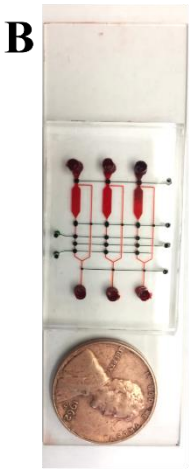
B

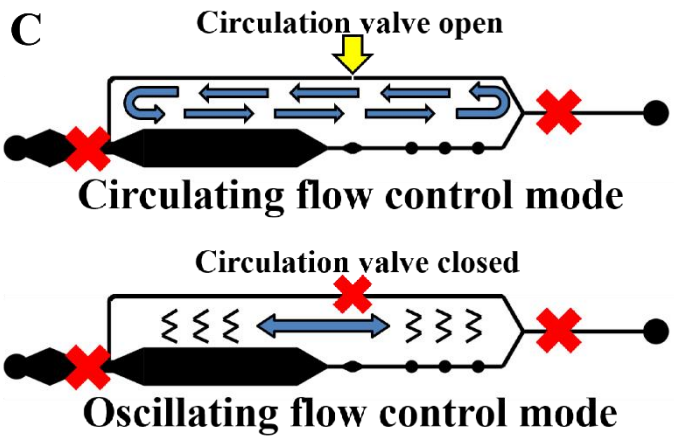
C
Circulation valve open
Circulating flow control mode
Circulation valve closed
Oscillating flow control mode

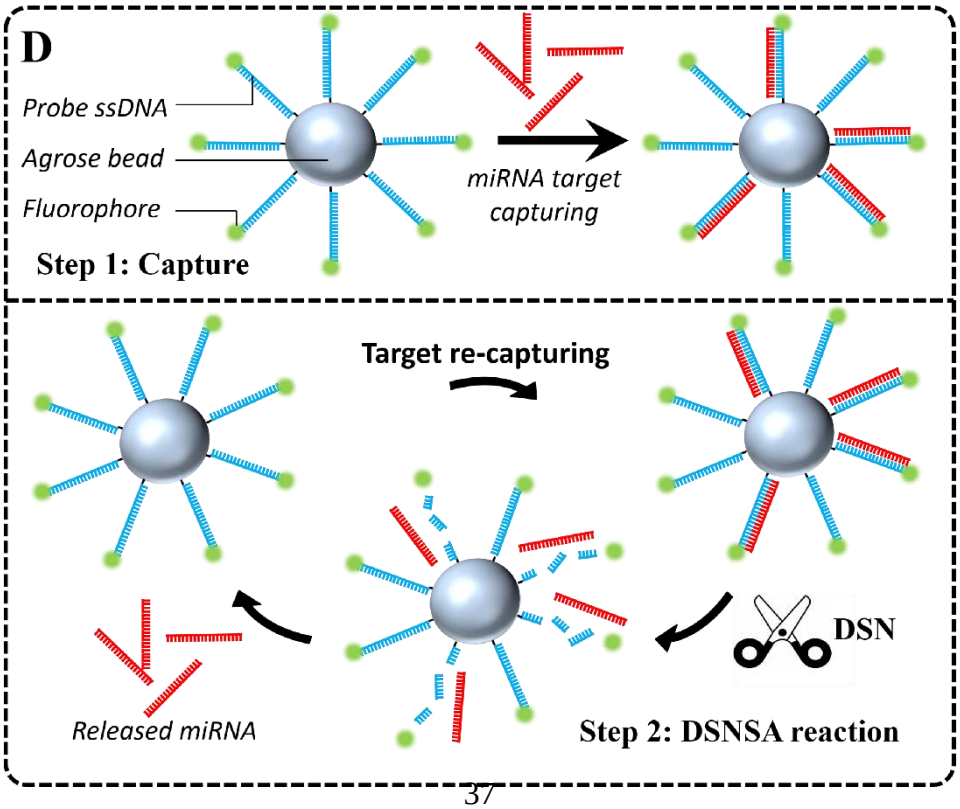
D
Probe ssDNA
Agrose bead
Fluorophore
Step 1: Capture
miRNA target capturing
Target re-capturing
DSN
Released miRNA
Step 2: DSNSA reaction

Figure 2-1. Illustration of the On-chip DSNSA mediated miRNA assay. (A) Illustration of the chip design. The chip involves a pneumatic control layer, a fluidic layer, and a glass substrate. Three valves are used to change flow direction for different working modes; A bead chamber is used to trap agarose beads inside the chip; A detection chamber is used for fluorescence signal amplification. (scale bars in each photo are 150 μm) (B) photo of an assembled chip, with red dye filled in the bottom flow channels and green dye filled in the top pneumatic control circuit. (C) Schematic of the circulating-flow-control mode and the oscillating-flow-control mode designed for improving the mixing during the DSNSA reaction. (D) Schematic of the On-Chip DSNSA principle step: (1) Solid-phase miRNA capture. In this step, the target miRNA molecules are captured by the ssDNA probe conjugated on the surface of the beads while the sample solution is flowing through the beads packed inside the beads chamber (2) DSNSA reaction step, during which the fluorescent ssDNA capture probes of the DNA-miRNA hybrids are cleaved by DSN and release the fluorophore and the miRNA. The capture and cleavage cycle keep being repeated until the end of this step, and the fluorescence is then measured to determine the concentration of the analyte miRNA.

Result and discussion

Chip design and assay principle

The principle of our method is to utilize the microfluidic reaction system to promote the DSN enzymatic reaction while reducing the amount of expensive DSN enzyme needed. To further enhance the analytical sensitivity and speed, we intended to construct a total analytical system that combines sample processing (i.e., isolation and enrichment of specific miRNAs from biological samples) and miRNA quantification by DSNSA assay in one on-chip workflow. This capacity would enable direct miRNA detection without the need of total RNA purification which can result in variability in yield, sequence bias, cross contaminations, and RNA degradation.[108, 152] The design and the integrated microfluidic device are presented in Figure 2-1A. It is a multi-layer device that consists of a PDMS pneumatic control layer, a PDMS fluidic layer, and a glass substrate. A photo of an assembled chip was shown in Figure 2-1B, in which the pneumatic channels were filled with green dye and the fluidic channels were filled with red dye. In the pneumatic control layer, the 100 μm-high control circuit designed for

precise delivery and routing of samples/reagents consists of a three-valve pump[153] and a set of lifting-gate valves[101] that control the input reservoir, output reservoir and circulation channel, respectively. The fluidic layer involves a beads chamber, a detection chamber, a circulation channel and a main flow channel. The 100 μm-high beads chamber was designed to trap and stack the 34 μm-diameter probe conjugated agarose beads for on-chip sample enrichment and the DSNSA reaction. The main flow channel and the circulation channel were both designed to be 25 μm in height to avoid the entrance of the agarose beads. The 100 μm-high detection chamber in 100 μm height is designed for the fluorescence detection while avoiding the signal interference from the fluorescent agarose beads. In addition, compared to the 25 μm-high flow channel, the detection chamber provides a 4 times higher optical distance, thus greatly enhancing the sensitivity of this fluorescence-based assay. The design of the circulation channel and the circulation valve enables two different mixing modes to promote the DSNSA reaction. As depicted in Figure 2-1C, the circulating-flow-control mode allows the reaction mixture except the agarose beads to flow along the channel circuit as the circulation valve is open. In contract, in the oscillating-flow-control mode, the circulation channel is disabled by the closure of the circulation valve, and the reaction mixture is forced to flow oscillationally within the main channel.

The On-Chip assay strategy, as illustrated in Figure 2-1D, consists of a solid-phase miRNA capture step and a DSNSA-reaction step. In the capture step, the sample solution driven by the 4-step on-chip pumping flows through the beads which are stacked in the bead chamber. The target miRNA is then captured and enriched by the ssDNA capture probe immobilized on the agarose beads surface, whose sequence is designed to be complementary to that of the target miRNA. The DSNSA-reaction step is then carried out after replacing the buffer in the channel with the reaction master mix

and increasing the temperature. The DSNSA reaction relies on the nature of duplex-specific nuclease (DSN), which only hydrolyzes the DNA part of a DNA-miRNA hybrid and thus releases the miRNA. The released miRNA is subsequently captured by another probe and form a DNA-miRNA hybrid again, ready for next cleavage. Meanwhile, the fluorophore attached on the probe DNA strand is also released to serve as the source of the signal. The on-chip pumping keeps working using the same parameter set as in the capture step, during which the reaction system is sealed by the closure of both of the input valve and output valve to avoid the diffusion toward the inlet and outlet reservoirs. The reaction system is being stirred thoroughly by the on-chip pumping so that the DSNSA reaction can be expedited. In the meantime, the released fluorophore molecules are defusing homogenously to all channels including the detection chamber for the signal readout.

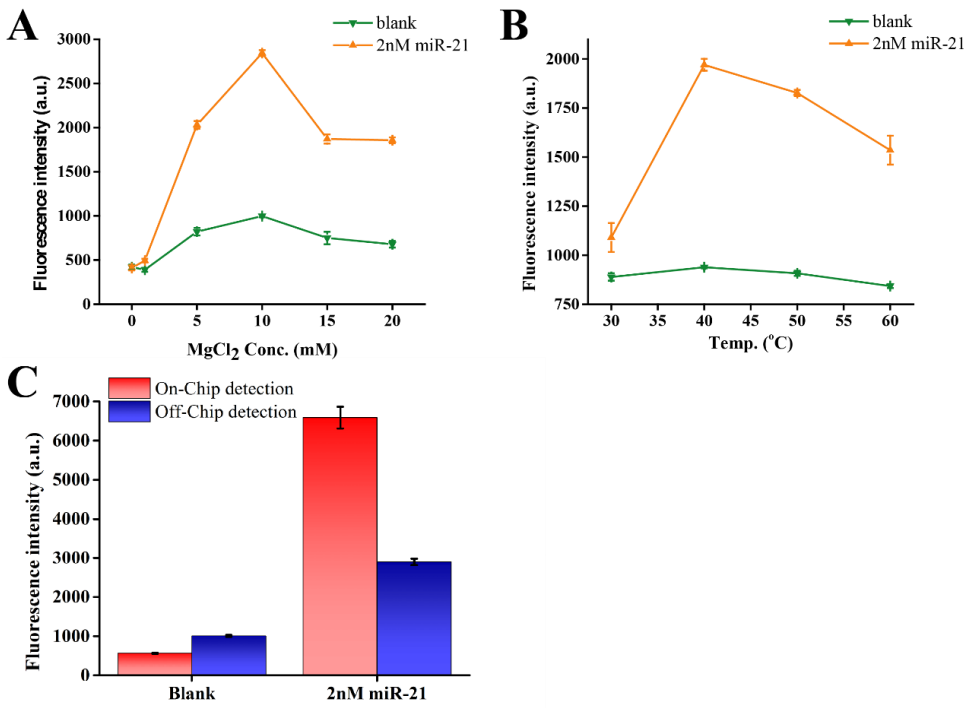

Figure 2-2. Off-chip optimization. (A) Optimization of $MgCl_2$ concentration (n=3). (B) Optimization of reaction temperature (n=3). (C) Comparison between the signal from the on-chip assay and the off-chip assay (n=3). The on-chip approach was performed with the circulating flow control mode during the on-chip DSNSA process.

Assay optimization

Although the reaction parameters of DSNSA reaction were well established in previous studies, the DSNSA on agarose surface has not been studied yet. To simplify the development of our on-chip DSNSA method, the optimization of reaction parameters, such as the concentration of $MgCl_2$ and the reaction temperature, was carried on via off-chip DSNSA assays. The concentration of $MgCl_2$ was optimized in reaction tubes due to the fact that the enzymatic activity of DSN can be impacted by the concentration of the Mg^{2+} ion in the reaction system. Interestingly, as presented in Figure 2-2A, it was observed that the signal intensity increasing along with the $MgCl_2$ concentration till 10 mM and then decreasing. This could be a result of the decrease in the DSN activity due to the increasing ionic strength.[134] Thus, 10 mM was picked as the optimum $MgCl_2$ concentration for our on-chip DSNSA assay. The reaction temperature was also investigated since it is an important parameter that determines the reaction rate of the DSN enzymatic reaction. We optimized the reaction temperature by performing the DSN reaction under different temperatures in the range from 30 to 60 °C in reaction tubes. As depicted in Figure 2-2B, the signal intensity reached the highest value at 40 °C and then dropped rapidly, while the reported working temperature of DSN could be as high as 60 °C.[134] This could be caused by the melting DNA-miRNA hybrids in high temperature due to the low melting temperature of miRNA. Therefore, 40 °C was determined to be the best working condition for the DSNSA reaction.

However, the large volume (>30 μL) of the off-chip assay requires a mass of DSN, which is not cost-effective. In addition, there is still room to improve the sensitivity due to the inefficient mixing of the beads during DSNSA assay. As demonstrated in Figure 2-2C, with our microfluidic device, a much higher signal was obtained while a lower background was achieved. This was due to the higher surface-

to-volume ratio in the micrometer scale microfluidic channel than that in a centrifuge tube. Meanwhile, the pumping system build in the chip also provides an efficient mixing for the reaction system, which expedited the DSNSA reaction.

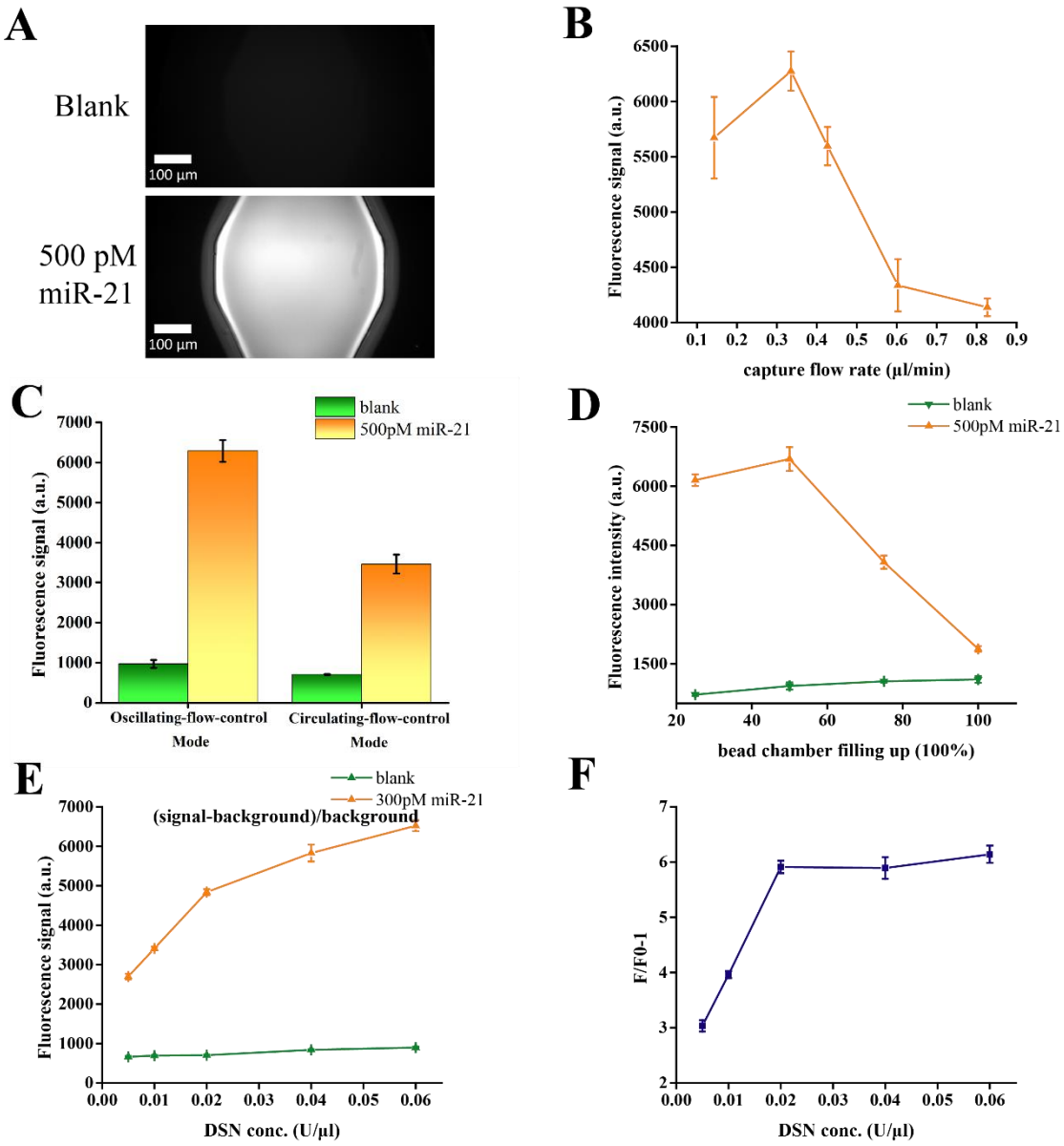

Figure 2-3. On-chip optimization. (A) Fluorescence images taken at the detection chamber after the on-chip DSNSA mediated assay for blank and 500 pM miR-21. (B) Optimization of the sample flow rate used in the solid-phase miRNA capture step (n=3). (C) Signal comparison between utilizing oscillating flow control mode and the circulating flow control mode during the DSNSA reaction (n=3). (D) Comparison of signal intensity of 300 pM miR-21 and blank with different beads amount (n=3). (E) Optimization of DSN concentration with 300 pM miR-21 and blank (n=3). (F) Background subtraction for optimization of DSN concentration shown in (E).

On-chip optimization

The optimized DSNSA mediated miRNA assay was employed on the microfluidic platform, on which the fluorescence signal could be measured at the detection chamber, as demonstrated in Figure 2-3A. A solid-phase miRNA capture step was integrated into the on-chip assay prior to the DSNSA reaction. In the capture step, the flow rate of the sample solution is an important parameter that greatly influences the sample capture efficiency. A high flow rate will shorten the capture time, but it will also reduce the time of the interaction between the target miRNA molecules and the ssDNA capture probes, resulting in a decrease of capture efficiency. In our chip, the flow rate can be controlled by employing different pumping parameter sets for the on-chip pump, as described previously.[153] To optimize the flow rate for the sample capture step, we tested 0.14, 0.34, 0.43, 0.60, 0.83 μL/min as the flow rate of 30 μL of 500 pM miR-21, followed with on-chip DSNSA detection with the same reaction condition. As shown in Figure 2-3B, flow rates higher than 0.34 μL/min caused signal dropping, which indicated insufficient capture efficiency. Interestingly, a slower flow rate also leads to signal reduction, presumably attributed to the degradation of miRNA when held at room temperature for too long. Hence, 0.34 μL/min was selected to be the optimum flow rate for the on-chip sample capture process. For 30 μL of sample solution, it required less than 1.5 h to finish the capture step.

The mixing process is crucial to promote the DSNSA reaction. To achieve a satisfactory thoroughly mixing, we designed a circulation channel and a circulation valve to enable the circulating-flow-control mode and the oscillating-flow-control mode, as above mentioned. The on-chip pump kept working with the same parameter set for both of the mixing modes, but the reaction system was mixed in a different way according to the status of the circulation valve, as illustrated in Figure 2-1C. To seek

out the optimum mixing strategy for the on-chip DSNSA assay, we compared these two mixing modes by analyzing 30 μL 500 mM miR-21. As shown in Figure 2-3C, it was notably the signal of 500 pM miR-21 from the oscillating flow mode was almost as twice as that from the circulating flowing mode, while the background remained nearly unchanged. The relatively lower mixing efficiency of the circulating-flow-control mode could be explained by the lack of contact between the miRNA and the probe-conjugated agarose beads when the released miRNA molecules were flowing in the circulation channel. Consequently, in terms of the mixing efficiency, the oscillating-flow-control mode performs way better than the circulating-flow-control mode and thus was picked as the optimums mixing strategy for the on-chip DSNSA reaction.

The amount of probe conjugated agarose beads filling in the beads chamber is significant to both the solid-phase miRNA capture step and the DSNSA-reaction step. More beads will provide more binding sites for the target miRNA capture, but could cause problems such as an increase of background. To determine the optimum beads amount filled into the chamber, we filled the chamber with different amounts of beads and performed the on-chip DSNSA assay on 30 μL of 500 pM miR-21. As illustrated in Figure 2-3D, although the background went up as the number of beads increased, the signal started to decrease when the beads fill out the chamber over 50%. This could be due to the decreased volume of the reaction master buffer within the channel caused by the increased space occupied by the agarose beads. Thus the total amount of DSN was not enough to maintain the enzymatic reaction rate, resulting in low efficient signal amplification. Therefore, filling the chamber 50 % with the beads was chosen to be the best condition for the on-chip DSNSA miRNA assay.

The concentration of DSN is vital for the DSNSA reaction in terms of both assay sensitivity and reagent consumption. To optimize the DSN concentration, the on-chip

DSNSA mediated miRNA assay was carried out on 30 μL of 300 pM miR-21 with five different DSN concentrations from 0.005 to 0.06 U/μL. As shown in Figure 2-3E, although the signal of miRNA increased along with the rise of the DSN concentration, the background performed the same. To accurately evaluate the impact of different DSN concentrations, we subtracted the background as illustrated in Figure 2-3F. It was obvious that the signal reaches a platform after 0.02 U/μL, which indicated that a DSN concentration higher than 0.02 U/μL would not help to increase the sensitivity of this assay. Therefore, 0.02 U/μL was selected to be the optimum concentration of DSN for our on-chip DSNSA miRNA assay. In this DSN concentration, compared to the 0.6 U DSN consumption in each 30 μL-volume off-chip assays, it is noted that the on-chip method only required 0.1U of DSN since only 5 μL working solution containing DSN was needed for each test, which greatly reduced the cost.

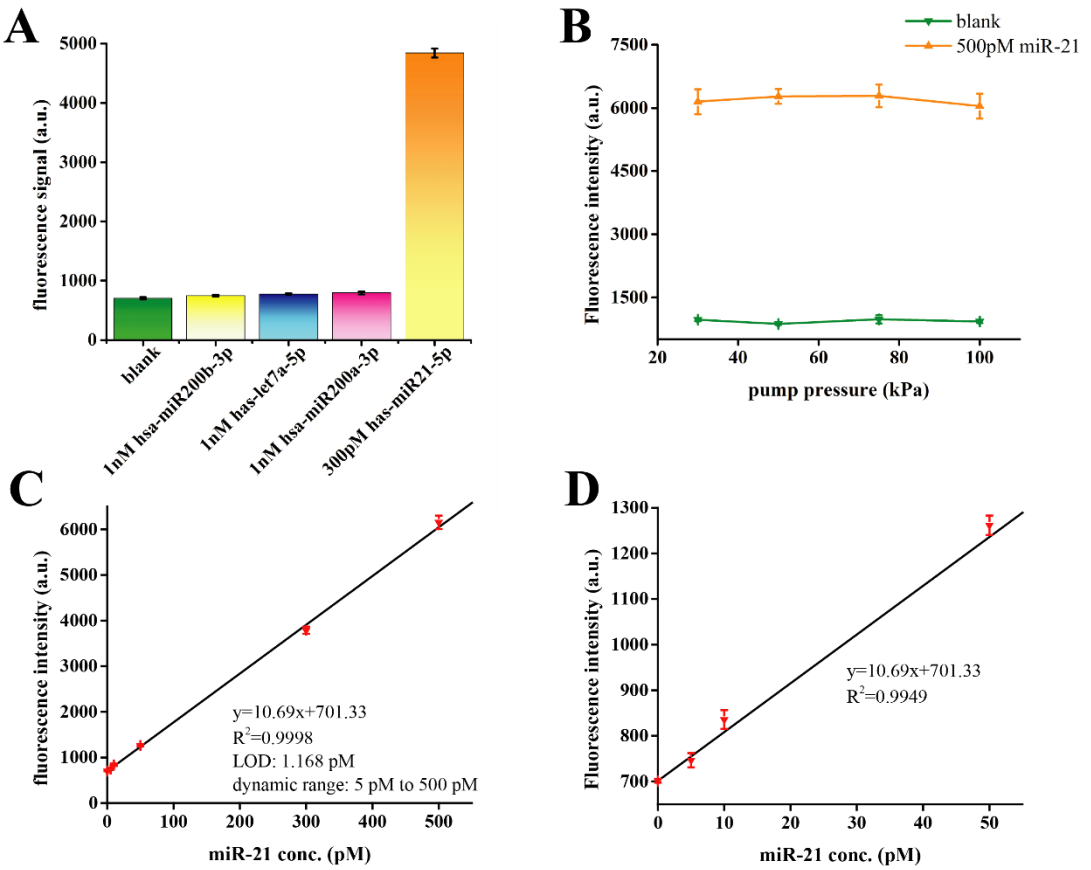

Figure 2-4. Analytical performance of the on-chip DSNSA mediated miR-21 assay. (A) Specificity test of On-chip DSNSA miR-21 assay (n=3). (B) Signal intensity comparison of 500 pM miR-21 and blank under different pump pressure during the reaction step (n=3). (C) Calibration curve of miR-21 by On-Chip DSNSA on overall dynamic range. (D) Calibration curve of miR-21 by On-Chip DSNSA on low concentration range.

Although the specificity of the DSNSA miRNA assay has been well studied, it is still important to verify it on our microfluidic platform. To investigate the specificity of the on-chip DSNSA mediated miRNA assay, high concentration (1 nM) of Let7a, Let7b, miR-200a, and miR-200b were measured by using the miR-21 probe, respectively. As depicted in Figure 2-4A, the signal intensity of these high concentrated non-target miRNAs from the assay was all at blank level, while only 300 pM of miR-21 obtained a fluorescence signal in high intensity, which indicated the specificity of the DSNSA mediated miRNA assay remained excellent on our on-chip platform.

Good reproducibility is essential for our approach when performed on different instruments, in which case the pump pressure applied on the pneumatic control circuit is the major variable. To assess the reproducibility of our method, we performed the on-chip DSNSA assay on 30 μL of 500 pM miR-21 with diverse pump pressures from 30 kPa to 100 kPa. As shown in Figure 2-4B, neither the signal intensity nor the blank level was significantly impacted by the change of pressure. This result revealed that our method was qualified with excellent reproducibility and capable to tolerate large variation of pump pressure that could possibly occur when performed on different instruments.

We calibrated the on-chip DSNSA mediated miRNA assay with synthetic miR-21 under the optimum reaction conditions. As illustrated in Figure 2-4C, the linear range of our approach is from 5 to 500 pM. The correlation equation was $Y=10.69X+701.33$ ($R^2=0.9998$), in which Y represents the fluorescence intensity observed at the detection chamber, and X represents the concentration of miR-21 in unit of pico-molar. A detection limit at 1.168 pM was obtained based on 3σ method. Furthermore, a good linear relationship was retained even in the low concentration range (<50 pM), as shown in Figure 2-4D. In addition, compared to the off-Chip assay, our on-chip platform provides >60-folds decreased limited-of-detection, which is due to the increased surface-to-volume ratio enabled by the microfluidic platform, as well as the enhanced mixing efficiency assisted by the oscillating-flow-control mode. These results demonstrated that our microfluidic platform greatly increased the sensitivity of the DSNSA miRNA assay.

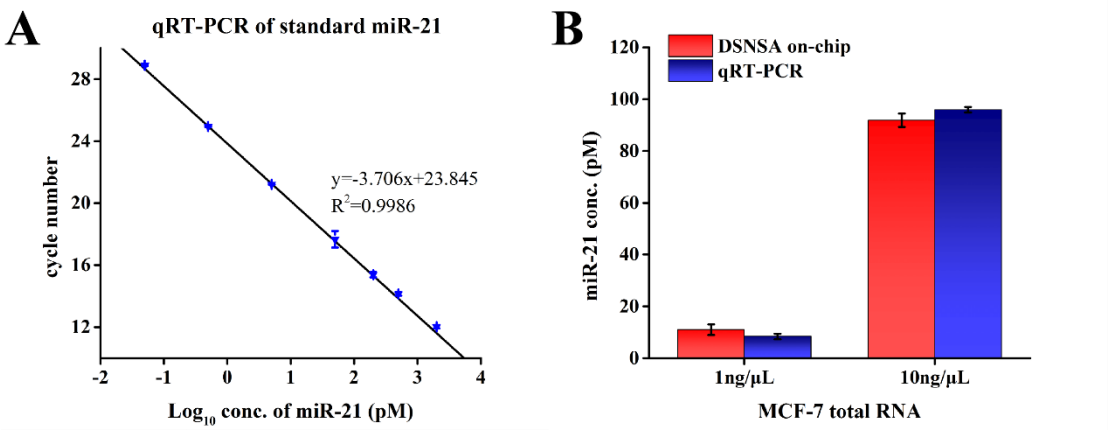

Figure 2-5. Detection of miR-21 in total RNA with the on-chip DSNSA mediated miRNA assay and commercial RT-qPCR. (A) Calibration curve of miR-21 by using RT-qPCR. (B) miR-21 measurement on total RNA extraction from MCF-7 cell line by using On-chip DSNSA and RT-qPCR. Error bars represent standard deviation (n=3).

Testing with biological samples

To investigate the applicability of our on-chip DSNSA method on real biological specimens, we measured the miR-21 in the total RNA extracted from a breast adenocarcinoma cell line MCF-7, and the commercial stem-loop RT-qPCR Taqman™ miRNA assay was employed as the validation. As shown in Figure 2-5A, a calibration curve of miR-21 standard was prepared with the commercial RT-qPCR method for the purpose of quantitative measuring of miR-21 in the total RNA sample. For the quantitation of miR-21 in the total RNA extracted from MCF-7 cell line, 1 mg/ml extracted total RNA was diluted to 10 ng/μL and 1 ng/μL and measured by our on-chip approach and the commercial RT-qPCR method. As shown in Figure 2-5B, the concentration of miR-21 in 10 ng/ml and 1 ng/ ml of the total RNA measured by our on-chip DSNSA approach was 91.9 ± 2.62 pM and 10.99 ± 2.04 pM, respectively. These results matched that from the commercial RT-qPCR method, which were 95.92 ± 1.06 pM and 8.4 ± 1.08 pM, respectively. This suggests that our method is capable to proceed biological samples with high accuracy and robustness. In addition, compared to the

standard RT-qPCR method, our on-chip method does not require a reverse transcription method and can process the sample within the chip with high automation. Such capability not only minimizes the human errors existing in the laboratory operation process, but also reduce the potential sample contamination and RNA degradation, thus holding great promise for its potential adaptability to a variety of applications, such as clinical diagnosis.

Conclusion

We have successfully developed a low-cost, sensitive, and easy-to-use on-chip DSNSA-mediated assay for miRNA detection. Our method integrated the sample enrichment and the DSNSA mediated miRNA assay in one streamlined analysis workflow and obtained a LOD at 1.168 pM (35.04 amol) of miR-21 and a dynamic range from 5 to 500 pM with excellent specificity and robustness. As a proof-of-concept, we used our method to quantitatively measure the miR-21 in the total RNA extracted from the MCF-7 cell line, and the result was verified with the commercial stem-loop RT-qPCR miRNA assay. Our on-chip approach greatly improved the competitivity of the DSNSA miRNA assay, and thus potentially can be utilized in numerous fields, such as clinical diagnosis and point-of-care testing.

Chapter 3. Quantitative measurement of exosomal mRNAs with a 3D-nanopatterned microfluidic chip coupled with droplet digital PCR

Introduction.

Rapid progress in early-stage diagnostics and precision therapy calls for new tools for the ultrasensitive detection of disease-specific biological particles in bodily fluids, such as circulating tumor cells (CTCs) and extracellular vesicles (EVs).[27, 154-156] Exosomes, a subtype of EVs secreted by mammalian cells with a typical size range of 30–150 nm, have been implicated in many biological processes, including immune response, tumorigenesis and metastasis.[157, 158] Thus, circulating exosomes are emerging as a new paradigm of "liquid biopsy" for non-invasive cancer diagnosis.[156, 159] However, tumor-associated exosomes in biofluids can be very rare during the early stages of disease development. Thus, it is imperative to develop new biosensing capabilities for the ultrasensitive and specific analysis of disease-associated exosome subtypes in the background of normal cell-derived vesicles. Current "gold standard" methods for exosome capture and characterization, such as ultracentrifugation (UC) and Western blot (WB), suffer from poor isolation efficiency, low sensitivity, time-consuming procedures, and large sample consumption. Microfluidics has been recently exploited to leverage exosome analysis; but the progress in improving sensitivity, speed, or multiplicity has been rather limited.[27, 160]

Biosensing largely relies on targets interacting with surface-immobilized probes for affinity capture. In such interfacial processes, mass transfer of targets to the surface

and the equilibrium and kinetics of binding reactions are the fundamental factors that govern sensing performance.[161] Microfluidics and nano-engineering approaches have been extensively explored to address these limitations. Many micromixing methods, including herringbone mixer, have been developed to promote microscale mass transfer.[162, 163] Two-dimensional (2D) nano-engineering[164] offers an effective means to enhance the interfacial binding of biomolecules,[165, 166] exosomes,[160] and cells.[167] In addition to the limits of mass transfer and binding reaction, it was recently reported that flow stagnation and hydrodynamic resistance due to the non-slip condition at the liquid-solid interface restrict the convection of slow-diffusing particles to the surface, which significantly reduces binding efficiency.[168-170] To address these boundary effects, a microfluidic chip integrated with 3D nanoporous microposts was developed by micropatterning carbon-nanotube (CNT) posts inside microchannels. Compared to solid microposts, the nanoporous CNT microposts permit the drainage of liquid through the nanopores, greatly reducing the near-surface flow stagnation and hydrodynamic resistance to enhance surface binding of particles of 40 nm to ~15 μm. [168-170] These studies present a creative strategy for microfluidic integration of 3D nanostructures to overcome the boundary effects; however, fabrication of 3D CNT patterns is highly sophisticated and time consuming.

As discussed above, previous approaches sought to individually or partially overcome the fundamental limits in mass transfer, surface reaction, and boundary effects, which presents a major conceptual constraint in leveraging the biosensing performance. Here we report an integrated, comprehensive strategy that addresses these three limits simultaneously in one device. Our approach, termed multiscale integration by designed self-assembly (MINDS), exploits microfluidically engineered colloidal self-assembly (CSA)[171] to achieve simple, large-scale integration of 3D nanostructured

functional microelements. We used the MINDS to combine micro-patterning and 3D nanostructuring of a widely used functional microelement, herringbone mixer for flow manipulation and molecular recognition. We showed that this 3D nanostructured herringbone (nano-HB) addresses the aforementioned limits in one device (Figure 3-1a) as it: 1) effectively promotes microscale mass transfer of bioparticles;[172, 173] 2) increases surface area and probe density to enhance binding efficiency and speed; and 3) permits drainage of the boundary layer of fluid through the pores of a nano-HB, which reduces near-surface hydrodynamic resistance[168, 169] and enriches particles near the surface to enhance surface binding of particles.

As a result, the nano-HB chip afforded an extremely low limit of detection of 10 exosomes μL^{-1} (200 exosomes per assay) for spiked-in standards and enabled quantitative detection of low-level exosome subpopulations in blood plasma that are otherwise indiscernible to the conventional flat-channel microfluidic chips. Coupling ddPCR method with our MINDS chip, we demonstrated quantitative detection of circulating exosomal CD24 mRNA, epithelial cell adhesion molecule (EpCAM) mRNA, and folate receptor alpha (FRα) mRNA to detect ovarian cancer using 100 μL of plasma, indicating the potential applications of our technology to liquid biopsy-based cancer diagnosis.

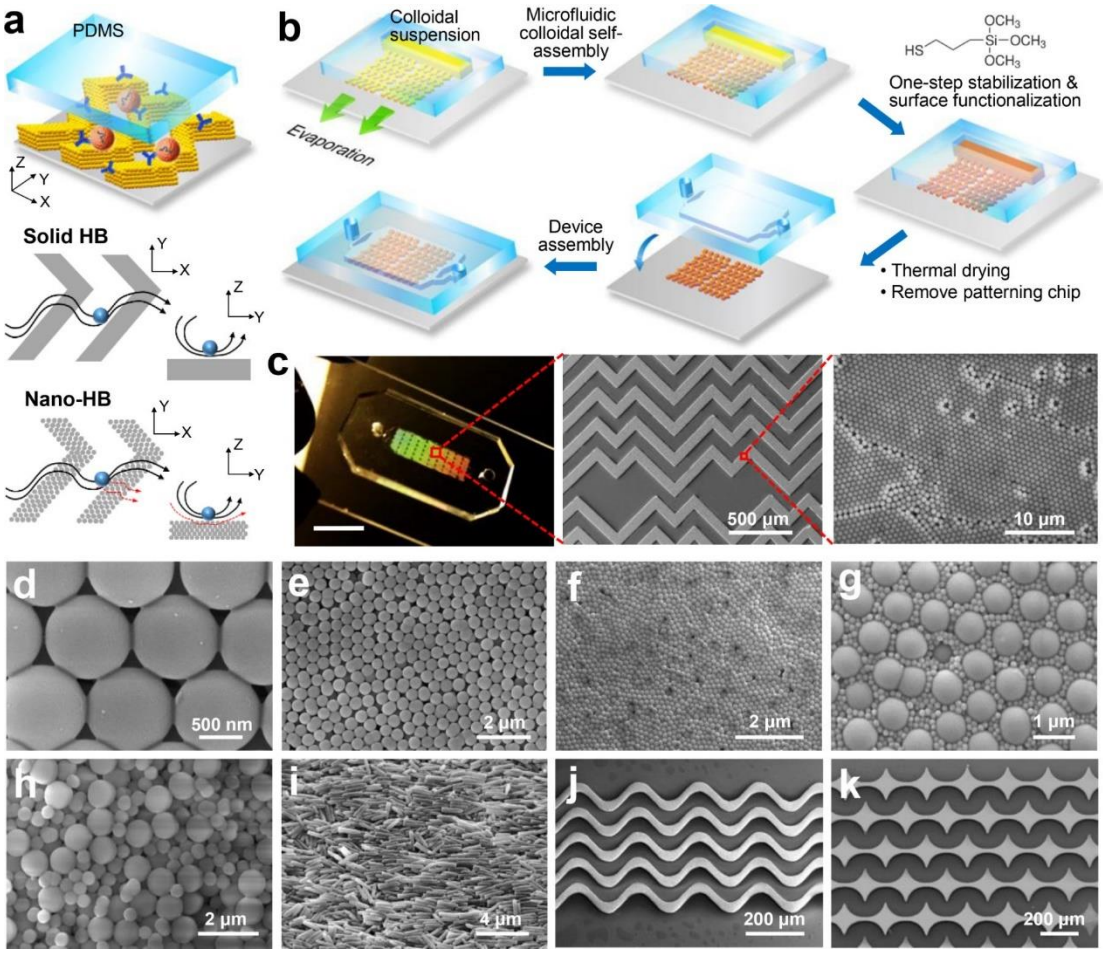

Figure 3-1. Multiscale Integration by Designed Self-assembly (MINDS). (a) Conceptual illustration of the MINDS strategy that improves biosensing by 3D nanostructuring of microfluidic elements, e.g., herringbone (HB) mixer. Conventional solid HB mixer creates microvortices to promote mass transfer of targets. A particle will experience hydrodynamic resistance near a solid surface that reduces direct surface contact. In a 3D nanoporous HB (nano-HB) chip, fluid near the surface can be drained through the porous structure (red dashed lines) to increase the probability of particle-surface collisions. (b) The workflow for fabricating a 3D nano-HB chip by MINDS. (c) A nano-HB chip fabricated with 960-nm silica colloids. The digital photo exhibits Bragg diffraction of light (scale bar, 5 mm). The SEM images show a high-quality, crack-free HB array patterned on a glass substrate with a crystalline nanoporous structure. (d) Silica necks were formed between the contacting particles by treatment with 5% 3-MPS. (e, f) SEM images of mono-assembled nano-HBs with silica colloids of 520 and 170 nm. (g) A well-ordered binary lattice composed of 170 and 960 nm silica colloids at equal mass ratio. (h) A randomly organized nano-HB co-assembled with 520 and 960 nm silica colloids at a 1:1 mass ratio. (i) An anisotropic microstructure assembled from silica nanorods with an averaged diameter of 238 ± 32 nm and length of 1.34 ± 0.26 μm. (j, k) Fabrication of crack-free, 3D nanostructured sinusoidal ribbon (j) and concave diamond arrays (k) using designed microfluidic channels to engineer evaporative self-assembly of 960 nm colloids.

Results

Designable 3D Nanostructuring of Functional Microelements by MINDS.

Fabrication of a MINDS-chip is illustrated Figure 3-1b and detailed in the Methods section. A nano-HB mixer was constructed by using a microchannel network to guide evaporation-driven CSA. A simple in situ treatment with (3-mercaptopropyl) trimethoxysilane (3-MPS) was developed to strengthen the assembled micropatterns and prime the surface for antibody conjugation in one step. After thermal drying and removing the patterning chip, the nano-herringbone pattern was aligned and sealed with an assay chip with ~50-μm high channels to construct a complete device. Figure 3-1c displays a nano-HB chip fabricated by MINDS using 960-nm silica colloids, which exhibited Bragg scattering of light by the embedded colloidal nanostructures. Scanning electron microscopy (SEM) imaging confirmed high-fidelity replication of the channel geometry by the engineered CSA and the 3D nanoporous crystalline structures (Figure 3-1c). The optimized 3-MPS treatment prevents the formation of cracks during thermal drying and minimizes the mechanical damages caused by removing the patterning chip, while preserving the nanoporosity. This is attributed to the formation of silica necks gluing the contacting nanoparticles (NPs) by hydrolysis and condensation reactions of 5% 3-MPS (Figure 3-1d). High concentrations of 3-MPS (e.g., 10%) can be used to completely fill the pores in nano-HBs (Figure 3-2), which allows us to fabricate solid-HB chips used in the following studies. Meanwhile, 3-MPS functionalizes the surfaces with sulfhydryl groups for antibody conjugation via maleimide reaction. Thus, this one-step treatment method greatly simplifies device fabrication.

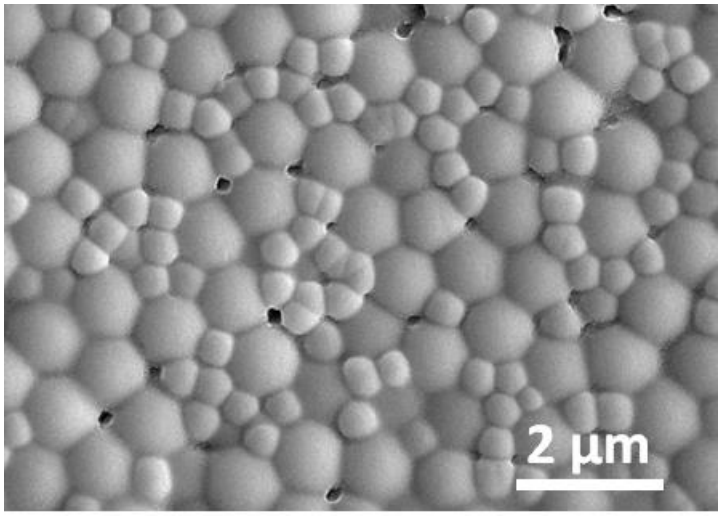

Figure 3-2. Fabrication of a solid-HB chip. A 520/960 nm binary colloidal structure was assembled and then treated by 10% 3-MPS to fill the interior pores, resulting in a solid-HB micropattern with the nano-textured surface.

The MINDS strategy allows us to conveniently engineer the morphology of 3D nano-HBs. We have demonstrated the nano-HBs fabricated with a variety of nanomaterials, including mono-assemblies of silica colloids of 960, 520 and 170 nm (Figure 3-1d-f), binary nanoparticle combinations (g, h), and silica nanorods (Figure 3-1i and Figure 3-9). Co-assembly of multi-component mixtures was tuned to create complex morphologies via controlling assembly variables, including particle size ratio and volume fraction.[174, 175] Co-assembly of 170 and 960 nm NPs of an equal volume fraction results in a unique morphology of hexagonally packed large particles surrounded by small particles (Figure 3-1g). In contrast, a 960/520 nm nano-HB was found to possess much higher structural disorder and porosity (Figure 3-1h). In addition to HB patterns, we have demonstrated high-fidelity patterning of complex microelements, such as a sinusoidal channel array previously reported for immunocapture of CTCs[176] (Figure 3-1j) and an array of concave diamonds (Figure 3-1k). These results suggest that utilizing the rich collection of nanomaterials and the flexibility of microfluidic design, the MINDS strategy affords broad applicability for

microscale integration of designable 3D nanostructures to develop new multiscale integrated biosensing systems.

Ultrasensitive Detection and Quantitative Protein Profiling of Exosomes.

Here we adopted a well-established HB design of 100 μm width and 225 μm pitch from the previous studies[177, 178] and investigated the nano-HBs of 15–35 μm height embedded in a 50 μm tall channel. The 25 μm height was found to provide the best flow mixing efficiency and signal/noise ratio for exosome detection (Figure 3-3).

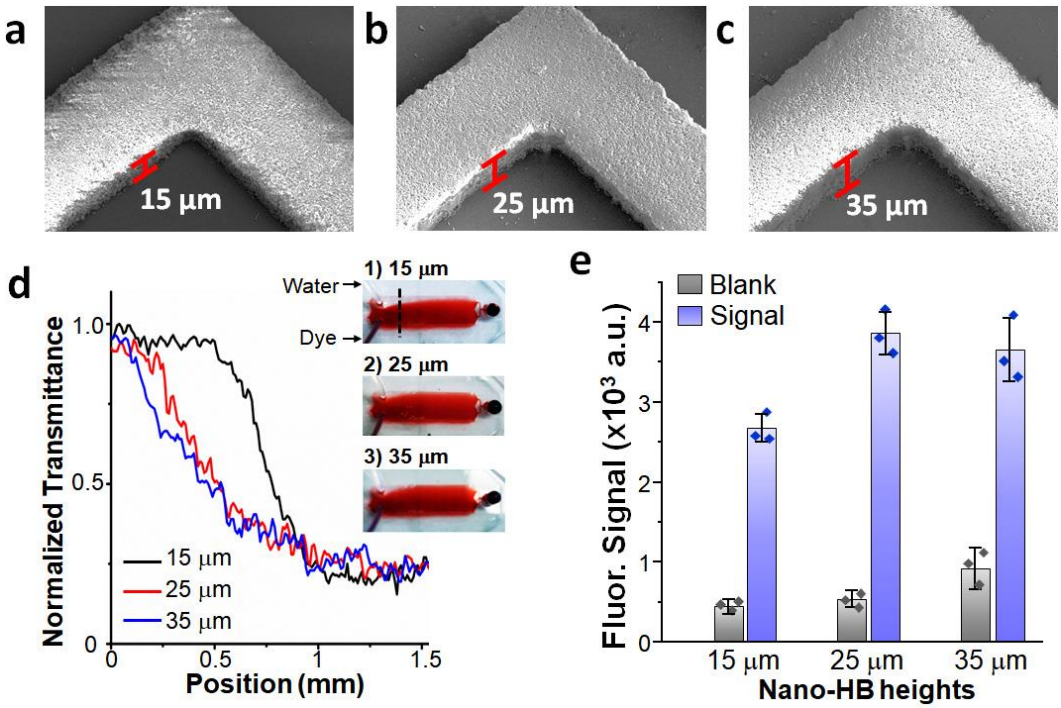

Figure 3-3. Optimization of the height of nano-HB for exosome detection. (a-c) SEM images of the nano-HBs with 15, 25 and 35 μm height, respectively. (d) Comparison of the flow mixing efficiency of the nano-HBs of variable heights. Nano-HBs were embedded within a 50-μm tall assay channel; water and dye solution were pumped through the channel in parallel at the same flow rate (1 μL/min). As shown by microscopic imaging (inset) and profiling the cross-sectional concentration gradient, the 25 and 30-μm tall nano-HBs provide better mixing efficiency than the 15-μm structure. (e) Comparative studies of nano-herringbones of variable heights for exosome detection. 105 μL-1 COLO-1 EVs were run through the chips for exosome capture by anti-CD81 mAb and detection by a mixture of mAbs against CD9, CD63 and EpCAM. The 25-μm tall nano-HB afforded the best signal/noise ratio for exosome detection. In all cases, the nano-HBs were fabricated using 960-nm silica particles. Error bars indicate one S.D. (n = 3).

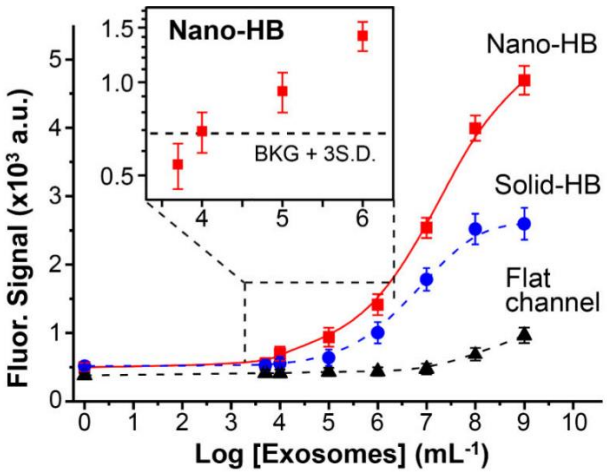

Figure 3-4. Calibration curves for quantifying total exosomes by the flat-channel, solid-HB, and nano-HB chips. Serial 10× diluted COLO-1 exosome standards were used with a mixture of anti-CD9, CD63, and EpCAM mAbs for detection.

With the optimized chip design and assay conditions, we calibrated and compared the nano-HB chips to the flat-channel and solid-HB devices for quantitative exosome detection (Figure 3-4). A mixture of anti-CD9, CD63, and EpCAM mAbs was used to quantify the overall exosomes captured on chip (Table 3-2). The flat-channel chip yielded a theoretical limit of detection (LOD) of 5.0×10^4 EVs μL^{-1}, calculated from the mean blank signal plus three standard deviations (n = 3). The solid-HB chip afforded a much lower LOD of 3.2×10^2 μL^{-1}, as a result of its substantially better mixing efficiency and larger surface area. 3D nano-HB chips further reduced the LOD to 10 μL^{-1} (i.e., 200 vesicles in a 20 µL sample, Figure 3-4 inset), and expanded the dynamic range over four orders of magnitude. Considering the solid-HB also has nanostructured exterior surface (Figure 3-2), this direct comparison with the solid-HB assay supports that the enhancement in sensitivity arises from small boundary flow drainage through the nano-HBs that increases vesicle-surface interactions and the accessible binding surface area, while preserving the HB's ability to enhance flow

mixing in microchannels. Our data suggest that our nano-HB chip offers better exosome detection sensitivity than the existing methods,[27, 160] including a nano-plasmonic sensor that requires at least 3,000 exosomes per assay.[156]

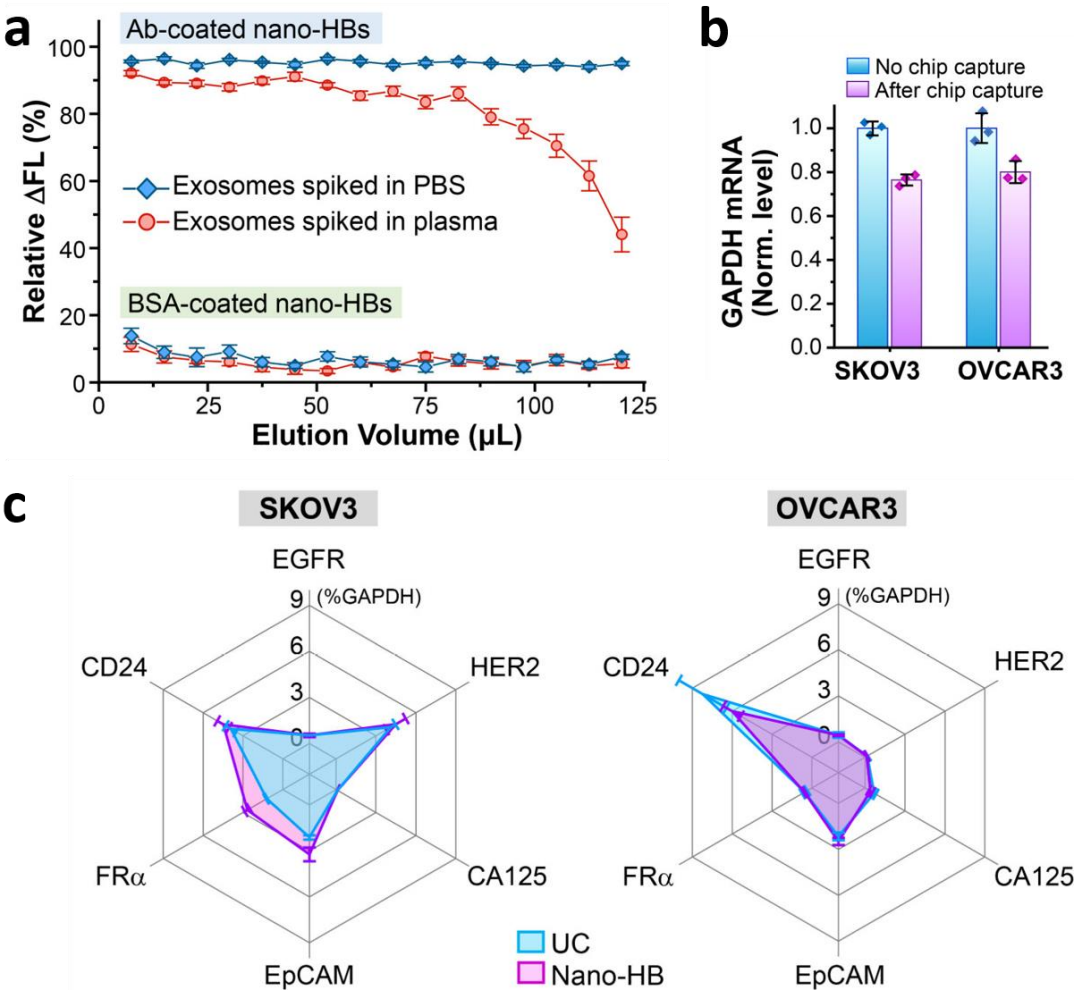

Figure 3-5. 3D engineered Nano-HB chip affords efficient immunocapture of exosomes. (a) Immunological and non-specific capture of COLO-1 exosomes as a function of injected sample volume assessed using an mAb or BSA-coated nano-HB chip, respectively. DiO dye-stained exosomes were spiked in PBS or 10× diluted human plasma (106 μL−1) and injected continuously through the chips at 0.5 μL/min. 2 μL eluent was collected at the outlet every 15 min and measured by a micro-volume plate reader to determine the reduction in fluorescence signal with respect to that of the original sample. (b) Capture efficiency of nano-HB chip measured by the GAPDH mRNA level. EVs isolated and concentrated from SKOV3 and OVCAR3 cell culture media by UC were spiked in PBS (106 μL−1) and 100 μL of the solution was run on the chip. Captured exosomes were eluted out for droplet digital PCR (ddPCR) quantification. The GAPDH mRNA levels in chip-captured exosomes were normalized by that in the same amount of EVs measured without chip capture. (c) Profiles of six mRNA markers measured in the chip-captured SKOV3 and OVCAR3 exosomes in comparison with the vesicles isolated and concentrated by UC. Exosome capture and elution on the nano-HB chip was performed as in (b) and the levels of individual mRNAs measured by ddPCR were normalized against GAPDH. Anti-CD81 mAb was used for exosome capture in all cases. Error bars, one S.D. (n = 3).

Evaluation of Exosome Immunocapture on Nano-HB Chip.

We evaluated the capture capacity and efficiency of nano-HB chips by monitoring the amount of exosomes depleted from the sample solution flowing through the nano-HB chip.[179] To this end, DiO dye-stained COLO-1 EVs were spiked in either PBS or 10-fold diluted patient plasma at 10^6 μL^{-1} and injected continuously into the BSA- or CD81 mAb-coated chips at 0.5 µL/min. 2 µL of eluent was sampled at the outlet every 15 min and measured with a micro-volume plate reader to determine the decrease of fluorescence intensity (ΔFL) caused by exosome depletion relative to the signal level of the sample before capture (Figure 3-5). A very small ΔFL was observed on the BSA-coated chips (5.5 ± 0.98% of original sample for PBS and 5.3 ± 1.1% for plasma media), indicating minimal matrix effects on the nano-HB chip. Exosome capture on the Ab-modified chips constantly resulted in a high ΔFL (95 ± 2%) for spiked PBS over 250 min injection, i.e., an accumulated sample volume of 125 µL. The plasma was estimated to contain $>10^{10}$ EVs per mL by UC and NTA. These unlabeled vesicles and other particulate species in plasma compete for the flow access into nano-HBs and/or the surface binding sites. Despite the vast background, a consistent ΔFL of 86% to 92% was observed for capturing exosomes spiked in diluted plasma over up to 82 µL volume loaded, which remained at 75% at 100 µL. Thus, the current nano-HB chip affords sufficient capacity for sensitive and quantitative analysis of up to 10 µL undiluted plasma. If needed, the capture capacity can be readily expanded by scaling up the chip size or the number of channels.

The capture performance of nano-HB chip was further evaluated for downstream analysis of mRNA contents of exosomes using the commercial droplet digital PCR (ddPCR) technique. Here we were focused on two ovarian cancer (OvCa) cell lines, SKOV3 and OVCAR3, which are commonly used in vitro cell culture models

representative of high-grade serous OvCa, the most aggressive subtype that accounts for nearly two-thirds of all OvCa-related deaths.[180] Designed for non-invasive cancer diagnosis using small sample volumes (<100 μL, Figure 3-5a), our microfluidic device has limited preparative sample processing capacity for bulk mRNA analysis; thus we used EVs isolated and concentrated by UC for on-chip immunocapture to yield sufficient exosomes for off-chip RNA extraction, cDNA synthesis, and ddPCR, following the established protocols.[34, 156] To assess the capture efficiency, 100 μL UC-concentrated SKOV3 and OVCAR3 EVs (10^6 μL^{-1}) were run on the chips and the captured exosomes were eluted out for ddPCR quantification of GAPDH mRNAs (Figure 3-5b). The GAPDH mRNA levels in chip-captured exosomes were measured to be 76.5 ± 2.6% for SKOV3 and 80.1 ± 5.0% for OVCAR3 relative to the initial samples. To assess the nano-HB chip for exosomal mRNA profiling in comparison to UC isolation, we detected six tumor-associated markers that have been identified in OvCa-derived exosomes,[156] human epidermal growth factor receptor 2 (HER2), epidermal growth factor receptor (EGFR), FRα, CA-125, EpCAM, and CD24. The combined assay of on-chip purification and ddPCR analysis reported an mRNA pattern consistent to that of the UC-purified SKOV3 and OVCAR3 EVs, respectively (Figure 3-5c and Figure 3-6). These results further demonstrated the validity of the nano-HB chip for exosome immunocapture. High capture efficiency of the nano-HB chip compares favorably with the recently reported methods,[179, 181, 182] which permits sensitive exosome detection.

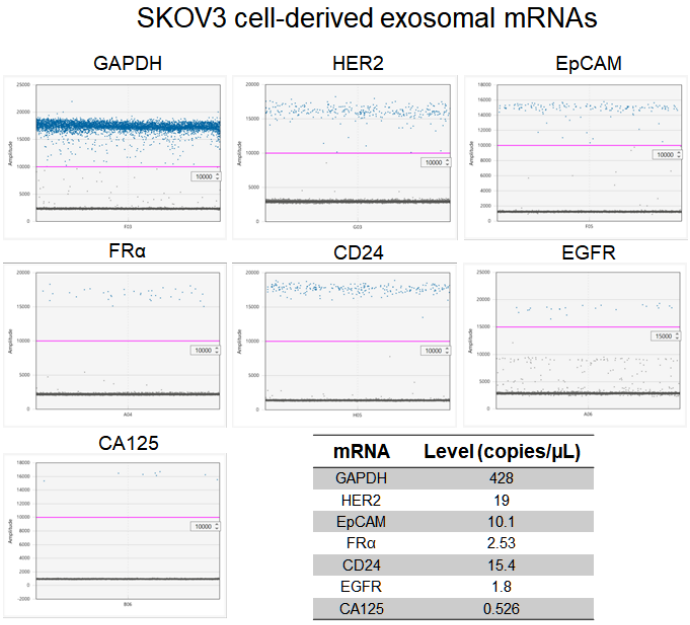

mRNA	Level (copies/μL)
GAPDH	428
HER2	19
EpCAM	10.1
FRα	2.53
CD24	15.4
EGFR	1.8
CA125	0.526

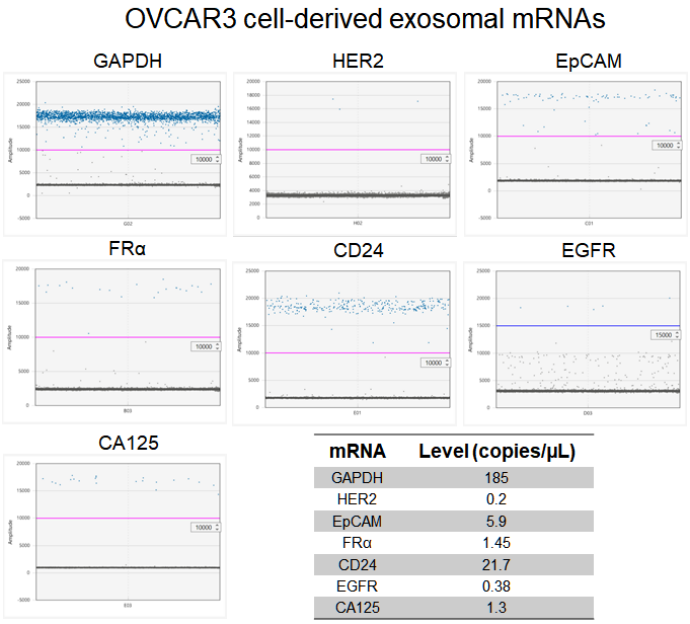

mRNA	Level (copies/μL)
GAPDH	185
HER2	0.2
EpCAM	5.9
FRα	1.45
CD24	21.7
EGFR	0.38
CA125	1.3

Figure 3-6. Representative results from droplet digital PCR (ddPCR) experiments for mRNA profiling of EVs isolated from two OvCa cell lines by UC.

Clinical Analysis of Circulating Exosomes for Cancer Diagnosis.

As a proof-of-concept, we adapted the nano-HB system to assess circulating exosomes as a non-invasive tool for diagnosis of OvCa. We examined plasma samples collected from OvCa patients (n = 10) and age-matched non-cancer controls (n = 5) (Table 3-1) by the combined assay of nano-HB capture and ddPCR. Our exosomes

profiling results show the universal presence of CD24 mRNA, EpCAM mRNA and FRα mRNA in exosomes from the OvCa cell lines and patient plasma (Figure 3-7 and Figure 3-8), revealed the advantages of our technology for highly sensitive and specific analysis of tumor-derived circulating exosomes with minimal sample consumption, which are particularly compelling for the development of non-invasive tools for preclinical screening and early-stage diagnosis of cancer.

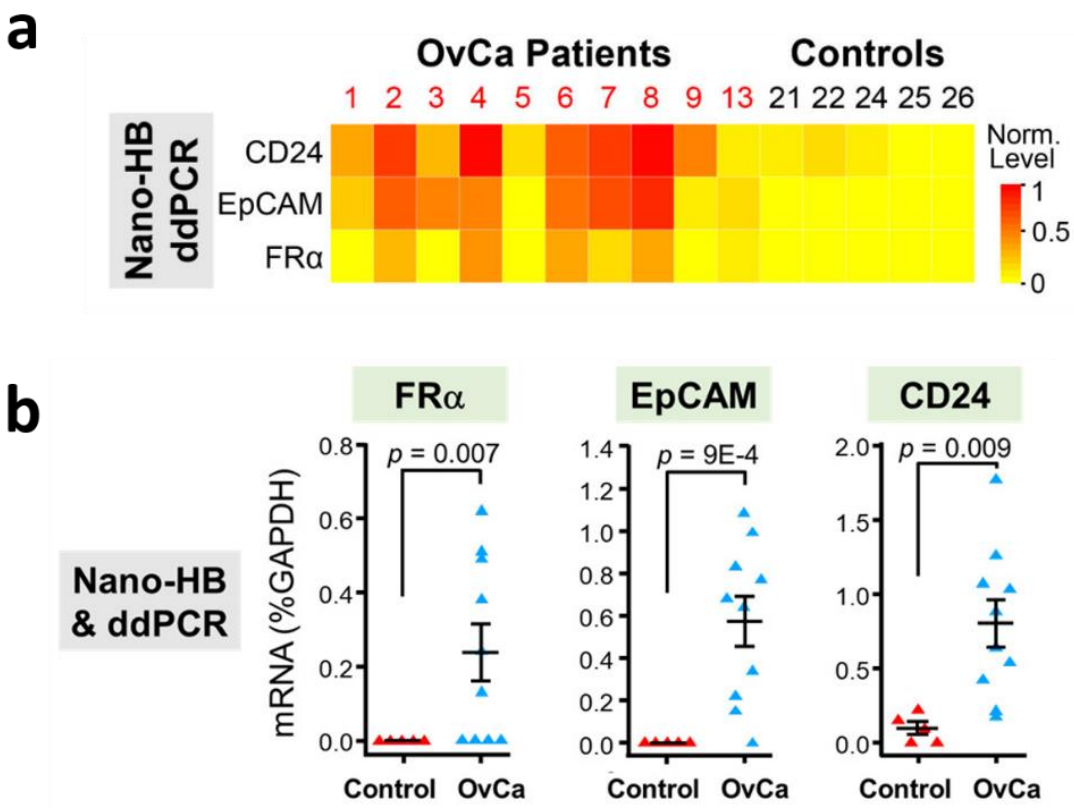

Figure 3-7. Clinical sample analysis. (a) Exosomal marker patterns measured with the combined nano-HB capture and ddPCR of mRNAs. Plasma samples collected from OvCa patients (n = 10) and age-matched non-cancer controls (n = 5) was assayed in triplicate. For mRNA analysis, 100 µl plasma from each patient was diluted tenfold and run through 2 8-channel nano-HB chips to ensure fast and efficient exosome capture. (b) Diagnostic performance of exosome analysis using the nano-HB ELISA chip coupled with ddPCR.

Patient #4

mRNA	Level (copies/μL)
GAPDH	82.1
CD24	1.02
EpCAM	0.696
FRα	0.523

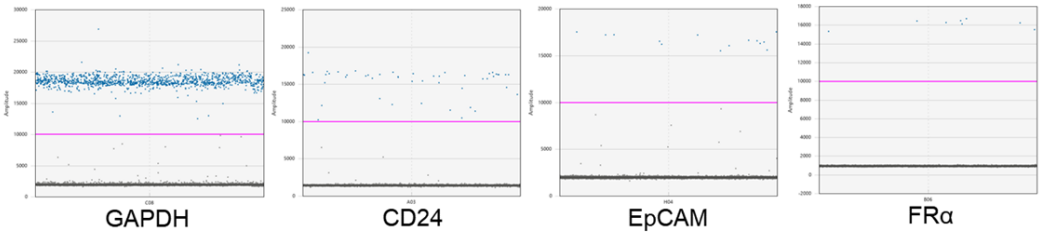

Patient #8

mRNA	Level (copies/μL)
GAPDH	87.9
CD24	1.53
EpCAM	1.08
FRα	0.379

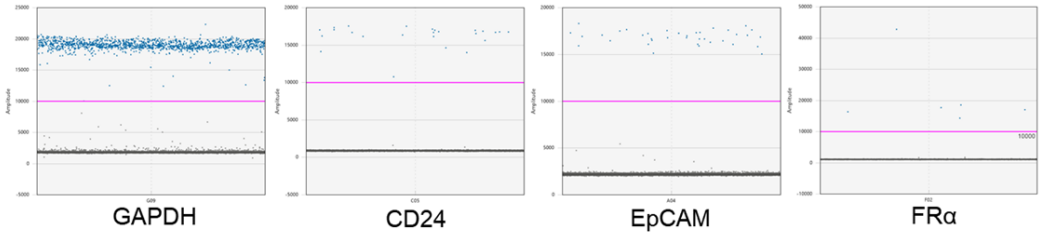

Control #21

mRNA	Level (copies/μL)
GAPDH	55.9
CD24	0.124
EpCAM	0
FRα	0

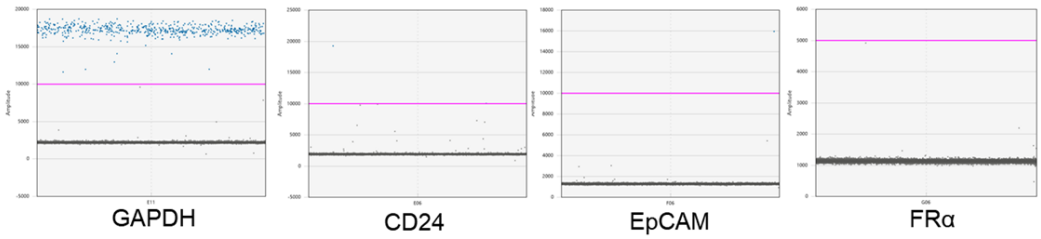

Figure 3-8. Representative results for nano-HB chip based ddPCR analysis of exosome mRNA markers in clinical plasma samples. 100 μL plasma samples were diluted by 10 times and run through two 8-channel nano-HB chips in parallel to capture exosomes in 2 h. Anti-CD81 mAb was used for exosome capture. Captured exosomes were eluted out and total RNA was extracted for ddPCR detection of individual targets following the standard protocols.

Table 3-1. Plasma samples

Samples for Exosome Profiling					
OvCa patients	**Age**	**Stage**	**Histology**	**Pathology**	**Tissue**
1	72	IIIC	High grade serous adenocarcinoma	Malignant	
2	67	IIA	High grade papillary serous carcinoma	Malignant	
3	70	IIIC	High grade serous carcinoma	Malignant	
4	80	IIIC	Metastatic high grade papillary serous carcinoma	Malignant	
5	66	IV	Metastatic high grade serous carcinoma	Malignant	
6	65	IIIB	High grade serous carcinoma	Malignant	
7	66	IIIC	High grade serous carcinoma	Malignant	
8	64	IIIC	High-grade serous adenocarcinoma	Malignant	Tested
9	61	IIIC	Metastatic high grade papillary serous carcinoma	Malignant	
10	53	IIIC	High grade papillary serous adenocarcinoma	Malignant	
11	74	IIA	High grade serous carcinoma	Malignant	Tested
12	55	IIIA	Metastatic ovarian carcinoma	Malignant	
13	75	IIIC	Mixed epithelial carcinoma: serous and endometrioid (50%)	Malignant	Tested
14	53	IIIC	High grade serous carcinoma	Malignant	
15	65	IIA	Mucinous adenocarcinoma	Malignant	
16	65	IIIC	High grade serous carcinoma	Malignant	
17	58	IA	Mucinous cystadenocarcinoma	Malignant	
18	58	IIIC	High grade serous carcinoma	Malignant	
19	51	IIA	Low grade serous carcinoma	Malignant	
20	63	IIA	Serous adenocarcinoma	Malignant	
Non-cancer control	**Age**	**Stage**	**Histology**	**Pathology**	**Tissue**
21	51	n/a	No history of cancer	Control	
22	53	n/a	No history of cancer	Control	
23	50	n/a	No history of cancer	Control	
24	52	n/a	No history of cancer	Control	
25	53	n/a	No history of cancer	Control	
26	52	n/a	No history of cancer	Control	
27	54	n/a	No history of cancer	Control	
28	56	n/a	Benign inclusion cysts	Benign	
29	67	n/a	Mucinous cystadenoma	Benign	
30	58	n/a	Serous cystadenoma	Benign	

Discussion

Microfluidic integration of nanostructures attracts enormous interests as it combines the advantageous micro- and nano-scale phenomena to immensely improve biosensing44, 45.[183, 184] However, device-scale microfluidic integration of 3D complex nanostructures has been a long-standing challenge. Standard nanofabrication techniques have been mainly used for small-scale 2D nano-patterning on planar surfaces. Existing 3D micro/nanofabrication techniques, such as proximity field nanopatterning,[185] multi-beam holographic lithography,[186] and femtosecond laser printing,[187] require expensive, sophisticated facilities and labor-intensive, time-consuming fabrication procedures, which severely limits their scalability and practicality for routine applications. Nano-engineering of microfluidic sensing devices mostly involves surface modification of microfabricated elements with nanomaterials, yielding essentially 2D nanostructured sensing surfaces.[164, 179, 184, 188] Alternatively, CSA enables simple, cost-effective fabrication of 3D nanomaterials with complex morphologies and have received extensive applications to material synthesis and photonics.[183, 189] However, its bioanalytical applications remain largely underexplored. The MINDS strategy presents an enabling approach for developing new microfluidic nanosensing technologies. Compared to standard nanolithography, this bottom-up method affords several advantages: 1) simple and programmable 3D assembly of complex nanostructures; 2) inherent compatibility with standard soft lithography for designed assembly and integration of device-scale nanostructures; and 3) broad applicability for nanobiosensing because it combines flexible and scalable microfluidic engineering with a wide spectrum of available nanomaterials.[183]

Probing circulating exosomes has attracted rapidly increasing interests in clinical care, especially for non-invasive diagnosis and monitoring of patient response

to treatment. Efficient isolation and specific measurement of disease-associated exosomes, often present in low concentrations in biofluids, remains challenging for conventional technologies. While microfluidics provides a uniquely suitable technology to surmount these challenges, existing microfluidic technologies have yielded limited improvement in exosome analysis3, 8.[27, 160] In contrast to these techniques, the MINDS approach provides a simple yet powerful multi-scale engineering strategy to simultaneously address the fundamental limits in mass transfer, reaction characteristics, and boundary effects. It was shown that 3D nano-engineering of a herringbone mixer by the MINDS approach preserves the HB's performance in enhancing mass transfer, reduces the boundary flow resistance to promote surface-exosome interactions, and immensely increases the surface area for binding. These distinct advantages result in an ultrasensitive system that permits rapid and specific immunosensing of tumor-related exosomes, e.g., FRα+ exosomes, which present at an undetectable concentration in biological samples for conventional methods. We showed that our technology can be adapted to exosome profiling in various cancer types, providing an enabling tool to facilitate the studies of biological functions and clinical relevance of exosomes.

Overall, our proof-of-concept clinical analyses should validate the ability of our technology for not only sensitive quantification of total circulating exosomes but also for exosome profiling to identify potential disease fingerprints for non-invasive OvCa diagnosis and stratification. In principle, our nano-HB chip is applicable to a broad spectrum of targets of biomedical significance, including circulating tumor cells.[172, 173, 178] Therefore, our method provides a useful tool to facilitate the development of new biosensing technologies and clinical biomarkers.

Methods

Reagents and Materials

Monodispersed silica colloids were ordered from Bangs Laboratories Inc. (3-Mercaptopropyl) trimethoxysilane (3-MPS), 4-Maleimidobutyric acid N-hydroxysuccinimide ester (GMBS), polyvinylpyrrolidone (PVP, MW~40,000), anhydrous ethanol, 1-pentanol (≥99%), and sodium citrate dihydrate (99%) were purchased from Sigma-Aldrich. Ammonia (28%) and tetra-ethyl orthosilicate (TEOS, 98%) were obtained from Fisher Scientific. The ELISA kits for EpCAM, CD24 and FRα were ordered from R&D Systems. Streptavidin conjugated β-Galactosidase (SβG), fluorescein-di-β-D-galactopyranoside (FDG), 3,3'-dioctadecyloxacarbocyanine perchlorate (DiO) lipophilic dye, Vybrant™ CM-DiO cell staining solution, and fluorescent nanoparticles (5% solid, Ex/Em 540/560 nm, actual size 46 nm) were purchased from Life Technologies. The detailed information of antibodies used in our studies was listed in Table 3-2 below. 1× phosphate-buffered saline solution (PBS) and SuperBlock buffer were from Mediatech, Inc and ThermoFisher Scientific, respectively. All other solutions were prepared with deionized water (18.2 MV-cm, Thermo Scientific). SβG and FDG were dissolved in PBS working solution (PBSW) at pH 7.4 which contain 0.5 mM DL-dithiothreitol (Sigma-Aldrich), 2 mM $MgCl_2$ (Fluka Analytical), and 5% bovine serum albumin (BSA, Sigma-Aldrich).

Table 3-2. The antibodies and ELISA kits used in this project.

Target	Vendor	Catalog No.	Clone
CD9 (biotin)	Ancell	156-030/mono mouse	C3-3A2
CD63 (biotin)	Biolegend	353018/mono mouse	H5C6
CD81 (biotin)	Ancell	302-030/mono mouse	1.3.3.22
CD81	Ancell	302-820/mono mouse	1.3.3.22
EpCAM (biotin)	Abcam	ab187270/mono mouse	MOC-31
EpCAM	Biolegend	324202/mono mouse	9C4
EpCAM ELISA kit	R&D Systems	DY960	
CD24 (biotin)	eBioscience	13-0247-80/mono mouse	SN3 A5-2H10
CD24	R&D Systems	AF5247	poly
FRα (biotin)	R&D Systems	BAF5646/poly goat	poly
FRα ELISA kit	R&D Systems	DY5646	
CA125 (biotin)	GeneTex	GTX44293/mono mouse	X306
CA125	Abcam	ab1107/mono mouse	X75
HER-2 (biotin)	eBioscience	BMS120BT/mono mouse	2G11
HER-2	eBioscience	BMS120/mono mouse	2G11
EGFR (biotin)	Abcam	ab24293/mono mouse	EGFR1
EGFR	BD Bioscience	555996/mono mouse	EGFR1
IgG (FITC)	Life Technologies	34-152-110413/ poly goat	poly

Microfabrication of PDMS Chips

The MINDS approach uses a patterning chip for microfluidic colloidal self-assembly and an assay chip for exosome analysis, both made of PDMS (Figure 3-1b). The PDMS chips were fabricated using standard photolithography, as detailed previously.[160] All silicon molds were patterned using SU-8 photoresist (MicroChem) following the procedures recommended by the manufacturer. For the patterning chips, we used SU-8 2010 to pattern the herringbone channel arrays with the heights of 15 μm, 25 μm and 35 μm by controlling the spin-coating speed. For the assay chips, SU-8 2050 was employed to pattern the flow channels of 50 μm in height. The prepared silicon molds were pre-treated by trichloro(1H, 1H, 2H, 2H-perfluorooctyl) silane under vacuum for 4 h. 33 g PDMS mixture at a 10 (base material): 1 (curing agent) ratio was

poured on the mold and cured in the oven at 70 °C for 4 h. PDMS slabs were peeled off from the molds and the access holes were punched.

Fabrication of Nano-Herringbone-Integrated Chips by MINDS

The process of MINDS based on microfluidically guided colloidal self-assembly is schematically illustrated in Figure 3-1b. Briefly, a PDMS patterning chip containing the herringbone channel array was sealed to clean glass slides without surface treatment. After 10 min sonication, 10 μL 10% w/v aqueous suspensions of monodisperse silica colloids was injected into the large solution reservoir shared by all channels. For co-assembly of colloids with different sizes, the total particle concentration of the mixed suspension was kept to be 10% w/v. The colloidal solution spontaneously filled the microchannels and stopped at individual channel outlets, due to the surface tension. The solution reservoir was sealed with a small piece of PDMS such that solvent evaporation from the open reservoir induced colloidal self-assembly to fully pack the microchannels. Colloidal suspension in the reservoir was then replaced by 5% 3-MPS to strengthen the mechanical stability of the assembled colloidal structures. The packed device was then completely dried at 80 °C for 1 h on a hotplate. After carefully peeling off the patterning chip, the self-assembled herringbone structure was aligned and sealed with a UV-Ozone-treated PDMS assay layer under a stereoscope. The assay channel is 10 mm long, 2 mm wide, and 50 μm tall, containing ten units of five herringbones.

Synthesis of Colloidal Silica Nanorods

Monodisperse silica nanorods with controlled aspect ratio were synthesized

following a published wet-chemical method[190] with minor modifications. Briefly, a solution was prepared by completely dissolving 30 g PVP in 300 mL 1-pentanol. 30 ml anhydrous ethanol, 8.4 ml ultrapure water, 2 ml of 0.18 M aqueous solution of sodium citrate dihydrate, 6.75 ml of fresh ammonia and 3 ml of TEOS were sequentially added into the PVP solution with hand shaking. The well-mixed solution was left in the fumehood without stirring to let the reaction proceed at the room temperature for ~4 h. The reaction mixture was then transferred into 50-mL centrifuge tubes. Monodisperse silica nanorods were purified by sequential centrifugation and washing: centrifuge at 2000× g for 1 h and re-disperse the sediment in ethanol; repeat the procedure at 1500× g for 15 min with ethanol (3 times) and water (3 times); and finally four times at 700× g for 15 min and disperse the purified nanorods in ~40 mL water. Using transmission electron microscopy (TEM), the dimensions of nanorods were determined to have an average diameter of 238 ± 32 nm and length of 1.34 ± 0.26 μm (Figure 3-9).

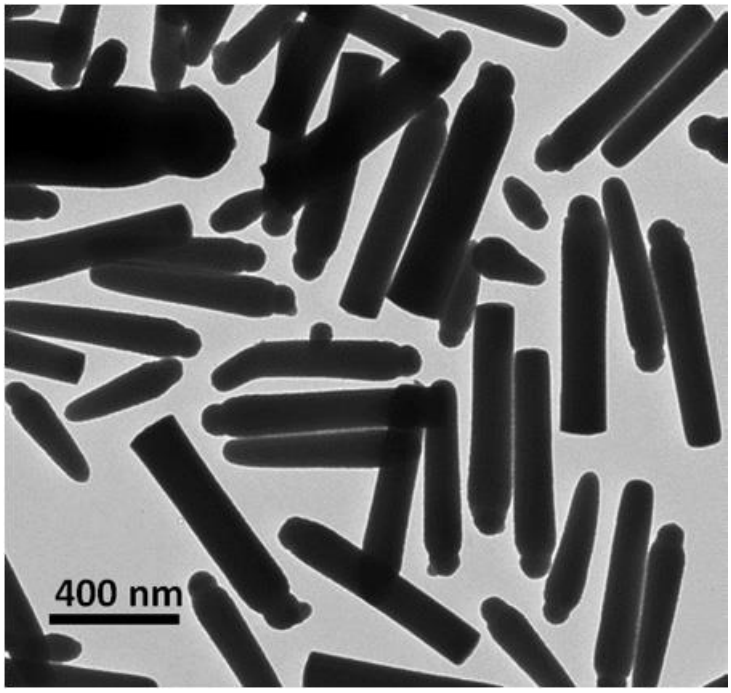

Figure 3-9. TEM image of synthesized monodisperse silica nanorods. The average diameter and length were determined to be 238 ± 32 nm and 1.34 ± 0.26 μm, respectively.

Cells and Culture Conditions

The human ovarian cancer cell lines SKOV3 and OVCAR3 were cultured in RPMI-1640 media with 10% (v/v) vesicle-depleted FBS, recombinant insulin (7.5 µg/mL), penicillin (100 U/mL), and streptomycin (100 µg/mL) at 37 °C in a humidified atmosphere with 5% CO_2. Vesicle-depleted FBS was prepared by centrifuging FBS for 18 h at 100,000× g and then passing the supernatant through a 0.22 µm filter. Cell lines were maintained between 40–80% confluency during which time the conditioned media was collected and replaced every 24 h. The collected media was immediately centrifuged at 2,000× g for 10 min to remove large cell debris and then stored at 4 °C until sufficient volume was pooled for exosome isolation.

Extracellular Vesicle (EV) Isolation

EVs were isolated by differential ultracentrifugation (UC) of approximately 300 mL of conditioned media for each cell line collected over a 1–2 week period. Pooled conditioned media was spun for 45 min at 10,000× g to pellet large vesicles. The supernatant was then spun at 100,000× g for 1 h to pellet EVs. The supernatant was carefully decanted to avoid disturbing the EV pellet until ~2 mL remained. The 2-mL samples from multiple tubes were pooled together into a 13.5 mL polypropylene Quick-Seal® centrifuge tube (Beckman Coulter) and then spun at 100,000× g for 1 h to pellet the washed EVs. The supernatant was quickly and carefully removed and the EV pellet was re-suspended in 100–200 µL of cold 0.22 µm-filtered PBS and stored in low-retention tubes at −80 °C. Isolated EVs were characterized with NTA using NanoSight LM10 to determine the size and concentrations. Protein concentration was measured using Bradford protein assay (Bio-Rad).

mRNA Analysis of OvCa Cell-Derived EVs

NTA counting reported a typical EV concentration of 10^7-10^8 mL^{-1} in SKOV3 and OVCAR3 cell culture media, which is ~10^2 to 10^4 fold lower than in human plasma. Because of the low concentration of EVs, hundreds of milliliters of the culture media were processed by UC to obtain sufficient amount of vesicles for droplet digital PCR (ddPCR) analysis of six mRNA markers. For bulk analysis of UC-purified OvCa EVs, total RNA was extracted from 40–60 μg EVs by RNAqueous™-Micro Total RNA Isolation Kit (Ambion) and then was reverse transcribed to cDNA using High-Capacity cDNA Reverse Transcription Kit (Applied Biosystems), per the manufacturer's protocol, respectively. PCR mix was prepared by mixing 1 μL of the obtained cDNA and the commercial pre-designed primer sets for each mRNA targets (PrimeTime® qPCR Assays, Integrated DNA Technologies) with QX200™ ddPCR™ EvaGreen® Supermix (Bio-Rad), following the manufacturer's recommendations. ddPCR was performed using the QX200™ Droplet Digital™ PCR System (Bio-Rad). The PCR protocol was: 5 min at 95 °C; 30 s at 95 °C, 1 min at 55 °C for 40 cycles; 5 min at 4 °C, 5 min at 90 °C. Background signal was determined for each assay and subtracted in data analysis to eliminate non-specific amplification. Measurement of each mRNA target was repeated at least three times with different batches of purified EVs. The concentrations of target mRNAs were normalized against GAPDH.

The nano-HB chip is designed for diagnostic exosome analysis using non-invasive sample volumes, which can run 20 −100 μL sample with a reasonable processing time (40–200 min). Chip isolation of exosomes from such small volume of cell culture medium was found not to yield sufficient amount of exosomes to detect the low-frequency mRNA targets by ddPCR. Based on the bulk mRNA analysis of UC-

isolated EVs, it was estimated that at least 10 mL culture media is needed for the nano-HB chip isolation and subsequent ddPCR analysis of the mRNA targets, which is beyond the sample processing capacity of the chip. Therefore, we used the UC-concentrated SKOV3 and OVCAR3 EVs to characterize the nano-HB capture for mRNA profiling of exosomes. To this end, 100 μL of the concentrated EVs (106 μL−1) was run on the chip modified with anti-CD81 capture antibody with protein G as the linker1. Captured exosomes were eluted out by flowing 20 μL Pierce™ IgG elution buffer (ThermoFisher) through the chip, which will dissociate capture antibodies from Protein G. We lysed the eluted exosomes, extracted total RNA, and performed ddPCR analysis of mRNA targets, as described above. Profiles of six mRNA markers measured in the chip-purified exosomes were compared with that of bulk analysis of UC-purified EVs.

Clinical Exosome mRNA Analysis

For mRNA analysis of exosomes in patient plasma, we have expanded the nano-HB chip to an 8-channel device to enhance the capacity and throughput for exosome capture. 100 μL plasma from each patient was diluted by 10 times and run through two 8-channel chips in 2 h to capture sufficient exosomes for subsequent ddPCR assays. Elution of the captured exosomes by 20 μL Pierce™ IgG elution buffer, exosome lysis, total RNA extraction, cDNA synthesis, and ddPCR assays were performed as described above.

Chapter 4. A microfluidic alternating-pull–push active digitization method for sample-loss-free digital PCR

Introduction

Digital polymerase chain reaction (dPCR) is an absolute quantitative method in which the bulk volume of a reaction mix is divided into 10^3-10^6 discrete compartments of nL-pL volumes, and massively parallel PCR assays are performed at the single-molecule level to quantify the targets using binomial Poisson statistics. Comparing with the conventional real-time PCR, dPCR is more reliable to detect trace amount of target gene and does not require a calibration curve. Because of its high sensitivity and robustness, dPCR has been widely applied in numbers of fields, including, single cell analysis,[107] detection of mutations,[191-197] copy number variations analysis,[198-200] detection of bacterium and viruses,[201-205] and detection of genetically modified organism.[206-208]

Sample digitization is a critical step in dPCR to ensure accurate quantification of the targets. Many applications involve the processing and measurement of very limited quantities of samples, such as single cells or extracellular vesicles enriched from biospecimen. Thus it is imperative to establish the ability to digitize minuscule liquid volume in order to implement dPCR in these applications. Current digitization methods, including water-in-oil emulsion,[74, 209-215] microwells,[216-218] and micro-valve based methods,[219, 220] have been well established mostly for the routine bulk bioassays. For instance, in the water-in-oil emulsion methods, a fraction of solution will be consumed to establish stable droplet formation and any droplets outside the size range will be filtered out for the size consistency of droplets.[221-223] For commonly used microwell-

based digitization, excess sample solution has to be injected to completely fill the microwells and the remaining portion will be removed to isolate individual microwells.[224-227]

Recent efforts have been invested into addressing the low sample digitization efficiency problem for integrated processing and analysis of volume-limited samples. A self-digitization method has been developed to exploit the interplay among microstructure geometry, surface tension of fluids, and flow rate to replace the oil phase filled in the nanoliter chambers/wells with an aqueous solution[228,229]. With this method, the entire volume of the aqueous solution injected into the chip can be dispensed into individual droplets isolated by microwells, achieving a nearly 100 % efficiency of sample digitization. The utilities of this microfluidic self-digitization method has been demonstrated by an array of applications, including single cell analysis[116] and low-cost genetic diagnosis.[230] Nonetheless, this method may have some limitations for certain applications, for example, the requirement of initial priming with an immiscible phase and stringent dependence on geometric design. Moreover, it needs external pump and tubing for flow delivery, which could introduce the dead volume to lower the overall sample digitization efficiency. Alternatively, a vacuum-driven, self-powered microwell array chip was designed for highly efficient sample digitization.[231] This polydimethylsiloxane (PDMS) chip relies on a specially designed, fractal tree-like branching microchannel network with identical distance between the chip inlet to each dead-end microwells to evenly distribute the sample solution into the microwells. The chip is pre-vacuumed so that the reagents can be passively loaded into the dead-end microwells through the microchannel circuit. While this device provides 100% sample compartmentalization, its working principle requires highly specialized channel design and the vacuum pre-packaging, which can compromise its scalability and amenability

to system integration and automation of functional modules for processing and analysis of complex biological samples.

Herein, we report a highly efficient microwell-based sample digitization method that is robust and inherently compatible with general design principles for microfluidic integration and automation. Our strategy, termed microfluidic alternating-pull-push active digitization (μAPPAD), presents a distinct mechanism from the existing methods for sample-loss-free digitization, as summarized in Table 4-1. It uses vacuum to load the solution into an array of microwells through an open-ended microhchannel, and meanwhile actuates pneumatic microvalves to periodically toggle the pressure/vacuum inside the microchannel to push the solution preferentially into the microwells rather than through the channel. Thus, this strategy not only affords a ~100% sample digitization efficiency, but also greatly reduces the volume variability of fluid compartmentalization. Both tandem- and parallel-channel chip designs were evaluated for the μAPPAD and sample digitization with the parallel-channel chip can be finished within 2 min, which is comparable with the existing device.[231] To assess the analytical performance of the μAPPAD chip, we calibrated it for absolution dPCR quantitation of λDNA across a range of concentrations. The result obtained with our chip matched well with the theoretical curve computed from Poisson statistic. Compared to the existing sample-loss-free digitization methods,[228, 229, 231] our method improves the robustness of sample digitization by eliminating the need of stringent microwell geometries and special channel design, but also benefits from the intrinsic amenability of the pneumatic valve technique with device integration and automation. Thus we envision that the μAPPAD technology provide a scalable and widely adaptable platform to promote the development of advanced lab-on-a-chip systems integrating microscale sample processing with dPCR for a broad scope of applications, such as single cell analysis of

tumor heterogeneity and genetic profiling of circulating exosomes directly in clinical samples.

Table 4-1. Comparison of the μAPPAD and previously reported microwell methods for sample-loss-free digitization

Digitization methods	Chip design	Digitization principle	Sample retention	Digitization efficiency	Filling time (min)
μAPPAD (this work)	Tandem open channel with valves	Vacuum-driven dead-end passive filling	100%	81.6 ± 4.4%	2.05 ± 0.04
		Valve-assisted pull–push active filling	100%	99.5 ± 0.3%	10.5 ± 1.3
	Parallel open channel with valves	Vacuum-driven dead-end passive filling	100%	28.7 ± 6.8%	0.81 ± 0.06
		Valve-assisted pull–push active filling	100%	94.6 ± 0.9%	1.86 ± 0.25
Self-digitization	Tandem open channel with side μwells[228]	Droplet formation governed by μwell geometry, interfacial tension of aqueous/oil phases, and flow rate	100%	100%	In minutes
	Parallel open channel with bottom μwells[229]		80–90%	95–100%	
Self-priming[231]	μwells with fractal branching channel	Vacuum-driven dead-end passive filling	100%	N/A	A couple of minutes

Materials and methods

Chemicals and materials

λDNA (dam–, dcm–) and Bovine Serum Albumin (BSA) were purchased from

Thermo Fisher Scientific (Waltham, MA, USA). The QX200™ EvaGreen® ddPCR Supermix was purchased from Bio-Rad (Hercules, CA, USA). The RNase free water was ordered from Fisher BioReagents (Fair Lawn, NJ, USA), and the Fluorinert® FC-40 was purchased from Sigma (Saint Louis, MO, USA). A pair of primers targeting the λDNA were ordered from Integrated DNA Technologies (IDT, Coralville, IA, USA),

forward primer: 5'-CGCGATATGCTGCGCTTGCT-3',

reverse primer: 5'-TAAGCACGAACTCAGCCAGAACGA-3'.

Microfluidic chip fabrication

The molds for both tandem and parallel channel designs were fabricated on 4" silicon wafers (p100) by using standard SU-8 photolithography. Briefly, for the mold of pneumatic layer, at first a base layer in 10 μm height was built with SU-8 2010 (MicroChem Corp., Newton, MA) on the surface of the silicon wafer, then the feature in 50 μm height was constructed with SU-8 2025 (MicroChem Corp., Newton, MA) on the base layer; for the mold of fluidic layer, a base layer in 10 μm height was fabricated with SU-8 2010, followed with a layer of 50 μm for channel features by using SU-8 2025, and then another layer in 50 μm height was built by SU-8 2025 to form a layer in total height of 100 μm for the sample introduction chambers and micro-chambers. After the photolithography, all the molds were treated with gas phase silanization by using Trichloro(1H,1H,2H,2H-perfluorooctyl)silane (Sigma-Aldrich, St. Louis, MO).

The pneumatic layer and fluidic layer were constructed by standard soft-lithography. To fabricate the pneumatic layer, 22 g mixture of Sylgard® 184 at a 10:1 (base: curing agent) weight ratio was poured onto the mold and incubated at 65 ºC for 2 hours to form a PDMS slab in 2 mm thick. The PDMS slab was then peeled off from the mold and cut according to chip size. Similarly, a 2 mm thick blank PDMS slab was

made with a blank mold. The blank PDMS slabs were then cut and hollowed out manually as the anti-evaporation layers. The anti-evaporation layer was permanent bonded on the pneumatic layer by using UV-ozone treatment. After bonding, holes of 1 mm diameter were punched as inlets of pneumatic control channels. To fabricate the fluidic layers, 6 g mixture of Sylgard® 184 at a 10:1 (base: curing agent) weight ratio was spin-coated on each mold by 500 rpm for 30 sec then 800 rpm for 30 sec, and then incubated at 65 °C for 1 hr. The pneumatic layer with the anti-evaporation layer was then carefully aligned on the fluidic layer, with permanent bonding by UV-ozone. After overnight incubation at 80 °C, the PDMS slab was then peeled off from the wafer. Holes in 2 mm diameter were punched as inlets and outlets of the fluidic channels. After staining each valve with 0.1 % (w/v) BSA solution, the PDMS slab was adhered on a piece of glass slide by UV-ozone treatment. The chip was stored in 100% humidity at 4 °C overnight, and then the chip would be ready to use.

Sample digitization

The chip and the pneumatic control system were set up as described in previous work.[153, 232] The on-chip valves and chambers were actuated with a positive pressure of 15 kPa and a vacuum of -87 kPa which is the maximum output of our vacuum pump (Welch, IL). To optimize the digitization process, 2.5 μL red food dye (Great Value, Bentonville, AR) was injected into the inlet reservoir and then introduced into the sample microchamber by the vacuum suction applied via the pneumatic layer, with the inlet valve closed. After all the red food dye flowed into the sample microchamber, 10 μL FC-40 oil was added into the inlet reservoir. The inlet valve was then opened and the outlet valve was actuated by the LabVIEW program to perform sample digitization driven by the vacuum applied to the microwell array. The video of the microwell filling

process was taken with an AM4113T digital microscope (Dino-Lite, Torrance, CA) to measure the digitization time. Bright-field images of the chips were taken on a microscope (Eclipse Ti2, Nikon Instruments Inc., Melville, NY) and analyzed by ImageJ (NIH) to determine the digitization efficiency.

On-chip dPCR

We firstly measured the concentration of the λDNA standard using an Implen NanoPhotometer (AH Diagnostics, Denmark), and then made a series dilution of the stock solution. The λDNA standards were added to the Bio-Rad QX200™ EvaGreen® ddPCR Supermix at the specific concentrations. When the inlet valve was closed, 2.5 μL sample mix (containing 1× QX200™ EvaGreen® ddPCR Supermix, 100 nM forward primer, 100 nM reverse primer, and λDNA template) was pipetted into the inlet reservoir and then sucked into the sample chamber by the vacuum applied on the top pneumatic chamber. After all the sample flowed into the sample chamber, 10 μL FC-40 was added into the inlet. Then the inlet valve was opened to let the sample and the FC-40 be filled into the microwell array using the valve-controlled μAPPAD method (5 sec Pull mode and 1 sec Push mode). After the completion of sample digitization, the pneumatic control chamber above the digital array was filled with water. A piece of glass slide was adhered on the anti-evaporation layer by epoxy glue (Gorilla Glue, Sharonville, Ohio.). Water was injected into the chamber of the anti-evaporation layer by a syringe. Then the whole chip assembly was placed on a T5000-A-IS In-situ adapter (Benchmark Scientific, Sayreville, NJ) in a thermal cycler (TC 9639, Benchmark Scientific, Sayreville, NJ). The thermal cycling protocol for on-chip dPCR was: hot start at 95 °C for 5 min, 15 sec of denaturation at 95 °C and 60 sec of annealing/extending at 60 °C for 33 cycles, then held at 4 °C. After PCR was done,

fluorescence images of the microwell array were taken by using a fluorescence microscope (Eclipse Ti2, Nikon Instruments Inc., Melville, NY) which equipped with a CCD camera (Prime 95B sCMOS Camera, Teledyne Photometrics, AZ), and analyzed using a free software program (ImageJ, NIH).

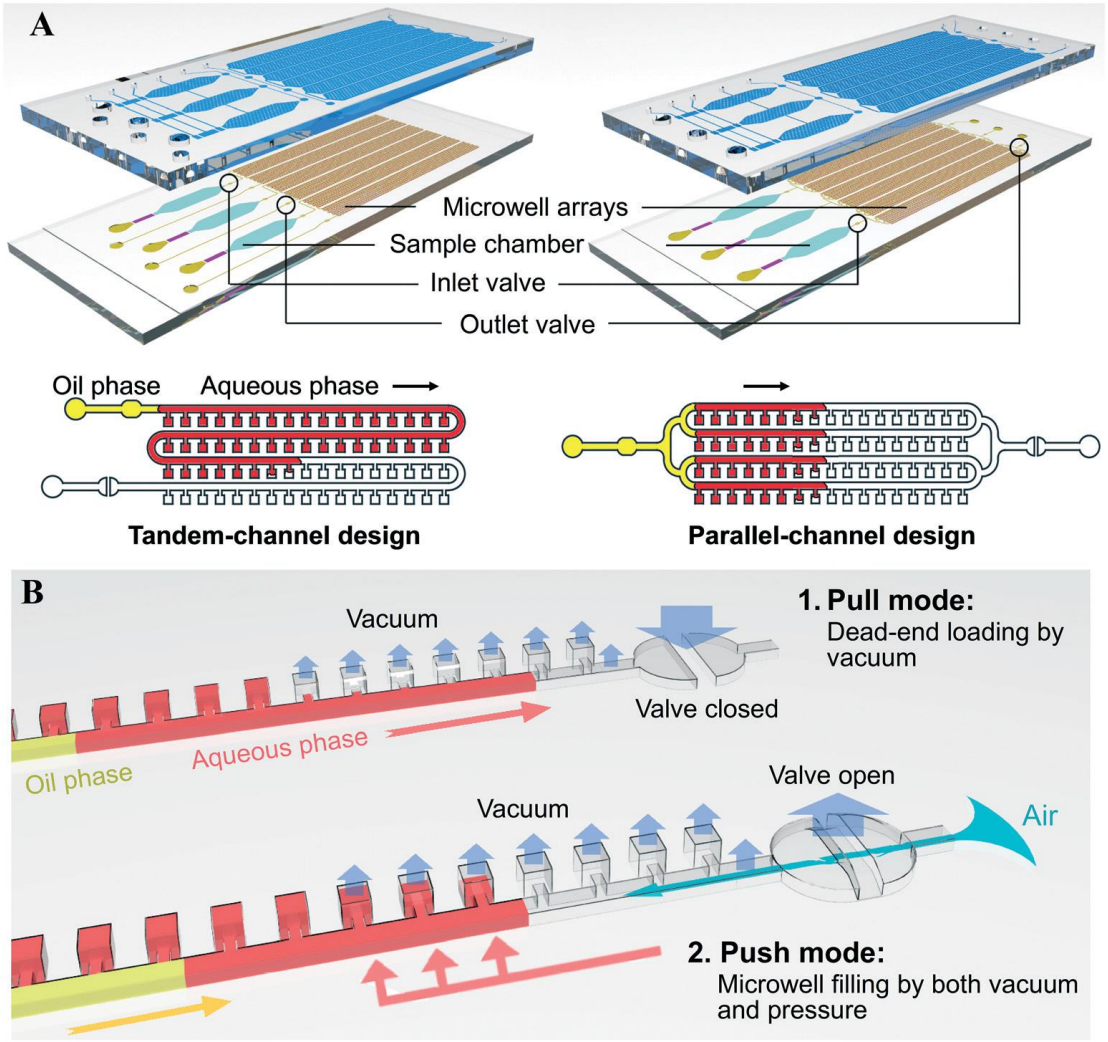

Figure 4-1. The µAPPAD chip designs. (A) Schematic of two microfluidic devices with the tandem-channel and parallel-channel designs. Both PDMS/glass chips consist of a pneumatic control layer and a fluidic channel layer bonded on a glass substrate. Each chip integrates three parallel units composed of a sample chamber connected with an array of 2000 microwells of 1.44 nL volume. The microwell array is flanked with the inlet and outlet valves. The volume of the sample chamber (2.5 µL) is ~10% smaller than the total volume of the microwells. (B) Schematic of the µAPPAD method showing the outlet valve operation to periodically switch the digitization process between the pull and push modes.

Result and discussion

Design and principle of the μAPPAD chip

We designed two μAPPAD chips, as shown in Figure 4-1A, which differ only in the arrangement of the digitization channels (tandem-channel or parallel-channel design). Both chips are assembled with a bottom fluidic layer and a top pneumatic layer and consist of three parallel units for simultaneous measurements. In each unit, a sample microchamber was connected to an array of 2000 microwells through either one main channel or 16 parallel channels. Dimensions of the main channels and reaction microwells in the digital array are illustrated in Figure 4-2. To achieve sample-loss-free digitization, the sample volume must be lower than the total microwell volume. Thus the sample chamber was designed to hold 2.5 μL sample, which is ~10 % less than the total volume of 2000 microwells (1.44 nL each). The microwell array is flanked by two pneumatic valves to control sample introduction and microwell filling. A pneumatic circuit was designed to actuate the sample chamber and control valves and to apply vacuum to the digital microwell array to drive the filling of microwells. The chip is fully automatically controlled by a homemade solenoid controller interfaced with a computer via a LabVIEW program described in our previous work.[153, 232] All the valves in this chip are the lifting gate microvalves,[101] which can be mechanically closed without any air pressure applied during thermal cycling for PCR.

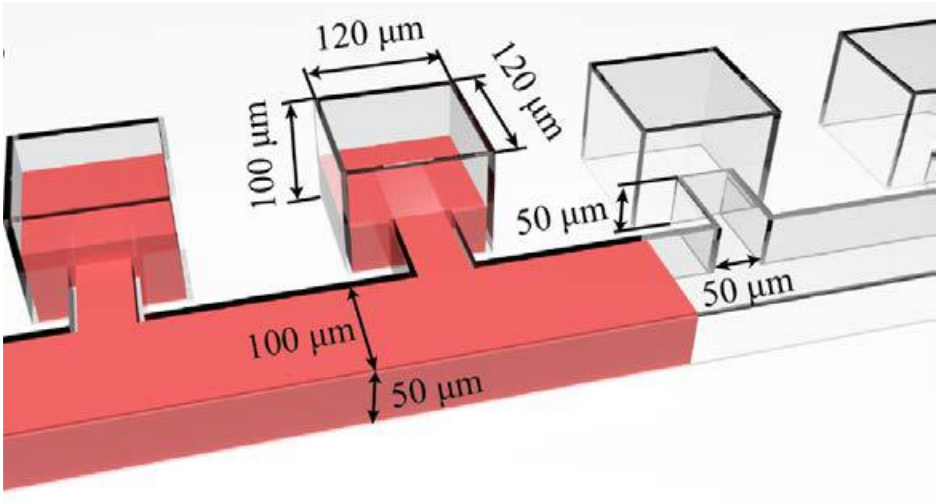

Figure 4-2. Dimensions of the microwells and the main channel in the µAPPAD device.

The principle of the µAPPAD method is sketched in Figure 4-1B. Enabled by the integration of a pneumatic control circuit, the digitization process in the µAPPAD chip can be periodically toggled between a "pull" mode and a "push" mode to achieve active filling of the microwells. In the pull mode, the outlet valve is closed to perform the conventional vacuum-driven dead-end filling, pulling the solution mainly through the main channel. Then the operation is switched to the "push" mode by opening the outlet valve to expose the main channel to the atmosphere, while maintaining the vacuum applied to the solution-isolated microwells through the top vacuum chamber (Figure 4-1A). Thus a pressure difference will be established between the main channel and those incompletely filled microwells. The higher pressure in the main channel will reverse the flow direction and push the aqueous phase to completely fill the microwells. Iterating the pull–push cycles will pull the sample solution plug further downstream until it is completely dispensed into the discrete microwells and isolated by the trailing oil phase.

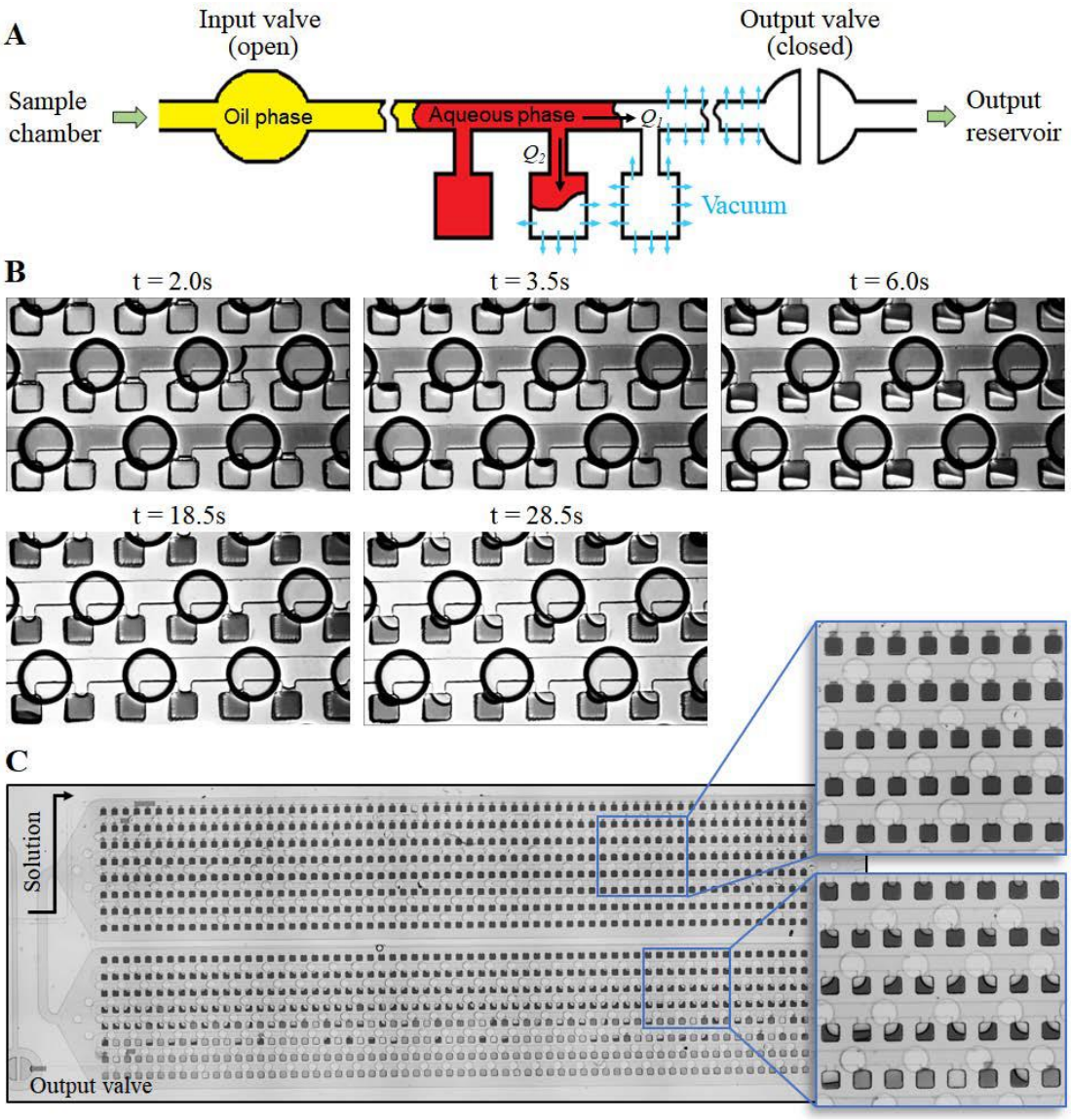

Figure 4-3. Dead-end filling of a limited sample volume on the µAPPAD chips. (A) Schematic of the dead-end microwell loading driven by the vacuum applied to the pneumatic chamber above the microwell array. The inlet valve is kept open and 2.5 µL aqueous solution held in the sample chamber is drawn through the channel and into the microwells at a volumetric flow rate of Q1 and Q2, respectively. The microwells are isolated by an oil phase immediately following the solution plug in the main channel. (B) Time-lapse images showing the process of incomplete microwell filling in a parallel-channel chip. The vacuum-driven flow of a dye solution in the main channels was seen to be too fast to completely fill the microwells before they were sealed by the oil plug. (C) A representative image of a tandem-channel chip after the sample digitization. The zoom-in images highlight the volume of solution loaded in the microwells decreases along the channel and the poor filling quality for the microwells close to the dead end of the channel.

Dead-end filling on μAPPAD chips

The μAPPAD method was developed from our initial efforts to implement and optimize the vacuum-driven dead-end filling method, which has been well demonstrated for microwell-based sample digitization, using our valve-integrated microfluidic chips. For the dead-end filling, a constant vacuum (−87 kPa) was applied to the vacuum chambers above the microwell array, while keeping the outlet valves closed with a positive pressure (15 kPa) (Figure 4-3A). Driven by the constant vacuum applied to the entire digitization array, a limited volume of aqueous solution in the sample chamber will be pulled through the main channel, loaded into the microwells, and sealed by the trailing FC-40 oil phase. However, this method consistently resulted in significant variation in compartmentalized volumes with a considerable fraction of microwells partially loaded with the solution. Using a parallel-channel chip, we investigated the dead-end filling process, as visualized in Figure 4-3B. It was seen that the solution was rapidly pulled across many microwells through the empty main channel while being slowly sucked into the microwells. Thus, a considerable fraction of microwells was only partially loaded with the solution before they were isolated by the oil phase, especially when the length of the solution plug has been largely shortened downstream of the main channel. This phenomenon was clearly manifested with the tandem-channel chip in which a much longer plug of solution can be formed than that in the parallel-channel chip. As shown in Figure 4-3C, the volume of solution compartmentalized in the microwells gradually decreases along the channel and the quality of microwell filling deteriorates significantly when getting closer to the dead end of the channel. Such significant variation in volume can cause inaccurate digital quantitation.

Our observations suggest two major factors that contribute to the poor sample

digitization performance by dead-end filling on our device. The first factor is the relative flow rate of the solution sucked through the main channel versus into the side microwells by the constant vacuum applied to the entire digitization array. As illustrated in Figure 4-3A, when the solution plug passes by a side microwell, the vacuum-induced negative pressure in the empty microwell competes with that in the main channel to pull the solution against the main flow into the microwell. It is reasonable to assume that a steady-state gas permeation flux across the thin PDMS membrane is established by the vacuum and that the amount of liquids pumped into the dead-end channel/microwell is equal to the amount of air sucked across the PDMS membrane.[233] Thus the volumetric flow rate inside the main channel (Q_1) should be much higher than that in individual microwells (Q_2), because of the much larger area of the main channel exposed to the vacuum. Such biased flow distribution largely limits the speed of microwell filling, which is unfavorable for the digitization of a limited sample volume. Second, distinct from other reported methods that used sufficient sample solution to ensure complete microwell filling, here a limited volume of fluid is injected into the channel and the length of the injected solution plug keeps decreasing when moving through the channel to load the microwells. As a result, the time to load the downstream microwells before they are sealed by the oil is progressively reduced, causing the deteriorating quality of fluid digitization seen in Figure 4-3C.

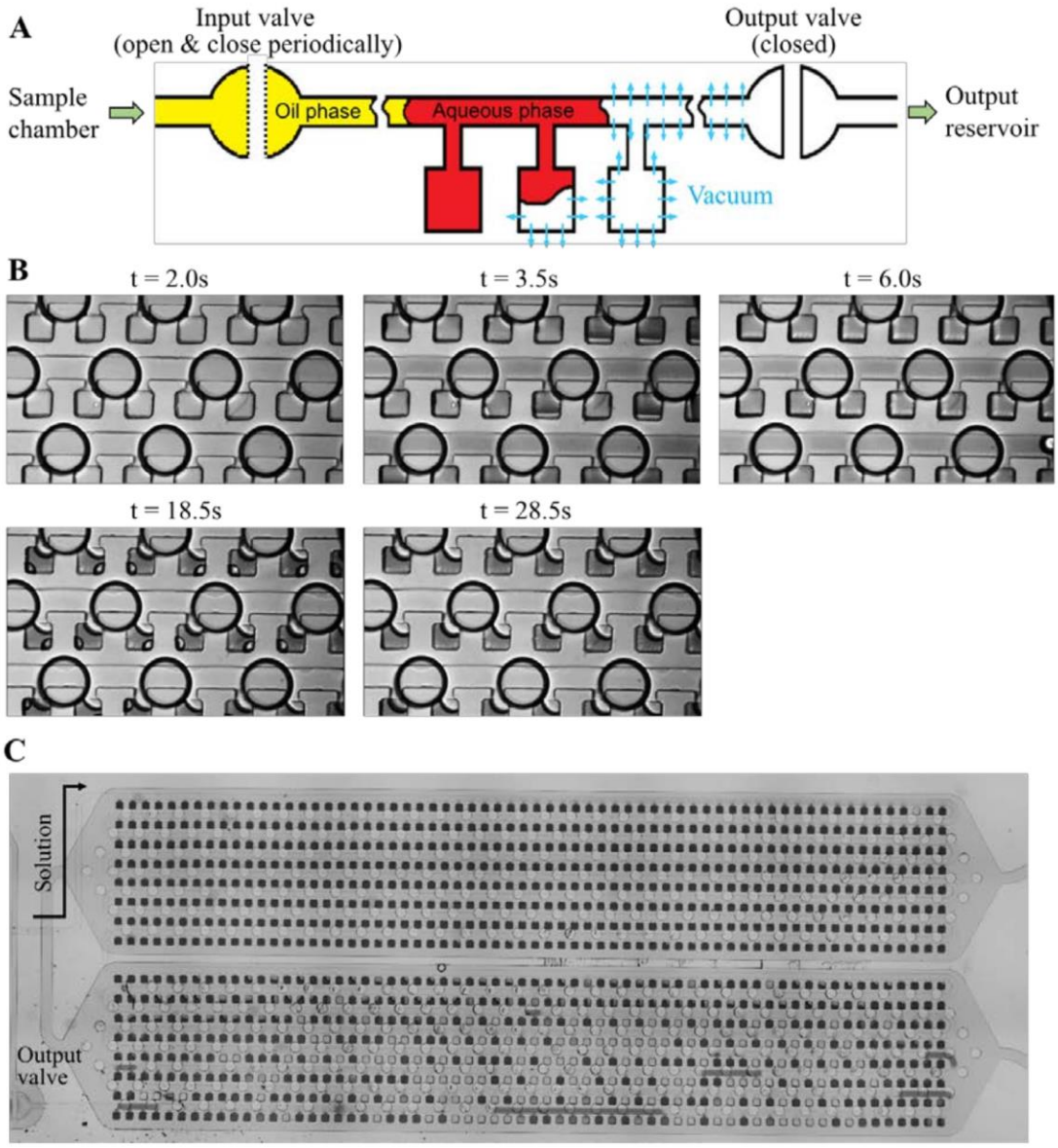

Figure 4-4. Pulsatile dead-end filling of microwells on the µAPPAD chips. (A) Schematic of the Pulsatile dead-end microwell loading. The inlet valve is periodically closed to pause the solution flow in the main channel. (B) Time-lapse images showing incomplete microwell filling in a parallel-channel chip. Closing the inlet valve periodically slowed the vacuum-driven flow of a dye solution in the main channels, but cannot completely fill the microwells before they were sealed by the oil plug. The time periods for closing and opening the inlet valve were set to 2 sec each in one cycle while keeping the outlet valve closed all the time. (C) A representative image of a tandem-channel chip after the sample digitization using the same valve actuation settings as in (B). Similar to the dead-end filling method, this modified dead-end filling approach resulted in decreasing solution volume loaded into the microwells along the channel and very poor sample digitization close to the dead end of the channel.

To preferentially load the solution into the microwells versus the main channel, we have tested a modified dead-end filling strategy in which the inlet valve was periodically closed to pause the vacuum-driven flow (Figure 4-4A). We varied the valve closing time over a wide range of 2 to 10 seconds while fixing the opening time at 2 seconds (i.e., close/open ratios of 1 to 10). However, it was found that this pulsatile dead-end filling method does not improve the digitization quality at all although it extends the time for filling microwells (Figure 4-4 B and C). The ineffectiveness of this method suggests that pausing the flow by closing the inlet valve does not change the relative pressure in the microwells versus the main channel to shift the flow distribution for complete filling of microwells. These findings pointed to the necessity of differentially modulating the pressure in the microwells and the main channel, which led to the development of our μAPPAD strategy as detailed below.

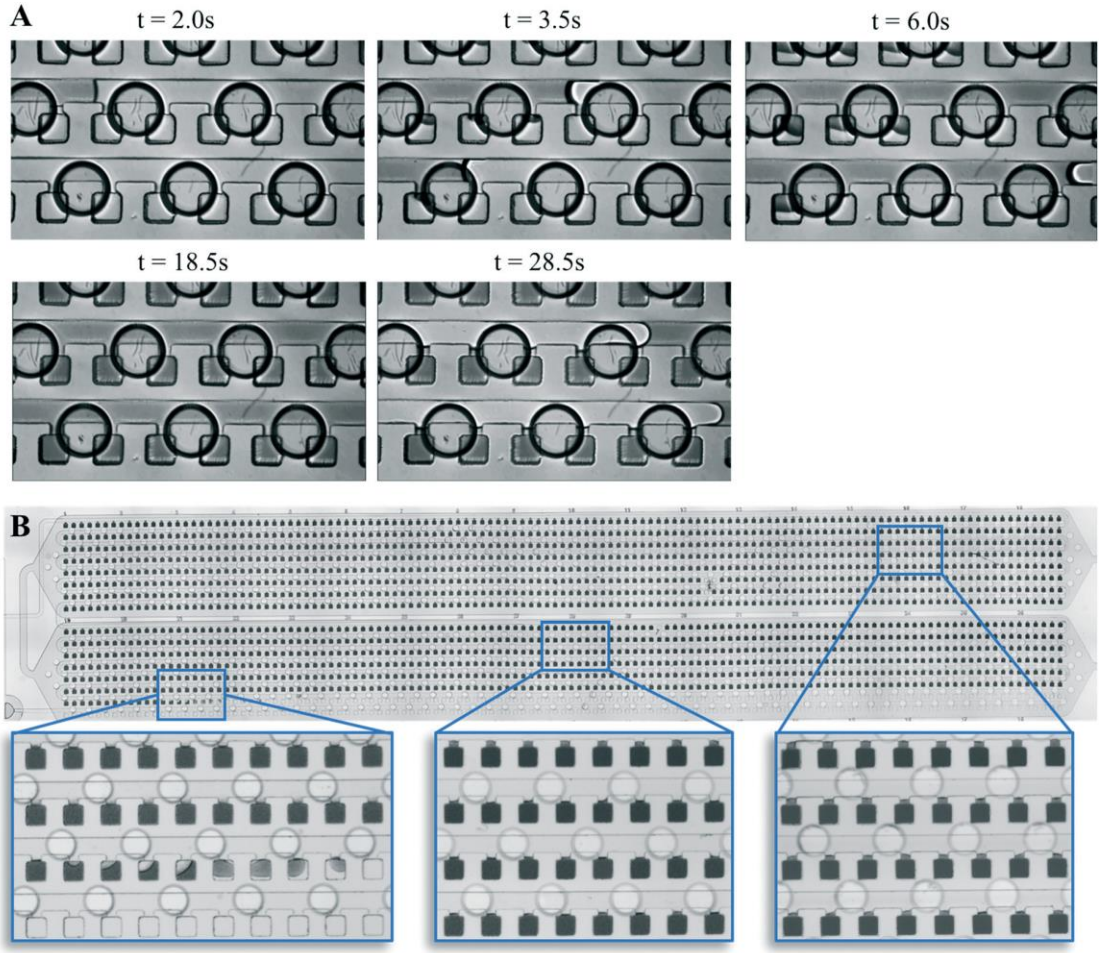

Figure 4-5. Efficient and uniform sample digitization enabled by the µAPPAD method. (A) Time-lapse images showing that the µAPPAD process was able to completely fill the microwells in a parallel-channel chip with a dye solution. (B) A representative image of a tandem-channel chip after the sample digitization using the µAPPAD method. The zoom-in images of different locations in the digitization array verify the complete filling of all the microwells exposed to the dye solution except for the last few ones. The time periods for closing and opening the outlet valve were set to 2 s each in one cycle while keeping the inlet valve open.

Development and optimization of the µAPPAD

Distinct from the continuous passive dead-end filling, our µAPPAD method is designed to enable active microwell loading by periodically toggling between the dead-end (pull) mode and the open-channel (push) mode, as sketched in Figure 4-1B. At the "push" mode, the outlet valve is opened to expose the main channel to the atmosphere, creating a pressure difference between the head of the aqueous solution plug and the

vacuumed microwells enclosed by the solution plug. Figure 4-5A clearly show that during the push mode, the higher pressure in the main channel can reverse the flow direction and drive the aqueous phase to completely fill the microwells. Using chips of different designs and microwell numbers, we demonstrated the ability of the μAPPAD method to fully load the microwells along the main channel except for the last few ones that were irregularly filled when the solution was nearly consumed, as exemplified by a tandem-channel chip with 2000 microwells (Figure 4-5B). Thus, in contrast to the passive dead-end loading methods, our μAPPAD method provides a new and robust means to enable uniform, highly efficient digitization of a limited sample volume.

We first optimized the μAPPAD for the tandem-channel design via investigating the settings of valve actuation that govern the performance of the two-mode sample digitization. The performance of the μAPPAD is quantified by a digitization efficiency defined as:

$$\text{Digitization Efficiency} = \frac{\text{Number of completely filled microwells}}{\text{Total number of completely filled and partially filled microwells}} \times 100\% \qquad (1)$$

The number of completely filled microwells was determined by counting the microwells filled with the solution up to the connecting channels. Based the dimensions shown in Figure 4-2,† the volume of a connecting channel is only 8.7% of that of the microwell. As verified in Figure 4-5B, all the microwells can be completely filled with a very small variation in the solution volumes inside the connecting channels. Thus the variation of the microwell-defined solution volumes was estimated to be ~6%, mostly due to the geometric variation resulting from microfabrication. As discussed above, the duration of the pull mode in each cycle controls the average speed of the solution flow in the main channel. To quantitatively assess its effect on the digitization quality, we varied the time for closing the outlet valve from 2 to 25 s while keeping the valve

opening time at 1 s. As seen in Figure 4-6A, when the period of the pull mode was varied from 2 to 5 s, our method could achieve complete loading of ~99.5% of the microwells, while greatly reducing the total time to complete the process from approximately 24 min to 10 min. As expected, further extending the duration of closing the outlet valve pulled the solution through the channel faster, but deteriorated the quality of sample digitization. These results suggest an optimal pull mode duration of 5 s needed to draw a sufficient amount of solution into the main channel for efficient microwell loading during the push mode.

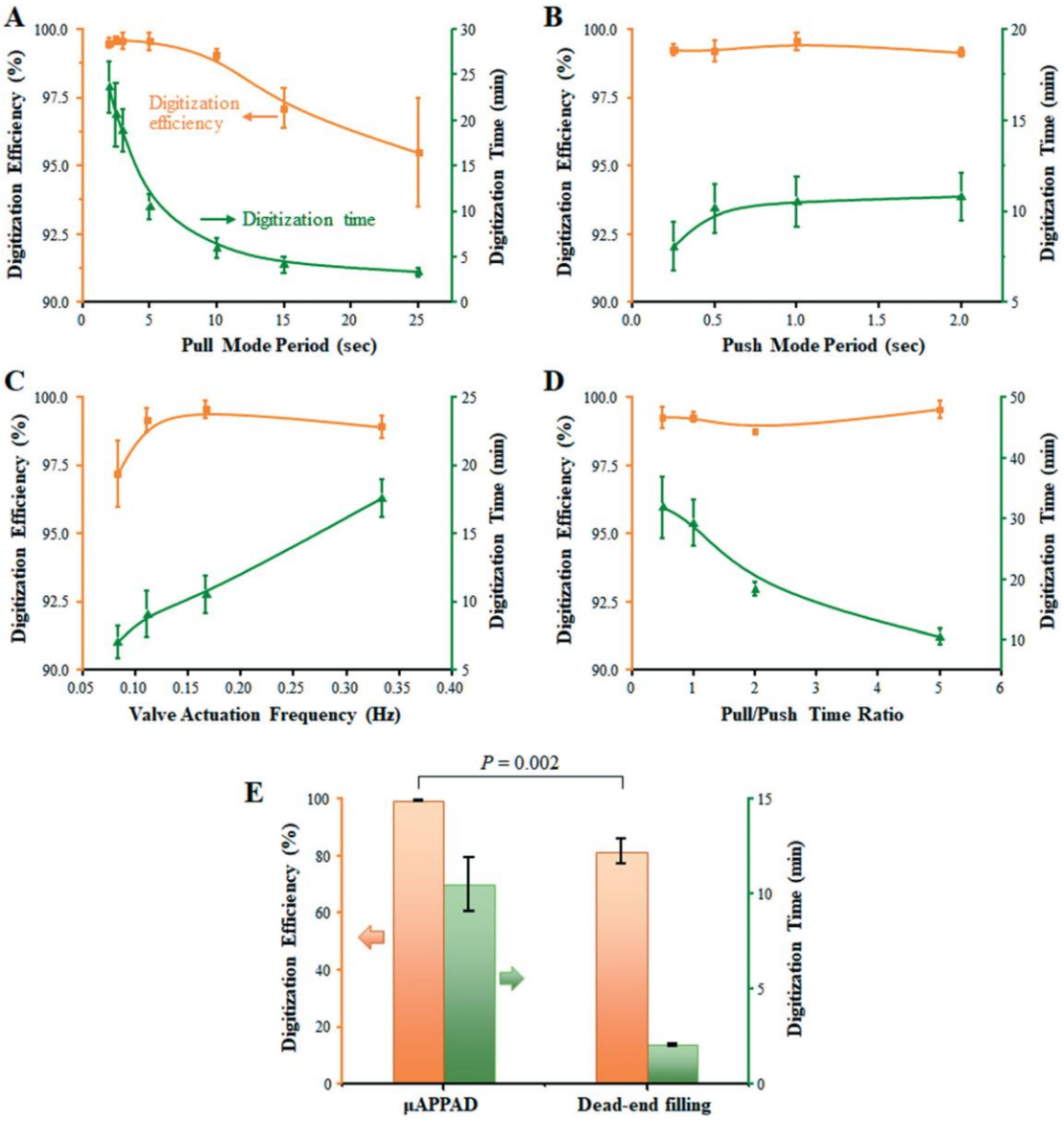

Figure 4-6. Optimization of the µAPPAD method for the tandem-channel chip. (A) Effects of the pull mode period on digitization efficiency and time were assessed with the push mode time fixed at 1 s in each valve actuation cycle. (B) Optimization of the push mode period with a fixed pull mode period of 5 s per valving cycle. (C and D) Assessment of the digitization efficiency and time by simultaneously varying the periods for both modes at a constant pull/push time ratio (C) and an overall frequency (D), respectively. Based on the results obtained in (A) and (B), the constant pull/push time ratio and overall frequency were determined to be 5 : 1 and 0.17 Hz, respectively. (E) Comparison of the optimal digitization performance of the µAPPAD with that of the conventional dead-end filling method. Error bars indicate one standard deviation (S.D., n = 3). Two-tailed Student's t-test was used to calculate the P value with 95% confidence.

We then assessed the push mode to optimize the time of exposing the main channel to a relatively positive pressure for microwell filling. In this case, the outlet valve was opened for a varying period after closing the valve for 5 s each cycle. As shown in Figure 4-6, the digitization efficiency remains consistently higher than 99% when the duration of the push mode was changed over a range of 0.25–2.0 s. This observation demonstrates the robustness of our μAPPAD for highly efficient digitization of a small-volume sample. Meanwhile, the total digitization time was observed to increase only slightly along with the push mode period. This could be due to extending the push mode period improving the microwell filling efficiency during each pull–push cycle and thus reducing the total number of push–pull cycles required to complete the sample digitization. We selected the optimal push mode time of 1.0 s for subsequent experiments, as it reliably provides the highest digitization efficiency of 99.5 ± 0.3%.

The results of the one-factor-at-a-time optimization of the pull and push modes were further validated by varying the periods for both modes at a constant pull/push time ratio and overall frequency, respectively. Figure 4-6C depicts the effects of the valve actuation frequency on the digitization performance assessed at the ratio of the pull/push periods optimized above (5 : 1). The optimal frequency was determined to be 0.17 Hz, which corresponds to the periods of 5 s and 1 s for the pull and push modes, respectively. As the frequency increased, the shortening time for both pull and push modes resulted in an increasingly longer digitization process, which can be attributed to the pull mode period affecting the digitization time more significantly than the push mode (Figure 4-6A and B). With the valve actuation frequency fixed at 0.17 Hz, we then changed the time ratio of the pull and push modes. As presented in Figure 4-6D, the pull/push time ratio does not impact the digitization efficiency significantly,

indicating that the tested range of the push time (1 to 4 s) was sufficient to load microwells efficiently. This is consistent with the observation in Figure 4-6B. However, the digitization time decreased significantly as the pull/push time ratio was increased to pull the solution through the channel faster, which was also observed in Figure 4-6A. These findings demonstrated that the quality of sample digitization is mainly controlled by the push mode while the speed is mostly determined by the pull mode. Collectively, these studies confirm the optimal periods of 5 s and 1 s for the pull and push modes, respectively. Using these valve actuation settings for a tandem-channel chip, the μAPPAD strategy afforded a substantially improved efficiency for digitizing small-volume samples compared to the conventional dead-end filling method (99.5 ± 0.3% versus 81.6 ± 4.4%, P = 0.002) (Figure 4-6E). We observed a relatively large variation in the filling time (Figure 4-6), which can be presumably attributed to three main factors: 1) chip-to-chip variation in microfabrication and chip assembly; 2) variation in experimental operation; 3) the change of PDMS surface chemistry overtime after UV ozone treatment. Despite such variable loading time (i.e., average flow rate in the main channel), it was seen that once optimized, our method afforded constantly high digitization efficiency with much less variability. These results suggest the robustness of our method for digitization of small sample volumes, which is important for reproducible absolute digital analysis.

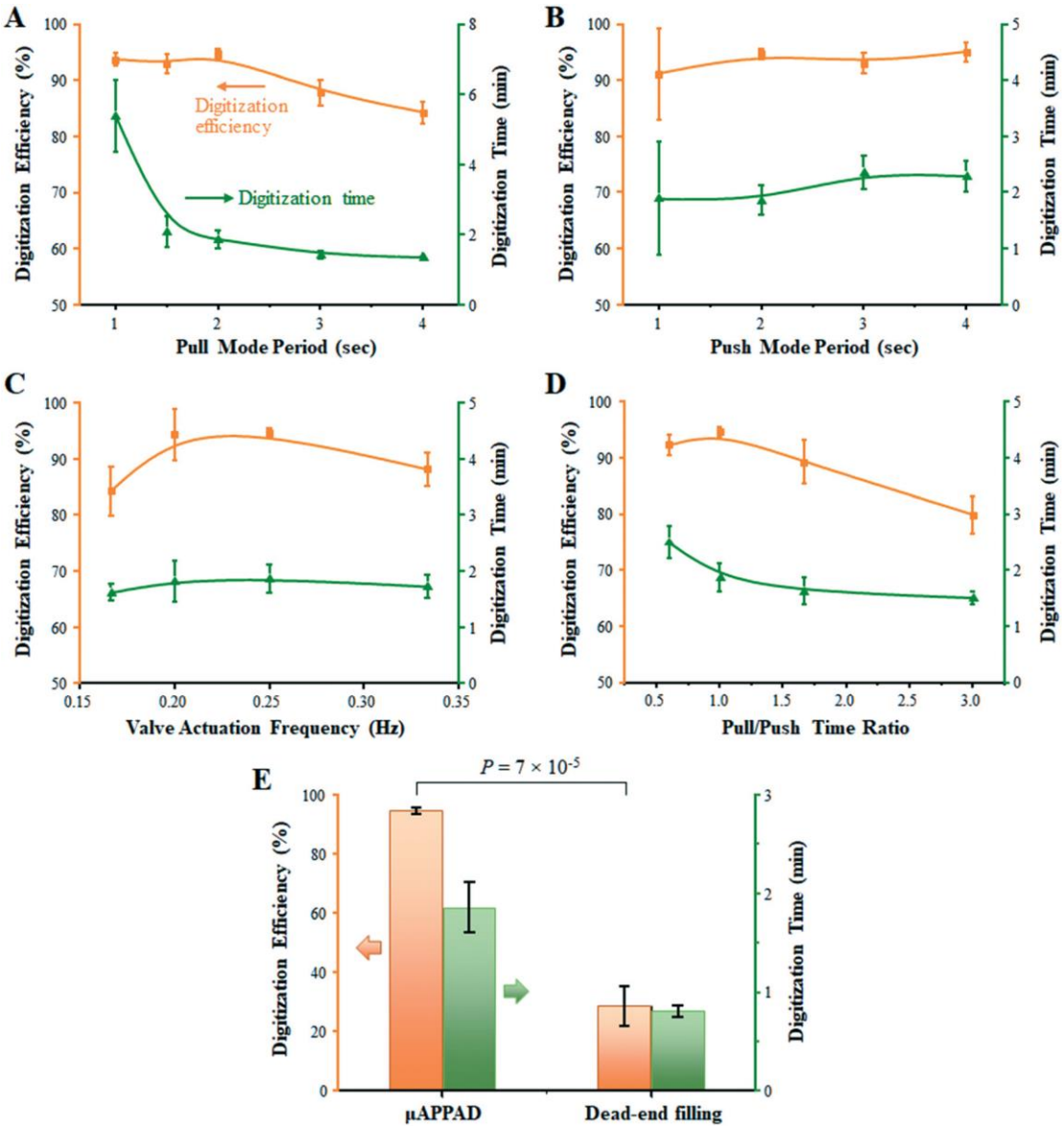

Figure 4-7. Optimization of the µAPPAD method with the parallel-channel chip. (A) Effects of the time period for the pull mode on the digitization performance were assessed with the push mode fixed at 2 s. (B) Optimization of the push mode period with a fixed pull mode period of 2 s. (C and D) The digitization performance assessed by simultaneously varying the periods for both modes at a constant time ratio of 1 : 1 (C) and an overall frequency of 0.25 Hz (D), respectively. (E) Comparison of the optimal digitization performance of the µAPPAD with that of the conventional dead-end filling method obtained with the parallel-channel chips. Error bars indicate one S.D. (n = 3). The P value was calculated by two-tailed Student's t-test with 95% confidence.

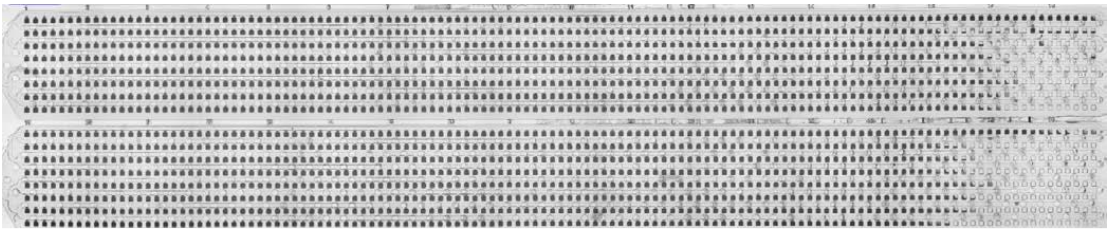

Figure 4-8. Sample digitization in a parallel-channel chip. Representative image of a parallel-channel chip after the sample digitization using the μAPPAD method shows the complete filling of all the microwells exposed to the dye solution except for the last few ones in each channel. The time periods for closing and opening the outlet valve were set to 2 sec and 3 sec, respectively, while keeping the inlet valve open.

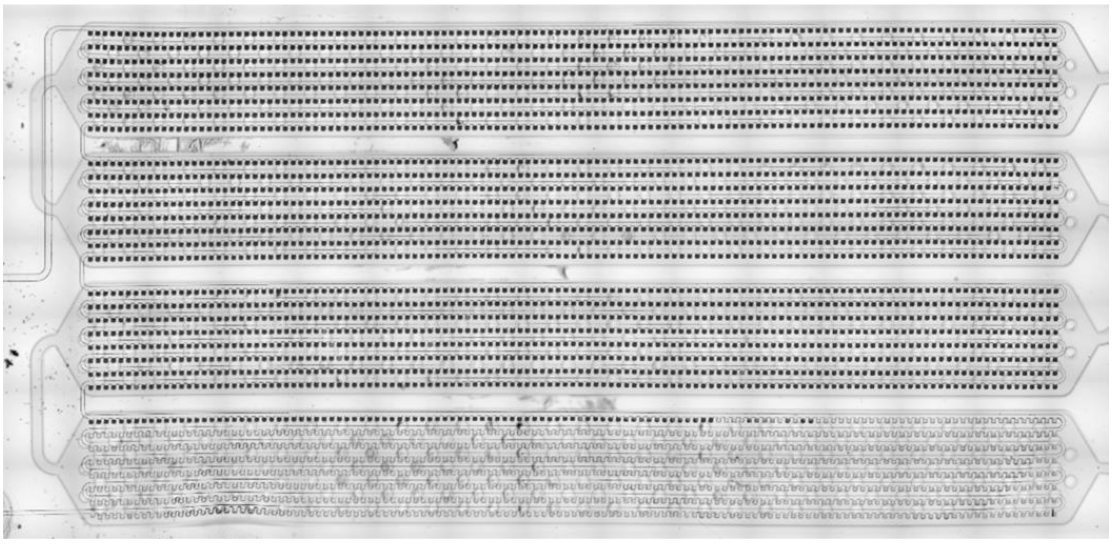

Figure 4-9. Robust and uniform sample digitization in a chip of different microwell geometries. The tandem-channel chip contains 4096 square microwells and each microwell is 60 μm in width and 100 μm in height. The main channel is 100 μm wide and 50 μm high. In this case, the μAPPAD process was conducted by closing and opening the outlet valve for 3 sec and 0.5 sec in each cycle, respectively.

It is noted that the quality improvement is traded off with the extended time for sample digitization (Figure 4-6E). To expedite the digitization process while maintaining the quality, we characterized the μAPPAD on a parallel-channel chip (Figure 4-8), following the same procedure described in Figure 4-6. The effects of the pull and push periods on the quality and time of sample digitization were found to be qualitatively consistent with those observed for the tandem-channel chip, as shown in Figure 4-7A and B. An optimal period of 2 s was determined for the pull and push

modes, respectively. These pull/push settings were confirmed via investigating the effects of the valve actuation frequencies (Figure 4-7C) and the ratio of the push and pull periods (Figure 4-7D). Such a difference in the optimal digitization settings is expected, because the parallel chip design has much shorter main channels than those of the tandem design and thus its digitization performance is more significantly influenced by the pull/push settings. The combination of a shorter pull step (i.e., slower flow in the main channels) and longer push step will enhance the rate of complete microwell filling in the short channels. Compared to the tandem-channel chip, the parallel chip design of the same microwell array reduces the digitization time from ~11 min to less than 2 min, but affords a slightly lower digitization efficiency of 94.6 ± 0.9% (Figure 4-7E). It was seen that the incomplete filling of microwells occurs when only an extremely small fraction of the solution was left in a main channel (Figure 4-5B). In the parallel-channel deice, such defective microwell loading in each channel sums up, leading to a relatively lower digitization efficiency (Figure 4-8). It is noted that the μAPPAD method significantly increased the digitization efficiency from 28.7 ± 6.8% for the dead-end filling to 94.6 ± 0.9% ($P = 7 \times 10^{-5}$, Figure 4-7E). Such improvement is much more significant that that obtained for the tandem-channel chip, which also demonstrates the effects of the channel length on the digitization efficiency. Overall, compared to other sample-loss-free digitization methods,[228, 229, 231] our method offers comparable or better digitization efficiency but better flexibility in chip design as the digitization principle of our method does not rely on the stringent microwell geometries, surface properties, and special channel design (Table 1). It is convenient to apply this method to chips with variable geometries and numbers of microwells (Figure 4-9) to achieve the desired analytical performance of dPCR. Nonetheless, other practical factors may affect the sample digitization quality. For instance, oil phases with different

viscosities can lead to variable flow rates in microchannels under a given vacuum pressure. In our case, the flow rate has been shown to affect both digitization efficiency and loading time (Figure 4-6 and Figure 4-7). The μAPPAD method can be readily optimized for specific chip designs and dPCR assays by fine tuning the valve operation and vacuum settings to achieve optimal sample digitization quality.

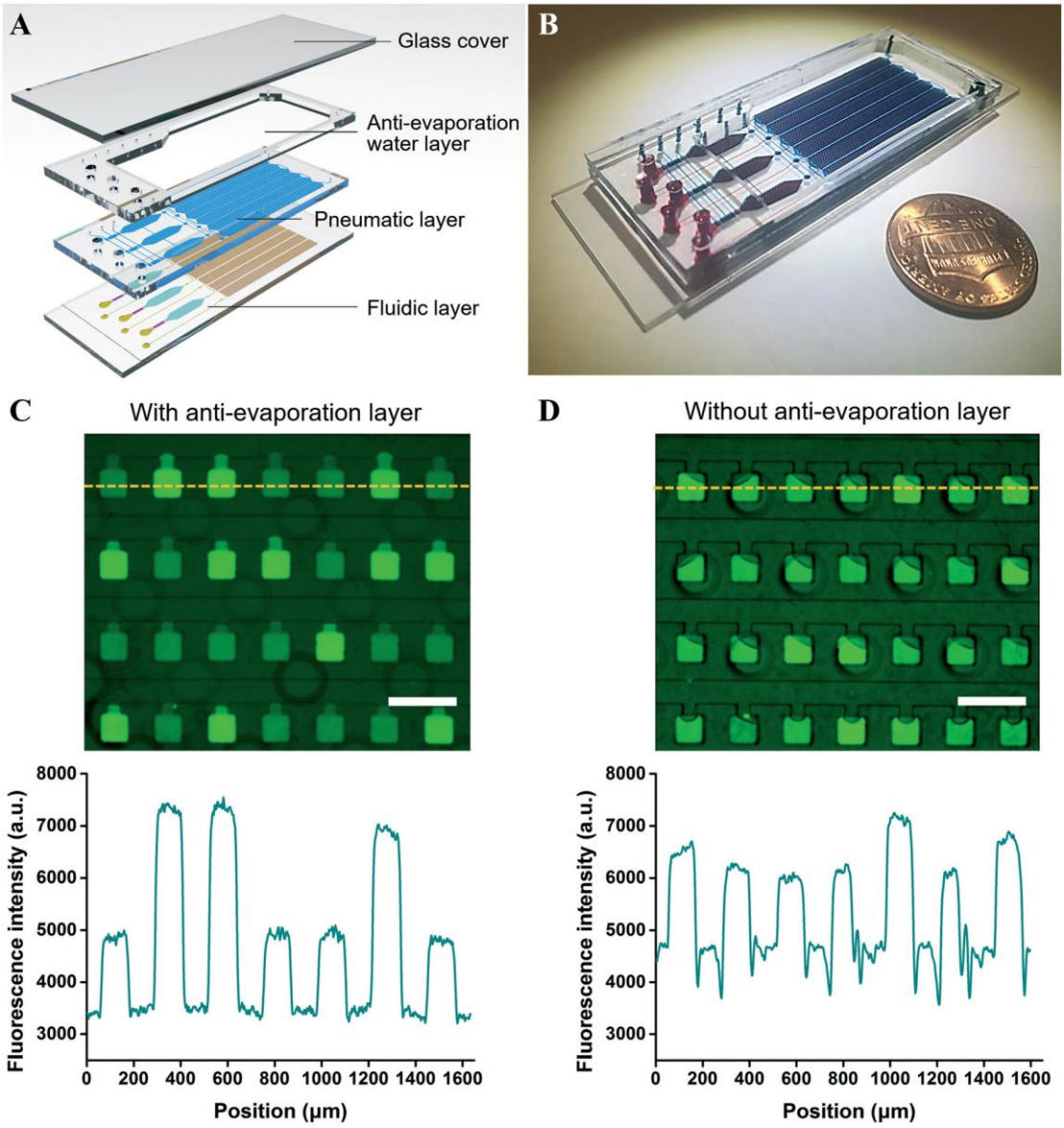

Figure 4-10. The μAPPAD chip-based dPCR system. (A) Exploded sketch and (B) a photo of the μAPPAD chip assembled with an anti-evaporation device for on-chip dPCR. The 2 mm thick anti-evaporation PDMS layer consists of a water chamber that protects the entire sample chamber and the microwell array and is topped with a piece of cover glass. (C and D) Comparison of the water evaporation in the chip with and without the anti-evaporation layer after thermal cycling. In both cases, the pneumatic channels/chambers in the μAPPAD chips were filled with water and then covered by a glass slide on the top. The signal intensity profiles were obtained by scanning across the fluorescence images as indicated by the dashed lines.

On-chip dPCR detection

As a proof-of-principle, we applied the μAPPAD chip for quantitative dPCR detection of λDNA. To prevent reagent evaporation in the PDMS device during thermal

cycling, we assembled the μAPPAD chip with a PDMS anti-evaporation layer and a glass slide on the top, as shown in Figure 4-10A and B. The PDMS anti-evaporation layer is permanently bonded on the pneumatic layer and contains a chamber that can be filled with more than 2 mL of water after sample digitization. As shown in Figure 4-10C, no discernable evaporation was observed in individual microwell-confined aqueous droplets after 33 cycles of PCR, and it is very easy to differentiate the positive and negative microwells. In contrast, without this anti-evaporation layer, severe evaporation was observed after thermal cycling so that the background signal largely increased to diminish the intensity difference between positive and negative microwells (Figure 4-10D). Thus, this chip construct was proven effective for preventing water evaporation to protect PCR reaction in the microwell-confined droplets. This method is low-cost and simple to use in comparison to existing methods, including pre-treating chips with 100% humidity[107] and coating chips with an electronic grade water-proof layer,[234] polyethylene water-proof layer,[235, 236] and parylene C film.[237] A similar anti-evaporation water chamber approach has been recently reported.[238] However, this method may not be compatible with the pneumatic valve-based microchip, because the valve may not work properly with a water chamber placed underneath.

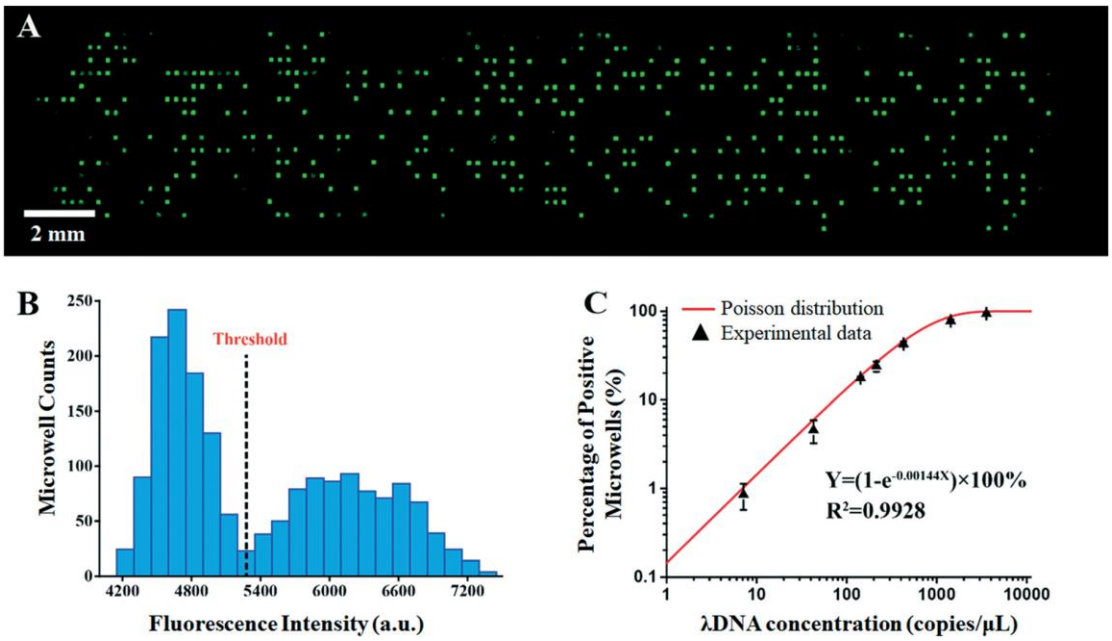

Figure 4-11. dPCR analysis performance assessed with a tandem-channel μAPPAD chip. (A) A representative fluorescence image of the entire microwell array after 33 cycles of PCR for detection of λDNA at a concentration of 214 copies per μL (11.2 pg mL−1). (B) A representative histogram of the fluorescence intensity in individual microwells after thermal cycling for detection of λDNA at a concentration of 428 copies per μL (22.4 pg mL−1). Two populations of the microwells are visualized and a threshold in the fluorescence intensity can be set to quantify the fraction of the positive reactions. (C) Log–log plot of the percentage of positive microwells measured for a range of λDNA concentrations (~7 to 3600 copies per μL). The solid line presents the theoretical prediction by the Poisson distribution, based on the microwell volume (1.44 nL), and its function was used as the regression curve to fit the experimental data to determine R2. Error bars indicate one S.D. (n = 3).

To demonstrate the application to quantitative genetic analysis, we measured λDNA as the model target using the tandem-channel chip. A series dilution of λDNA standards with concentrations ranging from ~7 to 3600 copies per μL were prepared and measured. 33 cycles of PCR were performed for each assay, which was repeated three times for each concentration. Figure 4-11A presents a representative fluorescence microscopy image of the post-PCR microwell chip for detection of λDNA at a concentration of 214 copies per μL. These fluorescence images were analyzed to plot the signal intensity histograms of the filled microwells, from which a threshold can be determined to distinguish the positive microwells from the negative microwells (Figure

4-11B). Based on that, the fraction of positive microwells over the total number of filled microwells was calculated and plotted as a function of λDNA concentration in a log–log calibration curve presented in Figure 4-11C. The plot shows a good linearity over a range of diluted λDNA concentrations and levels off as the DNA concentration increases. To verify the absolute quantification capability, the experimental results were compared to the theoretic curve predicted by the Poisson distribution,[230] based on the nominal volume of the microwells (1.44 nL). Very good agreement was observed between the experimental results and the theoretical curve ($R^2 = 0.9928$, Figure 4-11C), suggesting an excellent detection accuracy. This observation further verifies the ability of our μAPPAD method for robust and efficient digitization of small-volume samples to ensure accurate quantitation of target molecules. Extensive theoretical and experimental studies have demonstrated that the analytical performance of dPCR is governed by the number of reactions/microwells analyzed.[211, 231, 234, 239] Compared to the droplet dPCR technologies, the microwell-based devices have preset capacity for stochastic single-copy detection, which determines their detection sensitivity, accuracy, and dynamic range. Nonetheless, the array-type technologies afford a useful alternative platform with some distinct advantages, such as ease operation, high precision of controlling reaction volumes and numbers, and inherent compatibility with automated image registration and robotic liquid handling.[227] In this proof-of-concept study, a moderately sized μAPPAD device with a number of 2000 wells was used with the focus on demonstrating the high digitization quality of our method for quantitative dPCR. The sensitivity and dynamic range of this device can be readily customized for different applications by scaling up the size of the microwell array.

Conclusions

We have successfully developed a robust μAPPAD method for reproducible and highly efficient digitization of samples of limited volume. In contrast to the conventional vacuum-driven passive dead-end filling methods, our method employs integrated pneumatic valves to periodically manipulate air pressure inside the channels to greatly facilitate the microwell-based fluid compartmentalization. Using both tandem-channel and parallel-channel chips, we demonstrated that the μAPPAD method confers a digitization efficiency of 99.5 ± 0.3% and 94.6 ± 0.9%, respectively. The feasibility of the μAPPAD chip for digital genetic analysis was then assessed via absolution dPCR quantitation of λDNA across a range of concentrations. Compared to the existing methods, our technology is not only more flexible in the microwell/channel design, but also intrinsically amenable to the integration and automation of analytical functions on chip. Thus we envision that the μAPPAD technology should provide a useful platform to facilitate microfluidic integration of microscale sample processing with dPCR analysis, opening new opportunities for developing advanced lab-on-a-chip systems for a broad scope of applications, such as single cell analysis of tumor heterogeneity and genetic profiling of extracellular vesicles directly from clinical biofluid specimens.

Chapter 5. A microfluidic device for exosomal mRNA detection via on-chip digital one-step RT-PCR

Introduction

Exosomes, which are extracellular vesicles that are 30 – 150 μm in size, are found to be involved in intercellular interactions, including immune response suppression, tumor progression, angiogenesis, and metastasis.[30, 31, 240] Exosomes contain messenger RNAs (mRNAs) that are secreted from the origin cell.[33] These mRNAs are stable under the protection of the exosomes thus avoiding the degradation caused by the RNase in blood,[58, 59] and some of them are found to be relevant to a variety of diseases, such as ovarian cancer,[241] glioblastoma,[34] amyotrophic lateral sclerosis (ALS),[242] neurodegenerative disease,[243] prostate cancer,[244] Ewing Sarcoma,[119] melanoma and non–small cell lung cancer.[245] Therefore, the exosomal mRNA can be promising biomarkers for the diagnosis of diseases.[246] However, it is challenging to quantitatively measure the exosomal mRNAs due to its low abundance in exosomes.[247, 248]

The conventional methods for the quantitation of the mRNA are usually polymerase chain reaction (PCR) based methods, such as real-time RT-PCR,[249] nested PCR,[244] and droplet digital PCR (ddPCR),[250] which are all sensitive and robust. However, each of these approaches requires complicated sample preparation process, including exosome isolation, total RNA extraction and reverse transcription, which are tedious, time-consuming and labor costly, suffering from low isolation yield and large sample consumption.

Microfluidics is a platform that can integrate multiple functions in a single device and manipulate microiters to picoliters of fluids in its microchannels. Due to its high-sensitivity, low cost, robustness, low sample and reagent consumptions, a number of mRNA quantitative measurement methods based on the microfluidic technology have been developed, such as on-chip RT-qPCR,[106] on-chip digital PCR,[107, 116] on-chip RT-LAMP,[251] on-chip nucleic acid sequence-based amplification,[252] Nanostructured microelectrodes (NMEs),[117] etc. However, to our knowledge, there are only a few microfluidic approaches for exosomal mRNAs analysis. A microfluidic immuno-magnetic exosome RNA (iMER) platform, which integrated magnetic-bead-based exosome enrichment, on-chip RNA isolation and on-chip RT-qPCR in a single device, was developed for the MGMT and APNG mRNAs analysis in exosomes derived from glioblastoma multiforme.[118] However, this device required fully manual operations due to the built-in torque-activated valves. A microfluidic device that integrated on-chip enrichment and detection based on digital enzymatic signal amplification was developed for the quantitation of the EWS-FLI1 mRNA in Ewing Sarcoma (EWS)-derived EVs,[119] but this method did not integrate the exosome enrichment and lysis functions and still required off-chip exosome isolation and RNA extraction prior to the on-chip mRNA detection.

Previously, our group reported a sample-loss-free digitization method for on-chip digital PCR, referred to microfluidic Alternating-Pull-Push active digitization method (μAPPAD). We believe this technology can fit the requirements for the exosomal mRNAs analysis. Herein, we described a microfluidic device that integrated bead-capture of exosome, on-chip lysis and digital one-step reverse transcription polymerase chain reaction (RT-PCR) for the absolute quantitation of exosomal mRNAs. Our approach was able to measure the GAPDH mRNA down to 9 copies/μL in

0.5ng/ml the total RNA of human skeletal muscle. As a proof of concept, our method successfully detected the GAPDH mRNA in the exosome sample from MDA-MB-231 cell line. This on-chip exosomal mRNA detection method still needs further optimization, and we believe it will eventually achieve the goal of high-sensitive quantitative measurement.

Materials and methods

Chemicals and materials

The 1-Step RT-ddPCR Advanced Kit for Probes and the iScript™ RT-qPCR Sample Preparation Reagent were purchased from Bio-Rad (Hercules, CA). The SuperScript™ III Platinum™ One-Step RT-qPCR Kit, the Dynabeads® M-270 carboxylic acid, and the RNAqueous™-Micro Total RNA Isolation Kit were ordered from Invitrogen (Carlsbad, CA). Bovine Serum Albumin (BSA) and Ribolock RNase inhibitor were purchased from Thermo Fisher Scientific (Waltham, MA). Tween® 20 , Fluorinert® FC-40, 2-(N-morpholino)ethanesulfonic acid (MES), N-ethyl-N′ -(3-dimethylaminopropyl)carbodiimide hydrochloride (EDC), N-hydroxysuccinimide (NHS) were ordered from Sigma-Aldrich (St. Louis, MO). 20× EvaGreen® Dye was bought from Biotium (Fremont, CA). The RNase free water was ordered from Fisher BioReagents (Fair Lawn, NJ). Epoxy glue was purchased from Gorilla (Cincinnati, OH). Exosomes derived from MDA-MB-231 cell line were kindly provided by Dr. Liang Xu's Lab. Anti-CD81 was obtained from Ancell (Stillwater, MN). PrimeTime® qPCR Assays for GAPDH was purchase from IDT (Coralville, IA). Human GAPDH PrimePCR™ Probe Assay was bought from Bio-Rad.

Chip Fabrication

Standard SU-8 photolithography was employed on 4" silicon wafer (p100) for the fabrication of the molds for the pneumatic and fluidic layer, as previously described.[253] Briefly, for the pneumatic layer, the feature of 50 μm in height was fabricated by SU-8 2025 (MicroChem Corp., Newton, MA) on a 10 μm height base layer which is made of SU-8 2010 (MicroChem Corp., Newton, MA). For the fluidic layer, a base layer of 10 μm in height was coated on the wafer with SU-8 2010, on which the channel of 50 μm in height and chambers of 100 μm in height were constructed with SU-8 2025. All molds were treated with Trichloro(1H,1H,2H,2H-perfluorooctyl)silane (Sigma-Aldrich, St. Louis, MO) via gas-phase silanization. Soft lithography was utilized for the fabrication of the PDMS chip. Both of the 2 mm-thick anti-evaporation water layer and the 2 mm-thick pneumatic layer were fabricated with SYLGARD™ 184 Silicone Elastomer Kit (TDCC, Midland, Michigan) in a 10:1 ratio of the base to the curing agent. These two layers were permanently bonded by using UV-ozone. After the bonding, the combined upper layer PDMS slab was aligned and bonded to the fluidic layer, which was made by spin-coating the 10:1 Sylgard® 184 at a spin rate of 500 rpm for 60 sec on the mold and then incubated at 65 °C for 2 hours. UV-Ozone treatment and overnight incubation at 80 °C were applied to ensure permanent binding. Then the assembled PDMS slab was peeled off from the mold. 0.2 μL of 0.1% (w/v) BSA was employed to stain each lifting-gate valve to prevent valve failure caused by the adhesion on the glass surface. Finally, the assembled PDMS slab was adhered to a glass slide by using UV-Ozone. The chip was treated with 100 % humidity at 4 °C overnight before usage.

On-chip mRNA digital one-step RT-PCR

The sample mixture was prepared before the on-chip mRNA detection. 10 μL sample mixture consisted of 1 μL of RNA template, 5 μL of 2× Reaction Mix, 0.2 μL of Superscript III RT/ Platinum Taq mix, 0.1 μL of 20 μM forward and reverse primers mix, 0.5 μL of 2 % (v/v) Tween® 20, 0.5 μL of 20× EvaGreen Dye, 0.5 μL of 40 U/μL RNase inhibitor and 3.2 μL RNase-free water. For the on-chip mRNA detection, the sample mixture filled up the lysis chamber and the mixing chamber at first. Then the exceed sample solution in the inlet reservoir was replaced by FC-40, and the sample solution inside the chip was introduced into the digital chamber array via μAPPAD strategy, with 10 sec of pulling step and 0.5 sec of pushing step. Once the sample digitization was done, the pneumatic chamber above the digital array and the anti-evaporation layer would be filled with water, and the chip was sealed with a glass slide by using epoxy glue. The chip was then replaced on an in-situ adapter (T5000-A-IS, Benchmark, NJ, USA) in a thermal cycler (TC 9639, Benchmark, NJ, USA) for on-chip digital one-step RT-PCR, with reverse transcription at 50 ℃ for 5 min, reverse transcriptase denaturation at 95 ℃ for 3 min, denaturation at 95 ℃ for 15 sec and annealing/extending at 60 ℃ for 60 sec for 40 cycles, finally holding at 4 ℃. The fluorescence image of the digital area on the chip was taken with a Prime 95B sCMOS camera (Photometrics, AZ, USA) equipped on a fluorescence microscope (Eclipse Ti2, Nikon, NY, USA). The image was analyzed with ImageJ (NIH, MD, USA).

Preparation of the anti-CD81 coated magnetic beads

The anti-CD81 was coated on Dynabeads® M-270 carboxylic acid via NHS-amine cross-linkage according to the manual. Briefly, 100 μL magnetic beads were taken and washed with 25mM MES buffer (pH 5.0). The beads were then incubated

with MES buffer (pH 5.0) containing 25 mg/ml NHS and 25 mg/ul EDC for 30 min at room temperature. After the incubation, the beads were washed with 25 mM MES buffer (pH 5.0) and rotated with 60 µL 1mg/ml anti-CD81 overnight at 4 °C. After the cross-linkage, the beads were washed with 25 mM MES buffer (pH 5.0) and blocked with 1× PBS buffer (pH 7.0) containing 50 mM ethanolamine for 60 min, then washed with 1× PBS buffer (pH 7.0) containing 0.1% BSA and 0.1% Tween® 20, resuspended in 100 µL 1× PBS buffer (pH 7.0) and stored at 4 °C.

Off-chip exosome capture and On-chip exosomal-mRNA one-step dRT-PCR

For the off-chip capture, 1 µL exosome sample was mixed with 1 µL anti-CD81 coated magnetic beads and rotated overnight at 4 °C. The beads were washed with 1× PBS buffer containing 0.1 % (v/v) Tween® 20 and 0.1 % (w/v) BSA twice on the next day. Then the captured exosome would be ready for loading onto the chip. The RT-PCR master solution was prepared right before the on-chip mRNA detection. The master solution consisted of 20 µL of 2× Reaction Mix, 0.8 µL of Superscript III RT/ Platinum Taq mix, 0.4 µL of 20 µM forward and reverse primers, 2 µL of 2 % (v/v) Tween® 20, 2 µL of 20× EvaGreen Dye, 2 µL of 40 U/µL RNase inhibitor and 10.8 µL RNase-free water, for a total volume of 38 µL.

For the on-chip mRNA digital RT-PCR, the Bio-Rad iScript™ RT-qPCR Sample Preparation Reagent, as the lysis buffer, was pre-loaded to the lysis chamber at first. The inlet reservoir was washed with 1× PBS buffer for three times to clean out the remaining lysis buffer. The beads were then introduced into the inlet reservoir by using pipette and then dragged into the lysis chamber by a magnet under the chip. The chip was incubated at room temperature for 5 min for the on-chip lysis, meanwhile, the

solution in the inlet reservoir was replaced by the RT-PCR master solution. Once the incubation for lysis was finished, the exosome lysate and the RT-PCR master would be filled into the mixing chamber via dead-end filling. The exceeded master buffer remaining at the inlet reservoir was replaced by FC-40. When holding the chip on ice, the lysate was mixed with the RT-PCR solution homogeneously by the periodically pumping controlled by the pneumatic chamber above. After mixing, the sample mixture was introduced into the digital chamber array via μAPPAD strategy. After the sample digitization, the chip was filled with water and sealed with a glass slide on top, placed in a thermal cycler for on-chip one-step dRT-PCR, with reverse transcription at 50 °C for 5 min, reverse transcriptase denaturation at 95 °C for 3 min, denaturation at 95 °C for 15 sec and annealing/extending at 60 °C for 60 sec for 40 cycles.

Absolute quantitation of GAPDH mRNA in exosomes derived from MBA-MD-231 cell line with conventional one-step RT-ddPCR

Total RNA extraction was performed on 20 μL exosomes (9.45×10^8 exosomes/μl) derived from MDA-MB-231 cell line with RNAqueous™-Micro Total RNA Isolation Kit (Invitrogen), per the manufacturer's protocol. The conventional one-step RT-ddPCR was completed according to the manufacturer's manual. Briefly, the reaction mixture was prepared by mixing 1 μL total RNA extracted from the exosome sample, 5 μL of 2× Supermix, 2 μL of 200 U/μL Reverse Transcriptase, 1 μL of 300 mM DTT, 1 μL of Human GAPDH PrimePCR™ Probe Assay and 10 μL of RNase Free water for a total volume of 20 μL. The one-step RT-ddPCR was carried out on the QX200™ Droplet Digital™ PCR System (Bio-Rad). The thermal cycling condition was: 60 min at 50 °C; 10 min at 95 °C; 30 s at 95 °C, 1 min at 60 °C for 40 cycles; 10 min at 98 °C.

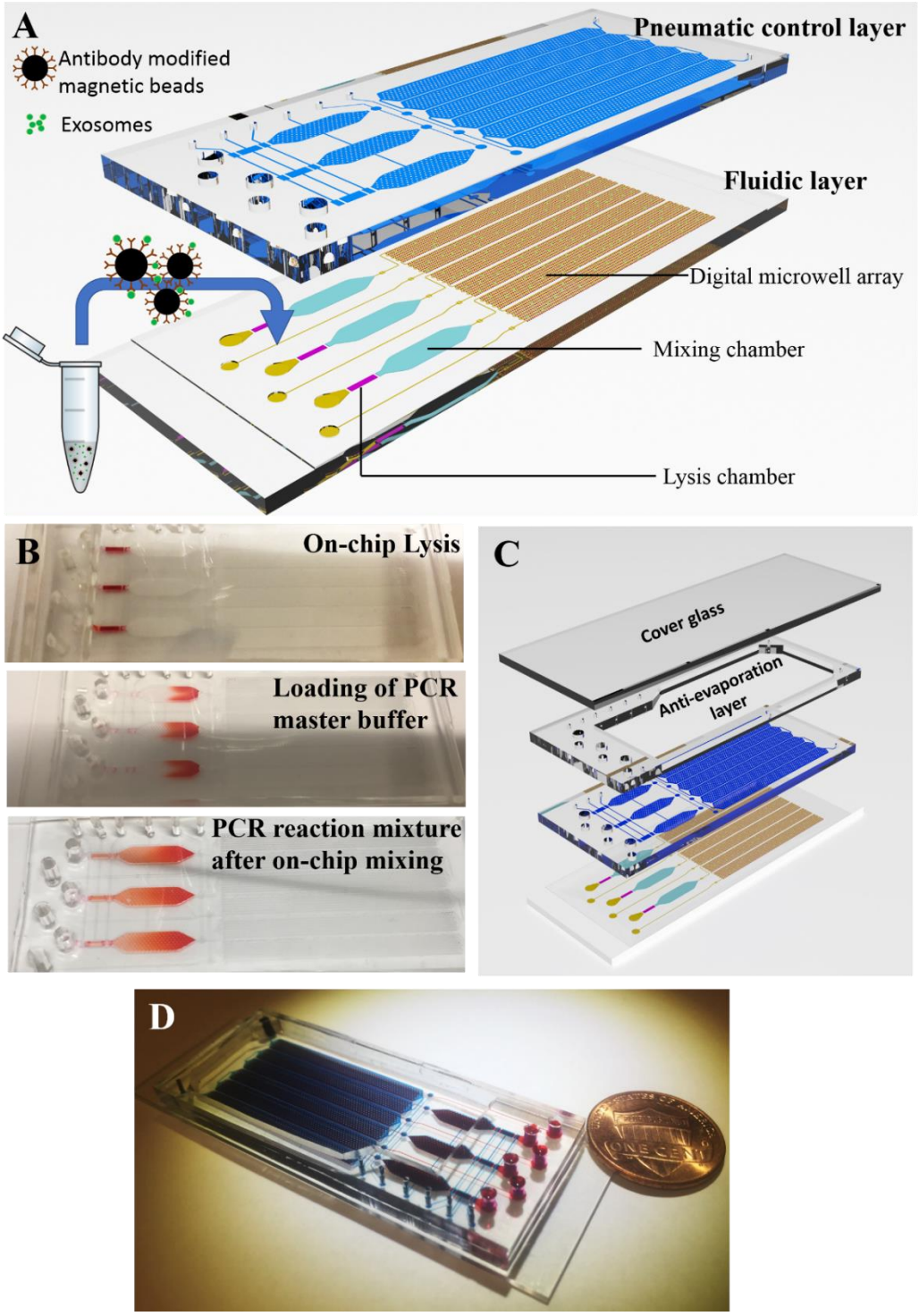

Figure 5-1. Illustration of the microfluidic platform for exosomal mRNA quantitation. (A) Schematic of pneumatic layer and fluidic layer for on-chip lysis, PCR reaction mixture preparation and sample digitization. (B) Images of the red food dye demonstration of the on-chip sample preparation before sample digitization, including lysis, PCR master buffer loading and on-chip mixing. (C) Illustration of the chip components before loading to chip onto thermal cycler. (D) An image of an assembled chip, with red dye filled in the fluidic channels and blue dye filled in pneumatic channels.

Results and Discussion

Chip design and the on-chip exosomal RNA detection workflow

Our microfluidic platform integrates on-chip exosome lysis, PCR reaction mixture preparation, and digital one-step RT-PCR for mRNA quantitation. As illustrated in Figure 5-1A, the chip consists of a pneumatic control layer and a fluidic layer. The pneumatic layer contains 50 μm high pneumatic circuits, used to control all the lifting-gate valves[101] and provide the vacuum for the dead-end filling for the sample loading and digitization. The fluidic layer consists of three parallel channels, and each channel contains a lysis chamber, a mixing chamber and a digital microwell array. The 100 μm high lysis chamber is where the magnetic bead-captured exosomes get lysed. As shown in Figure 5-1B, after the lysis, the PCR master buffer loaded at the input reservoir is introduced into the chip by the dead-end filling, carrying the exosome lysate into the 100 μm high mixing chamber. The mixture is mixed thoroughly by the reciprocating pumping of the pneumatic control chamber located above the mixing chamber. Then the reaction mixture is dispensed into the digital microwell array via alternating-push-pull active digitization method.[253] As demonstrated in Figure 5-1C, a water-filled anti-evaporation layer and a cover glass are employed to prevent the evaporation during the PCR reaction. An assembled chip is shown in Figure 5-1D, where the top cover glass was not installed for clearer sight.

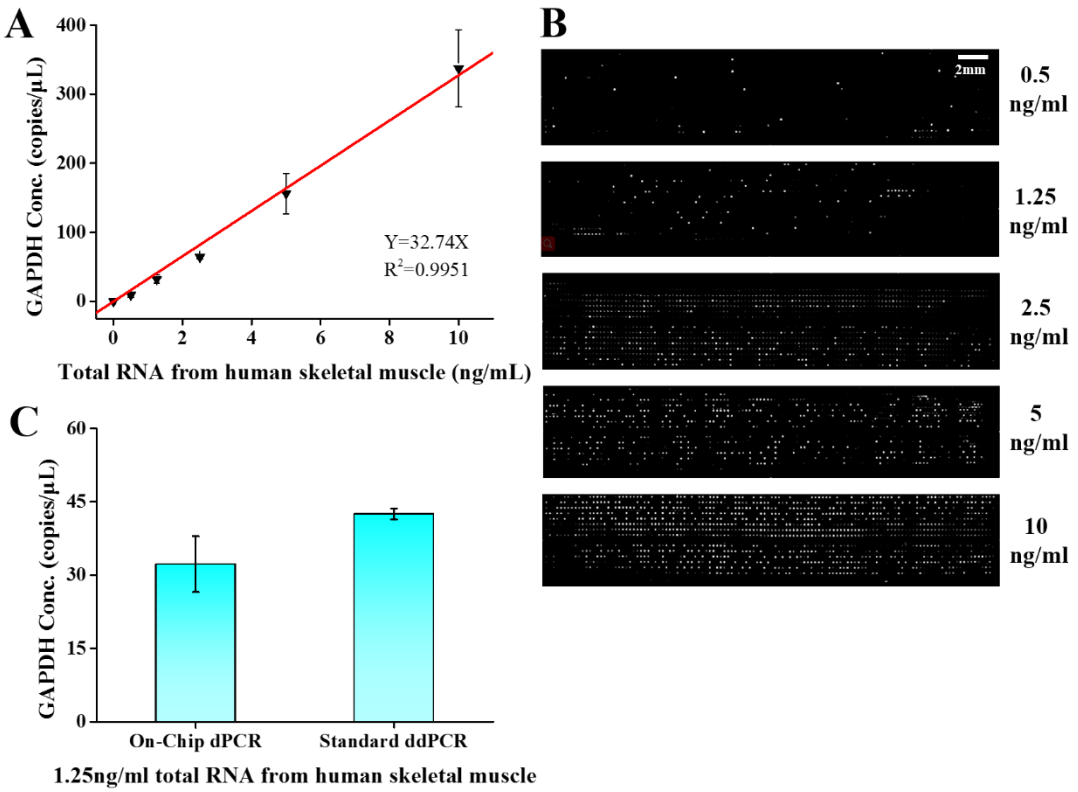

Figure 5-2. Absolute quantitation of GAPDH mRNA in human skeletal muscle total RNA. (A) On-chip GAPDH mRNA quantitation on series dilute total RNA samples (n=3). (B) Fluorescent images taken at the digital microwell array area for detection of GAPDH mRNA in different concentrations of human skeletal muscle total RNA (n=3). (C) Comparison of GAPDH mRNA quantitation result between the on-chip dPCR and the conventional ddPCR on 1.25 ng/ml human skeletal muscle total RNA sample.

On-chip absolute mRNA quantitation in human skeletal muscle total RNA

To investigate the analytical performance of the on-chip digital one-step RT-PCR module, the absolute quantitation of GAPDH mRNA in the human skeletal muscle total RNA was carried out via the on-chip approach. The copy number of the GAPDH mRNA was calculated based on Poisson statistic, as described previously.[253] As depicted in Figure 5-2A, a good linear relationship (R^2=0.9951) was obtained, and 9.27 ± 2.99 copies/μL GAPDH mRNA was detected in 0.5 ng/mL human skeletal muscle

total RNA. Examples of the fluorescent images of the on-chip dPCR GAPDH quantitation were demonstrated in Figure 5-2B. In addition, conventional ddPCR was performed to quantitatively measure the GAPDH mRNA in 1.25 ng/mL total RNA sample as a validation. As illustrated in Figure 5-2C, the concentration of GAPDH mRNA measured by on-chip dPCR (32.24 ± 5.72 copies/μL) matched the result of the conventional ddPCR (42.50 ± 1.14 copies/μL). These results revealed that the dPCR module integrated in our microfluidic platform is capable for absolute quantitative measurement of mRNA with high sensitivity and robustness, and its analytical performance is competitive compared to the conventional ddPCR method.

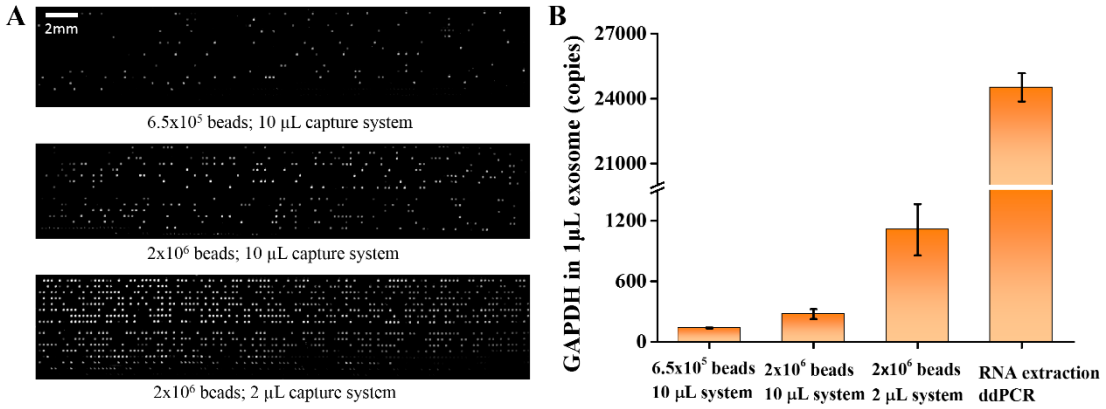

Figure 5-3. On-chip exosomal GAPDH mRNA detection. (A) Fluorescent images of on-chip GAPDH mRNA in exosomes from MDA-MB-231 cell line. (B) Results of GAPDH mRNA quantitation under different capture condition (n=3).

On-chip exosomal mRNA detection in exosome sample

To evaluate the capability to detect mRNA in exosome samples, the microfluidic platform was employed to target the GAPDH mRNA in the exosome of MDA-MB-231 cell line. The exosome sample was kindly provided by Dr. Liang Xu's Lab from the department of molecular biosciences of the University of Kansas, with a concentration of 9.45×10^{8} exosomes/μL measured by nanoparticle tracking analysis (NTA). 1 μL exosome was captured by antiCD-81 labeled magnetic beads, and being

loaded onto the microfluidic platform for GAPDH mRNA quantitation. The total copy number of the GAPDH mRNA was calculate was on the Poisson Statistic. As shown in Figure 5-3A, off-chip exosome immunoaffinity capture was performed in different conditions for the purpose of optimization. As demonstrated in Figure 5-3B, capturing 1 μL exosome with 2×10^6 beads in overall 10 μL capture system obtained higher on-chip GAPDH mRNA readout (274.51 ± 49.31 copies) than that with 6.5×10^5 beads (137.74 ± 3.85). Moreover, capturing 1 μL exosome with 2×10^6 beads in an overall 2 μL capture system gained even higher on-chip GAPDH mRNA readout (1110.44 ± 254.70 copies). These results suggested that a higher capture efficiency of the off-chip exosome bead-based enrichment was determined by more beads and smaller capture volume. However, it is noted that 1 μL of the exosome sample contained 24515.72 ± 655.00 copies of GAPDH mRNA, which was measured by the conventional one-step RT-ddPCR method. This data revealed that although the on-chip exosomal mRNA detection method performed well in a qualitative measure, its off-chip capture and the on-chip lysis still needs to be further optimized to achieve accurate quantitative measurement.

Conclusion

We have developed an exosomal mRNA detection approach that involves off-chip bead-based exosome enrichment, on-chip lysis, and on-chip one-step digital RT-PCR for mRNA quantitation. The microfluidic platform was capable of highly sensitive mRNA absolute quantitation without the requirement of a calibration curve. However, at this point, this approach is only capable of qualitative detection of mRNA in exosome, and further optimization of the off-chip enrichment and the on-chip lysis is still needed

to achieve the final goal of quantitative measurement of exosomal mRNA. We believe this method eventually can be utilized on the application for early cancer diagnosis by detecting the mutation gene transcripts that are encapsulated in exosomes, such as the EWS-FLI-1 transcript for Ewing Sarcoma.

Chapter 6. Conclusions and future plans

Summary of the thesis

Circulating miRNAs and exosomal mRNAs are promising biomarkers for the early cancer diagnosis via liquid biopsy. However, the detection of circulating miRNAs and exosomal mRNAs is challenging due to their low abundance in blood. Real-time reverse transcription polymerase chain reaction (RT-qPCR) is the gold standard for both miRNAs and mRNAs quantitation, but it requires labor-intensive total RNA extraction, large sample consumption, and expensive instrumentation. The aim of this dissertation is to seek for easy-to-use and economy alternative approach for the quantitative measurement of circulating miRNAs and exosomal mRNA.

For the detection of circulating miRNAs, our motivation is to develop a simple, inexpensive method that can be applied on various demands. As described in Chapter 2, we designed an automatic microfluidic platform that integrated the target miRNA enrichment and on-chip miRNA detection functions in a single workflow. This device took advantage of the Duplex specific nuclease signal amplification (DSNSA) mediated miRNA detection, which is a sensitive isothermal enzymatic amplification approach that does not require sophisticated temperature control via expensive instrumentations. Our method improved the sensitivity of DSNSA, reduced the cost of each assay, and prevented the possible contamination during sample preparation. This is the first microfluidic device designed for expediting the DSNSA-mediated miRNA detection approach. We believe this on-chip approach can be useful in many applications, including clinical diagnosis.

It is challenging to detect exosomal mRNAs due to their low abundance among

exosomes and the small portion of tumor-derived exosomes among total exosomes in plasma samples. Therefore, for the detection of exosomal mRNAs, our motivation is to seek out solutions that can greatly improve the speed and yield of the exosome isolation and enrichment and sensitively measure the mRNAs within exosomes. In Chapter 3, we described a nano-HB chip designed for high-efficient enrichment of exosome in plasma samples based on immunoaffinity capture. For the mRNA profiling, this device was coupled with droplet digital PCR, which is an ultra-sensitive approach with the capability of absolute quantitative measurement. Our nano-NB chip coupled with ddPCR method successfully realized highly sensitive detection of exosomal mRNA profiling. However, the captured exosome needed to be eluted and collected, undergoing total RNA extraction, reverse transcription and ddPCR for the final mRNA profiling. These complicated processing steps make the method labor-intensive and expensive. Also, sample loss cannot be avoided during sample processing, and potential contamination may occur. To address this problem, the whole processing must be integrated altogether within one device and automation must be enabled.

To develop a highly integrated microfluidic system for convenient, rapid, and sensitive exosomal mRNA detection, one of the most important portions is to embed the digital PCR (dPCR) module into the device. However, conventional solutions to achieve on-chip dPCR suffered from a sample-loss issue during the sample dispensing process, which caused sensitivity reduction. In Chapter 4, we introduced a microfluidic alternating-pull–push active digitization (μAPPAD) method to address this problem. This automatic approach achieved a high sample digitization efficiency by using pneumatic valve control to periodically manipulate air pressure inside the chip to greatly facilitate the vacuum-driven partition of solution into microwells. With this method, sample-loss-free on-chip dPCR can thus be achieved, which made us one step

closer to the goal of developing an integrated exosomal mRNA detection platform.

In my on-going project, which was introduced in Chapter 5, we attempted to integrate the off-chip magnetic bead-based immunoaffinity exosome enrichment, on-chip lysis, PCR reaction mixture preparation and the on-chip digital one-step RT-PCR functions in a single device. The chip performed well on mRNA quantitation in total RNA samples, and qualitative detection can be achieved in exosome samples isolated from cell culture media. Further optimizations on the off-chip exosome capture and the on-chip lysis are still demanded for the goal of quantitatively measure the mRNA with exosomes.

Future plans

To enable the quantitative measurement of exosomal mRNA in our integrated exosomal mRNA detection system, optimizations on the off-chip exosome capture and the on-chip lysis are required, as mentioned above. Although a qualitative detection was achieved for the GAPDH in the MDA-MB-231 exosome sample, the concentration obtained from our microfluidic system was way much lower than that from conventional coupling method of total RNA extraction and droplet digital one-step RT-PCR, indicating either a low capture efficiency of the off-chip exosome capture, or a failure of the on-chip lysis. To investigate the capture performance of the off-chip exosome capture, a series of experiments need to be done. The capture efficiency can be obtained by testing exosome's tetraspanins (e.g. CD81, CD9, CD63) in the supernatant before and after the bead capture. If the capture efficiency is not satisfactory, further optimization must be done, including adjusting the number of beads used for capture and the density of antibody immobilized on the bead surface. For the on-chip

lysis, although the lysis buffer was obtained from a commercial kit which was claimed to have a lysis efficiency over 95 %, unsatisfactory lysis still could occur because the lysis buffer might diffuse into the inlet reservoir when the magnetic beads were being transferred into the lysis chamber, leading to a decrease of lysis reagent concentration. If so, we need to adjust the concentration of the lysis buffer. Also, alternative lysis reagents (e.g. Triton X-100) can be applied if the current lysis buffer does not work. Once the issues are solved and the exosomal mRNA quantitation can be achieved, we plan to apply our highly integrated microfluidic exosomal mRNA detection system in the clinical diagnosis of Ewing Sarcoma by detecting the exosomal EWS-FLI-1 fusion transcript in patients' plasma. As mentioned previously, the EWS-FLI-1 mutation is specific to the Ewing Sarcoma, caused by chromosomal translocation.[48] The EWS-FLI-1 mRNA was observed not only in the tumor cells but also in the tumor-derived exosomes in the bloodstream.[119, 254] We believe our approach is able to facilitate the clinical diagnosis of Ewing Sarcoma via liquid biopsy.

Moreover, there is still room for improvement in our integrated microfluidic exosomal mRNA analysis system. In the current design, an overnight off-chip bead-based exosome enrichment step was required, which was time-consuming and might introduce contamination when transferring samples to the chip. To address this problem, we plan to integrate the nano-HB exosome-capture module into the mRNA analysis chip. Thus, a fully automatic microfluidic total analysis system for exosomal mRNA analysis can be developed, involving functions of on-chip exosome enrichment, on-chip lysis, PCR reaction mix preparation and on-chip digital one-step RT-PCR. We envision that this platform can contribute to not only the exosomal mRNAs profiling, but also the detection of exosomal miRNAs and lncRNA. Besides its applications related to exosome, we believe our microfluidic system can be applied to broad

applications, e.g. Viral RNA analysis.

Reference

1. Siegel, R. L.; Miller, K. D.; Jemal, A., Cancer statistics, 2020. *CA: A Cancer Journal for Clinicians* **2020,** *70* (1), 7-30.
2. Perakis, S.; Speicher, M. R., Emerging concepts in liquid biopsies. *BMC medicine* **2017,** *15* (1), 75.
3. Halpern, E. J., Contrast-enhanced ultrasound imaging of prostate cancer. *Reviews in urology* **2006,** *8* (Suppl 1), S29.
4. Zhi, H.; Ou, B.; Luo, B.-M.; Feng, X.; Wen, Y.-L.; Yang, H.-Y., Comparison of ultrasound elastography, mammography, and sonography in the diagnosis of solid breast lesions. *Journal of ultrasound in medicine* **2007,** *26* (6), 807-815.
5. Cheng, H.-D.; Shan, J.; Ju, W.; Guo, Y.; Zhang, L., Automated breast cancer detection and classification using ultrasound images: A survey. *Pattern recognition* **2010,** *43* (1), 299-317.
6. Henschke, C. I., Computed tomography screening for lung cancer: principles and results. *Clinical cancer research* **2005,** *11* (13), 4984s-4987s.
7. Swensen, S. J.; Jett, J. R.; Hartman, T. E.; Midthun, D. E.; Sloan, J. A.; Sykes, A.-M.; Aughenbaugh, G. L.; Clemens, M. A., Lung cancer screening with CT: Mayo Clinic experience. *Radiology* **2003,** *226* (3), 756-761.
8. Bach, P. B.; Jett, J. R.; Pastorino, U.; Tockman, M. S.; Swensen, S. J.; Begg, C. B., Computed tomography screening and lung cancer outcomes. *Jama* **2007,** *297* (9), 953-961.
9. Lowe, V. J.; Boyd, J. H.; Dunphy, F. R.; Kim, H.; Dunleavy, T.; Collins, B. T.; Martin, D.; Stack Jr, B. C.; Hollenbeak, C.; Fletcher, J., Surveillance for recurrent head and neck cancer using positron emission tomography. *Journal of clinical oncology* **2000,** *18* (3), 651-651.
10. Tsuyoshi, H.; Yoshida, Y., Diagnostic imaging using positron emission tomography for gynecological malignancy. *Journal of Obstetrics and Gynaecology Research* **2017,** *43* (11), 1687-1699.
11. Nahas, C. S.; Akhurst, T.; Yeung, H.; Riedel, E.; Markowitz, A. J.; Minsky, B. D.; Paty, P. B.; Weiser, M. R.; Temple, L. K.; Wong, W. D., Positron emission tomography detection of distant metastatic or synchronous disease in patients with locally advanced rectal cancer receiving preoperative chemoradiation. *Annals of surgical oncology* **2008,** *15* (3), 704-711.
12. DeMartini, W.; Lehman, C.; Partridge, S., Breast MRI for cancer detection and characterization: a review of evidence-based clinical applications. *Academic radiology* **2008,** *15* (4), 408-416.
13. Morrow, M.; Waters, J.; Morris, E., MRI for breast cancer screening, diagnosis, and treatment. *The Lancet* **2011,** *378* (9805), 1804-1811.
14. Brix, G.; Lechel, U.; Glatting, G.; Ziegler, S. I.; Münzing, W.; Müller, S. P.; Beyer, T., Radiation exposure of patients undergoing whole-body dual-modality 18F-FDG PET/CT examinations. *Journal of Nuclear Medicine* **2005,** *46* (4), 608-613.
15. Chawla, S. C.; Federman, N.; Zhang, D.; Nagata, K.; Nuthakki, S.; McNitt-Gray, M.; Boechat, M. I., Estimated cumulative radiation dose from PET/CT in children with malignancies: a 5-year retrospective review. *Pediatric radiology* **2010,** *40* (5), 681-686.

16. Miglioretti, D. L.; Johnson, E.; Williams, A.; Greenlee, R. T.; Weinmann, S.; Solberg, L. I.; Feigelson, H. S.; Roblin, D.; Flynn, M. J.; Vanneman, N., The use of computed tomography in pediatrics and the associated radiation exposure and estimated cancer risk. *JAMA pediatrics* **2013,** *167* (8), 700-707.
17. Mouliere, F.; Robert, B.; Arnau Peyrotte, E.; Del Rio, M.; Ychou, M.; Molina, F.; Gongora, C.; Thierry, A. R., High Fragmentation Characterizes Tumour-Derived Circulating DNA. *PLOS ONE* **2011,** *6* (9), e23418.
18. Diehl, F.; Schmidt, K.; Choti, M. A.; Romans, K.; Goodman, S.; Li, M.; Thornton, K.; Agrawal, N.; Sokoll, L.; Szabo, S. A., Circulating mutant DNA to assess tumor dynamics. *Nature medicine* **2008,** *14* (9), 985.
19. Parkinson, D. R.; Dracopoli, N.; Petty, B. G.; Compton, C.; Cristofanilli, M.; Deisseroth, A.; Hayes, D. F.; Kapke, G.; Kumar, P.; Lee, J. S., Considerations in the development of circulating tumor cell technology for clinical use. *Journal of translational medicine* **2012,** *10* (1), 138.
20. Young, R.; Pailler, E.; Billiot, F.; Drusch, F.; Barthelemy, A.; Oulhen, M.; Besse, B.; Soria, J.-C.; Farace, F.; Vielh, P., Circulating tumor cells in lung cancer. *Acta cytologica* **2012,** *56* (6), 655-660.
21. Bidard, F.-C.; Michiels, S.; Riethdorf, S.; Mueller, V.; Esserman, L. J.; Lucci, A.; Naume, B.; Horiguchi, J.; Gisbert-Criado, R.; Sleijfer, S., Circulating tumor cells in breast cancer patients treated by neoadjuvant chemotherapy: a meta-analysis. *JNCI: Journal of the National Cancer Institute* **2018,** *110* (6), 560-567.
22. El-Heliebi, A.; Hille, C.; Laxman, N.; Svedlund, J.; Haudum, C.; Ercan, E.; Kroneis, T.; Chen, S.; Smolle, M.; Rossmann, C., In situ detection and quantification of AR-V7, AR-FL, PSA, and KRAS point mutations in circulating tumor cells. *Clinical chemistry* **2018,** *64* (3), 536-546.
23. Harding, C. V.; Heuser, J. E.; Stahl, P. D., Exosomes: looking back three decades and into the future. *J Cell Biol* **2013,** *200* (4), 367-371.
24. Kowal, J.; Tkach, M.; Théry, C., Biogenesis and secretion of exosomes. *Current opinion in cell biology* **2014,** *29*, 116-125.
25. Colombo, M.; Raposo, G.; Théry, C., Biogenesis, secretion, and intercellular interactions of exosomes and other extracellular vesicles. *Annual review of cell and developmental biology* **2014,** *30*, 255-289.
26. Weidle, U. H.; Birzele, F.; Kollmorgen, G.; Rueger, R., The multiple roles of exosomes in metastasis. *Cancer Genomics-Proteomics* **2017,** *14* (1), 1-15.
27. He, M.; Zeng, Y., Microfluidic exosome analysis toward liquid biopsy for cancer. *Journal of laboratory automation* **2016,** *21* (4), 599-608.
28. Théry, C.; Zitvogel, L.; Amigorena, S., Exosomes: composition, biogenesis and function. *Nature reviews immunology* **2002,** *2* (8), 569-579.
29. Pan, B.-T.; Johnstone, R. M., Fate of the transferrin receptor during maturation of sheep reticulocytes in vitro: selective externalization of the receptor. *Cell* **1983,** *33* (3), 967-978.
30. Azmi, A. S.; Bao, B.; Sarkar, F. H., Exosomes in cancer development, metastasis, and drug resistance: a comprehensive review. *Cancer and Metastasis Reviews* **2013,** *32* (3-4), 623-642.
31. Tang, M. K.; Wong, A. S., Exosomes: Emerging biomarkers and targets for ovarian cancer. *Cancer letters* **2015,** *367* (1), 26-33.
32. Bobrie, A.; Théry, C., Exosomes and communication between tumours and the immune system: are all exosomes equal? *Biochemical Society Transactions* **2013,** *41* (1), 263-267.
33. Valadi, H.; Ekström, K.; Bossios, A.; Sjöstrand, M.; Lee, J. J.; Lötvall, J. O.,

Exosome-mediated transfer of mRNAs and microRNAs is a novel mechanism of genetic exchange between cells. *Nature cell biology* **2007,** *9* (6), 654-659.
34. Skog, J.; Würdinger, T.; Van Rijn, S.; Meijer, D. H.; Gainche, L.; Curry, W. T.; Carter, B. S.; Krichevsky, A. M.; Breakefield, X. O., Glioblastoma microvesicles transport RNA and proteins that promote tumour growth and provide diagnostic biomarkers. *Nature cell biology* **2008,** *10* (12), 1470-1476.
35. Théry, C.; Amigorena, S.; Raposo, G.; Clayton, A., Isolation and characterization of exosomes from cell culture supernatants and biological fluids. *Current protocols in cell biology* **2006,** *30* (1), 3.22. 1-3.22. 29.
36. Tauro, B. J.; Greening, D. W.; Mathias, R. A.; Ji, H.; Mathivanan, S.; Scott, A. M.; Simpson, R. J., Comparison of ultracentrifugation, density gradient separation, and immunoaffinity capture methods for isolating human colon cancer cell line LIM1863-derived exosomes. *Methods* **2012,** *56* (2), 293-304.
37. Salih, M.; Zietse, R.; Hoorn, E. J., Urinary extracellular vesicles and the kidney: biomarkers and beyond. *American Journal of Physiology-Renal Physiology* **2014,** *306* (11), F1251-F1259.
38. Taylor, D. D.; Shah, S., Methods of isolating extracellular vesicles impact down-stream analyses of their cargoes. *Methods* **2015,** *87*, 3-10.
39. Taylor, D. D.; Zacharias, W.; Gercel-Taylor, C., Exosome isolation for proteomic analyses and RNA profiling. In *Serum/plasma proteomics*, Springer: 2011; pp 235-246.
40. Gámez-Valero, A.; Monguió-Tortajada, M.; Carreras-Planella, L.; Beyer, K.; Borràs, F. E., Size-Exclusion Chromatography-based isolation minimally alters Extracellular Vesicles' characteristics compared to precipitating agents. *Scientific reports* **2016,** *6*, 33641.
41. Andreu, Z.; Rivas, E.; Sanguino-Pascual, A.; Lamana, A.; Marazuela, M.; González-Alvaro, I.; Sánchez-Madrid, F.; de la Fuente, H.; Yáñez-Mó, M., Comparative analysis of EV isolation procedures for miRNAs detection in serum samples. *Journal of extracellular vesicles* **2016,** *5* (1), 31655.
42. Greening, D. W.; Xu, R.; Ji, H.; Tauro, B. J.; Simpson, R. J., A protocol for exosome isolation and characterization: evaluation of ultracentrifugation, density-gradient separation, and immunoaffinity capture methods. In *Proteomic Profiling*, Springer: 2015; pp 179-209.
43. Oksvold, M. P.; Neurauter, A.; Pedersen, K. W., Magnetic bead-based isolation of exosomes. In *RNA Interference*, Springer: 2015; pp 465-481.
44. Soller, M., Pre-messenger RNA processing and its regulation: a genomic perspective. *Cellular and Molecular Life Sciences CMLS* **2006,** *63* (7-8), 796-819.
45. Vaklavas, C.; Blume, S. W.; Grizzle, W. E., Translational dysregulation in cancer: molecular insights and potential clinical applications in biomarker development. *Frontiers in oncology* **2017,** *7*, 158.
46. Bhat, M.; Robichaud, N.; Hulea, L.; Sonenberg, N.; Pelletier, J.; Topisirovic, I., Targeting the translation machinery in cancer. *Nature reviews Drug discovery* **2015,** *14* (4), 261-278.
47. Leibovitch, M.; Topisirovic, I., Dysregulation of mRNA translation and energy metabolism in cancer. *Advances in biological regulation* **2018,** *67*, 30-39.
48. Cidre-Aranaz, F.; Alonso, J., EWS/FLI1 target genes and therapeutic opportunities in Ewing sarcoma. *Frontiers in oncology* **2015,** *5*, 162.
49. Lin, F.; van Rhee, F.; Goldman, J.; Cross, N., Kinetics of increasing BCR-ABL transcript numbers in chronic myeloid leukemia patients who relapse after bone marrow transplantation. *Blood* **1996,** *87* (10), 4473-4478.

50. Froggatt, N. J.; Brassett, C.; Koch, D. J.; Evans, D.; Hodgson, S. V.; Ponder, B.; Maher, E. R., Mutation screening of MSH2 and MLH1 mRNA in hereditary non-polyposis colon cancer syndrome. *Journal of medical genetics* **1996,** *33* (9), 726-730.
51. El-Mahdani, N.; Vaillant, J.; Guiguet, M.; Prevot, S.; Bertrand, V.; Bernard, C.; Parc, R.; Bereziat, G.; Hermelin, B., Overexpression of p53 mRNA in colorectal cancer and its relationship to p53 gene mutation. *British journal of cancer* **1997,** *75* (4), 528-536.
52. Kopreski, M. S.; Benko, F. A.; Kwak, L. W.; Gocke, C. D., Detection of tumor messenger RNA in the serum of patients with malignant melanoma. *Clinical cancer research* **1999,** *5* (8), 1961-1965.
53. Wong, S. C. C.; Lo, S. F. E.; Cheung, M. T.; Ng, K. O. E.; Tse, C. W.; Lai, B. S. P.; Lee, K. C.; Lo, Y. D., Quantification of plasma β-catenin mRNA in colorectal cancer and adenoma patients. *Clinical Cancer Research* **2004,** *10* (5), 1613-1617.
54. Chen, X. Q.; Bonnefoi, H.; Pelte, M.-F.; Lyautey, J.; Lederrey, C.; Movarekhi, S.; Schaeffer, P.; Mulcahy, H. E.; Meyer, P.; Stroun, M., Telomerase RNA as a detection marker in the serum of breast cancer patients. *Clinical cancer research: an official journal of the American Association for Cancer Research* **2000,** *6* (10), 3823-3826.
55. Kopreski, M. S.; Benko, F. A.; Gocke, C. D., Circulating RNA as a tumor marker: detection of 5T4 mRNA in breast and lung cancer patient serum. *Annals of the New York Academy of Sciences* **2001,** *945* (1), 172-178.
56. Li, Y.; Elashoff, D.; Oh, M.; Sinha, U.; St John, M.; Zhou, X.; Abemayor, E.; Wong, D. T., Serum circulating human mRNA profiling and its utility for oral cancer detection. *J Clin Oncol* **2006,** *24* (11), 1754-1760.
57. Fugazzola, L.; Mihalich, A.; Persani, L.; Cerutti, N.; Reina, M.; Bonomi, M.; Ponti, E.; Mannavola, D.; Giammona, E.; Vannucchi, G., Highly sensitive serum thyroglobulin and circulating thyroglobulin mRNA evaluations in the management of patients with differentiated thyroid cancer in apparent remission. *The Journal of Clinical Endocrinology & Metabolism* **2002,** *87* (7), 3201-3208.
58. Di Liegro, C. M.; Schiera, G.; Di Liegro, I., Extracellular vesicle‐associated RNA as a carrier of epigenetic information. *Genes* **2017,** *8* (10), 240.
59. Wei, F.; Yang, J.; Wong, D. T., Detection of exosomal biomarker by electric field-induced release and measurement (EFIRM). *Biosensors and Bioelectronics* **2013,** *44*, 115-121.
60. Reddi, K.; Holland, J. F., Elevated serum ribonuclease in patients with pancreatic cancer. *Proceedings of the National Academy of Sciences* **1976,** *73* (7), 2308-2310.
61. Velu, V. K.; Ramesh, R.; Srinivasan, A., Circulating microRNAs as biomarkers in health and disease. *Journal of clinical and diagnostic research: JCDR* **2012,** *6* (10), 1791.
62. Almeida, M. I.; Reis, R. M.; Calin, G. A., MicroRNA history: discovery, recent applications, and next frontiers. *Mutation Research/Fundamental and Molecular Mechanisms of Mutagenesis* **2011,** *717* (1-2), 1-8.
63. Siomi, H.; Siomi, M. C., Posttranscriptional regulation of microRNA biogenesis in animals. *Molecular cell* **2010,** *38* (3), 323-332.
64. Yekta, S.; Shih, I.-h.; Bartel, D. P., MicroRNA-directed cleavage of HOXB8 mRNA. *Science* **2004,** *304* (5670), 594-596.
65. Zeng, Y.; Yi, R.; Cullen, B. R., MicroRNAs and small interfering RNAs can inhibit mRNA expression by similar mechanisms. *Proceedings of the National Academy of Sciences* **2003,** *100* (17), 9779-9784.

66. Bruce, J. P.; Hui, A. B.; Shi, W.; Perez-Ordonez, B.; Weinreb, I.; Xu, W.; Haibe-Kains, B.; Waggott, D. M.; Boutros, P. C.; O'Sullivan, B., Identification of a microRNA signature associated with risk of distant metastasis in nasopharyngeal carcinoma. *Oncotarget* **2015,** *6* (6), 4537.
67. Esquela-Kerscher, A.; Slack, F. J., Oncomirs—microRNAs with a role in cancer. *Nature reviews cancer* **2006,** *6* (4), 259-269.
68. Gantier, M. P.; McCoy, C. E.; Rusinova, I.; Saulep, D.; Wang, D.; Xu, D.; Irving, A. T.; Behlke, M. A.; Hertzog, P. J.; Mackay, F., Analysis of microRNA turnover in mammalian cells following Dicer1 ablation. *Nucleic acids research* **2011,** *39* (13), 5692-5703.
69. Kasinski, A. L.; Slack, F. J., MicroRNAs en route to the clinic: progress in validating and targeting microRNAs for cancer therapy. *Nature Reviews Cancer* **2011,** *11* (12), 849-864.
70. Sanders, R.; Bustin, S.; Huggett, J.; Mason, D., Improving the standardization of mRNA measurement by RT-qPCR. *Biomolecular detection and quantification* **2018,** *15*, 13-17.
71. Fan, J.-B., *Next-generation MicroRNA expression profiling technology: methods and protocols*. Springer: 2012.
72. Chen, C.; Ridzon, D. A.; Broomer, A. J.; Zhou, Z.; Lee, D. H.; Nguyen, J. T.; Barbisin, M.; Xu, N. L.; Mahuvakar, V. R.; Andersen, M. R., Real-time quantification of microRNAs by stem–loop RT–PCR. *Nucleic acids research* **2005,** *33* (20), e179-e179.
73. Meehan, K.; Clynick, B.; Mirzai, B.; Maslen, P.; Harvey, J.; Erber, W., HER2 mRNA transcript quantitation in breast cancer. *Clinical and Translational Oncology* **2017,** *19* (5), 606-615.
74. Wang, P.; Jing, F.; Li, G.; Wu, Z.; Cheng, Z.; Zhang, J.; Zhang, H.; Jia, C.; Jin, Q.; Mao, H., Absolute quantification of lung cancer related microRNA by droplet digital PCR. *Biosensors and Bioelectronics* **2015,** *74*, 836-842.
75. Baskerville, S.; Bartel, D. P., Microarray profiling of microRNAs reveals frequent coexpression with neighboring miRNAs and host genes. *Rna* **2005,** *11* (3), 241-247.
76. Kuo, W. P.; Jenssen, T.-K.; Butte, A. J.; Ohno-Machado, L.; Kohane, I. S., Analysis of matched mRNA measurements from two different microarray technologies. *Bioinformatics* **2002,** *18* (3), 405-412.
77. AC't Hoen, P.; Friedländer, M. R.; Almlöf, J.; Sammeth, M.; Pulyakhina, I.; Anvar, S. Y.; Laros, J. F.; Buermans, H. P.; Karlberg, O.; Brännvall, M., Reproducibility of high-throughput mRNA and small RNA sequencing across laboratories. *Nature biotechnology* **2013,** *31* (11), 1015.
78. Whitley, S. K.; Horne, W. T.; Kolls, J. K., Research techniques made simple: methodology and clinical applications of RNA sequencing. *Journal of Investigative Dermatology* **2016,** *136* (8), e77-e82.
79. Lisak, G.; Cui, J.; Bobacka, J., Paper-based microfluidic sampling for potentiometric determination of ions. *Sensors & Actuators: B. Chemical* **2015,** *207* (PB), 933-939.
80. Bhattacharjee, S.; Bhattacharya, B. B.; Chakrabarty, K., *Algorithms for Sample Preparation with Microfluidic Lab-on-Chip*. River Publishers: 2019.
81. Lung-Ming, F.; Chin-Lung, C.; Yao-Nan, W.; Chia-Yen, L., Microfluidic Mixing: A Review. *International Journal of Molecular Sciences* **2011,** *12* (5), 3263-3287.
82. Chen, C.; Skog, J.; Hsu, C.-h.; Lessard, R. T.; Balaj, L.; Wurdinger, T.;

Carter, B. S.; Breakefield, X. O.; Toner, M.; Irimia, D., Microfluidic isolation and transcriptome analysis of serum microvesicles. *Lab on a Chip* **2010,** *10* (4), 505-511.
83. Yang, F.; Liao, X.; Tian, Y.; Li, G., Exosome separation using microfluidic systems: size ‐ based, immunoaffinity ‐ based and dynamic methodologies. *Biotechnology Journal* **2017,** *12* (4), 1600699.
84. Viskari, P. J.; Landers, J. P., Unconventional detection methods for microfluidic devices. Weinheim, 2006; Vol. 27, pp 1797-1810.
85. Cygan, Z. T.; Cabral, J. T.; Beers, K. L.; Amis, E. J., Microfluidic platform for the generation of organic-phase microreactors. *Langmuir* **2005,** *21* (8), 3629-3634.
86. Li, L.-L.; Li, X.; Wang, H., Microfluidic Synthesis of Nanomaterials for Biomedical Applications. *Small Methods* **2017,** *1* (8), 1700140.
87. Song, Y.; Hormes, J.; Kumar, C. S. S. R., Microfluidic Synthesis of Nanomaterials. Weinheim, 2008; Vol. 4, pp 698-711.
88. Antia, M.; Herricks, T.; Rathod, P. K., Microfluidic approaches to malaria pathogenesis. Oxford, UK, 2008; Vol. 10, pp 1968-1974.
89. Kim, M. S.; Kim, T.; Kong, S.-Y.; Kwon, S.; Bae, C. Y.; Choi, J.; Kim, C. H.; Lee, E. S.; Park, J.-K., Breast Cancer Diagnosis Using a Microfluidic Multiplexed Immunohistochemistry Platform (Microfluidic Cancer Diagnosis). *PLoS ONE* **2010,** *5* (5), e10441.
90. Zhao, Z.; Yang, Y.; Zeng, Y.; He, M., A microfluidic ExoSearch chip for multiplexed exosome detection towards blood-based ovarian cancer diagnosis. *Lab on a Chip* **2016,** *16* (3), 489-496.
91. Liu, R. H.; Lee, A. P.; Lee, A. P., Integrated biochips for DNA analysis. Austin, Tex. : Landes Bioscience

New York : Springer Science+Business Media: Austin, Tex. : New York, 2007.
92. Fan, J.-B., *Next-generation MicroRNA expression profiling technology : methods and protocols*. New York : Humana Press: New York, 2012.
93. Sinkala, E.; Sollier-Christen, E.; Renier, C.; Rosas-Canyelles, E.; Che, J.; Heirich, K.; Duncombe, T. A.; Vlassakis, J.; Yamauchi, K. A.; Huang, H., Profiling protein expression in circulating tumour cells using microfluidic western blotting. *Nature communications* **2017,** *8* (1), 1-12.
94. Lecault, V.; White, A. K.; Singhal, A.; Hansen, C. L., Microfluidic single cell analysis: from promise to practice. *Current opinion in chemical biology* **2012,** *16* (3-4), 381-390.
95. Yun, H.; Kim, K.; Lee, W. G., Cell manipulation in microfluidics. 2013; Vol. 5, p 022001.
96. Kang, L.; Chung, B. G.; Langer, R.; Khademhosseini, A., Microfluidics for drug discovery and development: from target selection to product lifecycle management. *Drug discovery today* **2008,** *13* (1-2), 1-13.
97. Zhang, X.; Haswell, S. J., Materials matter in microfluidic devices. *MRS bulletin* **2006,** *31* (2), 95-99.
98. Becker, H.; Gärtner, C., Polymer microfabrication technologies for microfluidic systems. *Analytical and Bioanalytical Chemistry* **2008,** *390* (1), 89-111.
99. Leclerc, E.; Sakai, Y.; Fujii, T., Cell culture in 3-dimensional microfluidic structure of PDMS (polydimethylsiloxane). *Biomedical microdevices* **2003,** *5* (2), 109-114.
100. Xu, L.; Lee, H.; Jetta, D.; Oh, K. W., Vacuum-driven power-free microfluidics utilizing the gas solubility or permeability of polydimethylsiloxane (PDMS). *Lab Chip* **2015,** *15* (20), 3962-3979.

101. Kim, J.; Kang, M.; Jensen, E. C.; Mathies, R. A., Lifting gate polydimethylsiloxane microvalves and pumps for microfluidic control. *Analytical chemistry* **2012,** *84* (4), 2067-2071.
102. Unger, M. A.; Chou, H.-P.; Thorsen, T.; Scherer, A.; Quake, S. R., Monolithic microfabricated valves and pumps by multilayer soft lithography. *Science* **2000,** *288* (5463), 113-116.
103. Oh, K. W.; Ahn, C. H., A review of microvalves. 2006; Vol. 16, pp R13-R39.
104. Schudel, B. R.; Choi, C. J.; Cunningham, B. T.; Kenis, P. J. A., Microfluidic chip for combinatorial mixing and screening of assays. *Lab on a Chip* **2009,** *9* (12), 1676-1680.
105. Grover, W. H.; Skelley, A. M.; Liu, C. N.; Lagally, E. T.; Mathies, R. A., Monolithic membrane valves and diaphragm pumps for practical large-scale integration into glass microfluidic devices. *Sensors & Actuators: B. Chemical* **2003,** *89* (3), 315-323.
106. White, A. K.; VanInsberghe, M.; Petriv, I.; Hamidi, M.; Sikorski, D.; Marra, M. A.; Piret, J.; Aparicio, S.; Hansen, C. L., High-throughput microfluidic single-cell RT-qPCR. *Proceedings of the National Academy of Sciences* **2011,** *108* (34), 13999-14004.
107. White, A.; Heyries, K.; Doolin, C.; Vaninsberghe, M.; Hansen, C., High-throughput microfluidic single-cell digital polymerase chain reaction. *Analytical chemistry* **2013,** *85* (15), 7182-7190.
108. Cao, H.; Zhou, X.; Zeng, Y., Microfluidic exponential rolling circle amplification for sensitive microRNA detection directly from biological samples. *Sensors and Actuators B: Chemical* **2019,** *279*, 447-457.
109. Guo, S.; Lin, W. N.; Hu, Y.; Sun, G.; Phan, D.-T.; Chen, C.-H., Ultrahigh-throughput droplet microfluidic device for single-cell miRNA detection with isothermal amplification. *Lab on a Chip* **2018,** *18* (13), 1914-1920.
110. Zhang, K.; Kang, D.-K.; Ali, M. M.; Liu, L.; Labanieh, L.; Lu, M.; Riazifar, H.; Nguyen, T. N.; Zell, J. A.; Digman, M. A., Digital quantification of miRNA directly in plasma using integrated comprehensive droplet digital detection. *Lab on a Chip* **2015,** *15* (21), 4217-4226.
111. Zhang, H.; Liu, Y.; Fu, X.; Yuan, L.; Zhu, Z., Microfluidic bead-based assay for microRNAs using quantum dots as labels and enzymatic amplification. *Microchimica Acta* **2015,** *182* (3-4), 661-669.
112. Lee, H.; Shapiro, S. J.; Chapin, S. C.; Doyle, P. S., Encoded hydrogel microparticles for sensitive and multiplex microRNA detection directly from raw cell lysates. *Analytical chemistry* **2016,** *88* (6), 3075-3081.
113. Chapin, S. C.; Doyle, P. S., Ultrasensitive multiplexed microRNA quantification on encoded gel microparticles using rolling circle amplification. *Analytical chemistry* **2011,** *83* (18), 7179-7185.
114. Haider, M.; Ji, B.; Haselgrübler, T.; Sonnleitner, A.; Aberger, F.; Hesse, J., A microfluidic multiwell chip for enzyme-free detection of mRNA from few cells. *Biosensors and Bioelectronics* **2016,** *86*, 20-26.
115. Marcus, J. S.; Anderson, W. F.; Quake, S. R., Microfluidic single-cell mRNA isolation and analysis. *Analytical chemistry* **2006,** *78* (9), 3084-3089.
116. Thompson, A. M.; Gansen, A.; Paguirigan, A. L.; Kreutz, J. E.; Radich, J. P.; Chiu, D. T., Self-Digitization Microfluidic Chip for Absolute Quantification of mRNA in Single Cells. *Analytical Chemistry* **2014,** *86* (24), 12308-12314.
117. Mohamadi, R. M.; Ivanov, I.; Stojcic, J.; Nam, R. K.; Sargent, E. H.; Kelley, S. O., Sample-to-answer isolation and mRNA profiling of circulating tumor cells.

Analytical chemistry **2015,** *87* (12), 6258-6264.
118. Shao, H.; Chung, J.; Lee, K.; Balaj, L.; Min, C.; Carter, B. S.; Hochberg, F. H.; Breakefield, X. O.; Lee, H.; Weissleder, R., Chip-based analysis of exosomal mRNA mediating drug resistance in glioblastoma. *Nature communications* **2015,** *6* (1), 1-9.
119. Zhang, P.; Crow, J.; Lella, D.; Zhou, X.; Samuel, G.; Godwin, A. K.; Zeng, Y., Ultrasensitive quantification of tumor mRNAs in extracellular vesicles with an integrated microfluidic digital analysis chip. *Lab on a Chip* **2018,** *18* (24), 3790-3801.
120. Keller, A.; Leidinger, P.; Bauer, A.; ElSharawy, A.; Haas, J.; Backes, C.; Wendschlag, A.; Giese, N.; Tjaden, C.; Ott, K., Toward the blood-borne miRNome of human diseases. *Nature methods* **2011,** *8* (10), 841.
121. Sempere, L. F., Tissue slide-based microRNA characterization of tumors: how detailed could diagnosis become for cancer medicine? *Expert review of molecular diagnostics* **2014,** *14* (7), 853-869.
122. Galimberti, D.; Villa, C.; Fenoglio, C.; Serpente, M.; Ghezzi, L.; Cioffi, S. M.; Arighi, A.; Fumagalli, G.; Scarpini, E., Circulating miRNAs as potential biomarkers in Alzheimer's disease. *Journal of Alzheimer's Disease* **2014,** *42* (4), 1261-1267.
123. Weber, J. A.; Baxter, D. H.; Zhang, S.; Huang, D. Y.; How Huang, K.; Jen Lee, M.; Galas, D. J.; Wang, K., The microRNA spectrum in 12 body fluids. *Clinical chemistry* **2010,** *56* (11), 1733-1741.
124. Feng, J.; Xing, W.; Xie, L., Regulatory roles of microRNAs in diabetes. *International journal of molecular sciences* **2016,** *17* (10), 1729.
125. Femminella, G. D.; Ferrara, N.; Rengo, G., The emerging role of microRNAs in Alzheimer's disease. *Frontiers in physiology* **2015,** *6*, 40.
126. Farazi, T. A.; Spitzer, J. I.; Morozov, P.; Tuschl, T., miRNAs in human cancer. *The Journal of pathology* **2011,** *223* (2), 102-115.
127. Di Leva, G.; Croce, C. M., miRNA profiling of cancer. *Current opinion in genetics & development* **2013,** *23* (1), 3-11.
128. Tiberio, P.; Callari, M.; Angeloni, V.; Daidone, M. G.; Appierto, V., Challenges in using circulating miRNAs as cancer biomarkers. *BioMed research international* **2015,** *2015*.
129. Benes, V.; Castoldi, M., Expression profiling of microRNA using real-time quantitative PCR, how to use it and what is available. *Methods* **2010,** *50* (4), 244-249.
130. Redshaw, N.; Wilkes, T.; Whale, A.; Cowen, S.; Huggett, J.; Foy, C. A., A comparison of miRNA isolation and RT-qPCR technologies and their effects on quantification accuracy and repeatability. *Biotechniques* **2013,** *54* (3), 155-64.
131. Bissels, U.; Wild, S.; Tomiuk, S.; Holste, A.; Hafner, M.; Tuschl, T.; Bosio, A., Absolute quantification of microRNAs by using a universal reference. *Rna* **2009,** *15* (12), 2375-2384.
132. Git, A.; Dvinge, H.; Salmon-Divon, M.; Osborne, M.; Kutter, C.; Hadfield, J.; Bertone, P.; Caldas, C., Systematic comparison of microarray profiling, real-time PCR, and next-generation sequencing technologies for measuring differential microRNA expression. *Rna* **2010,** *16* (5), 991-1006.
133. Jensen, S. G.; Lamy, P.; Rasmussen, M. H.; Ostenfeld, M. S.; Dyrskjøt, L.; Ørntoft, T. F.; Andersen, C. L., Evaluation of two commercial global miRNA expression profiling platforms for detection of less abundant miRNAs. *BMC genomics* **2011,** *12* (1), 435.
134. Anisimova, V. E.; Rebrikov, D. V.; Shagin, D. A.; Kozhemyako, V. B.; Menzorova, N. I.; Staroverov, D. B.; Ziganshin, R.; Vagner, L. L.; Rasskazov, V. A.;

Lukyanov, S. A., Isolation, characterization and molecular cloning of Duplex-Specific Nuclease from the hepatopancreas of the Kamchatka crab. *BMC biochemistry* **2008,** *9* (1), 14.
135. Yin, B.-C.; Liu, Y.-Q.; Ye, B.-C., One-step, multiplexed fluorescence detection of microRNAs based on duplex-specific nuclease signal amplification. *Journal of the American Chemical Society* **2012,** *134* (11), 5064-5067.
136. Degliangeli, F.; Kshirsagar, P.; Brunetti, V.; Pompa, P. P.; Fiammengo, R., Absolute and direct microRNA quantification using DNA–gold nanoparticle probes. *Journal of the American Chemical Society* **2014,** *136* (6), 2264-2267.
137. Shen, W.; Gao, Z., Quantum dots and duplex-specific nuclease enabled ultrasensitive detection and serotyping of Dengue viruses in one step in a single tube. *Biosensors and Bioelectronics* **2015,** *65*, 327-332.
138. Lu, L.; Yang, B.; Kang, T., A dual amplification strategy for ultrasensitive detection of microRNA. *Applied Surface Science* **2017,** *426*, 597-604.
139. Zhang, K.; Wang, K.; Zhu, X.; Xu, F.; Xie, M., Sensitive detection of microRNA in complex biological samples by using two stages DSN-assisted target recycling signal amplification method. *Biosensors and Bioelectronics* **2017,** *87*, 358-364.
140. Bo, B.; Zhang, T.; Jiang, Y.; Cui, H.; Miao, P., Triple Signal Amplification Strategy for Ultrasensitive Determination of MiRNA Based on Duplex Specific Nuclease and Bridge DNA-Gold Nanoparticles. *Analytical chemistry* **2018**.
141. Reyes, D. R.; Iossifidis, D.; Auroux, P.-A.; Manz, A., Micro total analysis systems. 1. Introduction, theory, and technology. *Analytical chemistry* **2002,** *74* (12), 2623-2636.
142. Dittrich, P. S.; Tachikawa, K.; Manz, A., Micro total analysis systems. Latest advancements and trends. *Analytical chemistry* **2006,** *78* (12), 3887-3908.
143. Vilkner, T.; Janasek, D.; Manz, A., Micro total analysis systems. Recent developments. *Analytical chemistry* **2004,** *76* (12), 3373-3386.
144. Zeng, Y.; Wang, T., Quantitative microfluidic biomolecular analysis for systems biology and medicine. *Analytical and bioanalytical chemistry* **2013,** *405* (17), 5743-5758.
145. Sato, K.; Tachihara, A.; Renberg, B.; Mawatari, K.; Sato, K.; Tanaka, Y.; Jarvius, J.; Nilsson, M.; Kitamori, T., Microbead-based rolling circle amplification in a microchip for sensitive DNA detection. *Lab on a Chip* **2010,** *10* (10), 1262-1266.
146. Chapin, S. C.; Appleyard, D. C.; Pregibon, D. C.; Doyle, P. S., Rapid microRNA profiling on encoded gel microparticles. *Angewandte Chemie International Edition* **2011,** *50* (10), 2289-2293.
147. Ishihara, R.; Hasegawa, K.; Hosokawa, K.; Maeda, M., Multiplex MicroRNA detection on a power-free microfluidic chip with laminar flow-assisted dendritic amplification. *Analytical Sciences* **2015,** *31* (7), 573-576.
148. Arata, H.; Komatsu, H.; Hosokawa, K.; Maeda, M., Rapid and Sensitive MicroRNA Detection with Laminar Flow-Assisted Dendritic Amplification on Power-Free Microfluidic Chip (Sensitive MicroRNA Detection on Microfluidic Chip). *PLOS ONE* **2012,** *7* (11), e48329.
149. McArdle, H.; Jimenez-Mateos, E. M.; Raoof, R.; Carthy, E.; Boyle, D.; ElNaggar, H.; Delanty, N.; Hamer, H.; Dogan, M.; Huchtemann, T., "TORNADO"–Theranostic One-Step RNA Detector; microfluidic disc for the direct detection of microRNA-134 in plasma and cerebrospinal fluid. *Scientific reports* **2017,** *7* (1), 1-11.
150. Li, X.; Rout, P.; Xu, R.; Pan, L.; Tchounwou, P. B.; Ma, Y.; Liu, Y.-M., Quantification of microRNAs by coupling cyclic enzymatic amplification with

microfluidic voltage-assisted liquid desorption electrospray ionization mass spectrometry. *Analytical chemistry* **2018,** *90* (22), 13663-13669.
151. Zeng, Y.; Novak, R.; Shuga, J.; Smith, M. T.; Mathies, R. A., High-performance single cell genetic analysis using microfluidic emulsion generator arrays. *Analytical chemistry* **2010,** *82* (8), 3183-3190.
152. Cheng, L.; Sharples, R. A.; Scicluna, B. J.; Hill, A. F., Exosomes provide a protective and enriched source of miRNA for biomarker profiling compared to intracellular and cell-free blood. *Journal of extracellular vesicles* **2014,** *3* (1), 23743.
153. Wang, T.; Zhang, M.; Dreher, D. D.; Zeng, Y., Ultrasensitive microfluidic solid-phase ELISA using an actuatable microwell-patterned PDMS chip. *Lab on a Chip* **2013,** *13* (21), 4190-4197.
154. Schwarzenbach, H.; Nishida, N.; Calin, G. A.; Pantel, K., Clinical relevance of circulating cell-free microRNAs in cancer. *Nature reviews Clinical oncology* **2014,** *11* (3), 145.
155. Haber, D. A.; Velculescu, V. E., Blood-based analyses of cancer: circulating tumor cells and circulating tumor DNA. *Cancer discovery* **2014,** *4* (6), 650-661.
156. Im, H.; Shao, H.; Park, Y. I.; Peterson, V. M.; Castro, C. M.; Weissleder, R.; Lee, H., Label-free detection and molecular profiling of exosomes with a nano-plasmonic sensor. *Nature biotechnology* **2014,** *32* (5), 490.
157. Yáñez-Mó, M.; Siljander, P. R.-M.; Andreu, Z.; Bedina Zavec, A.; Borràs, F. E.; Buzas, E. I.; Buzas, K.; Casal, E.; Cappello, F.; Carvalho, J., Biological properties of extracellular vesicles and their physiological functions. *Journal of extracellular vesicles* **2015,** *4* (1), 27066.
158. Atay, S.; Banskota, S.; Crow, J.; Sethi, G.; Rink, L.; Godwin, A. K., Oncogenic KIT-containing exosomes increase gastrointestinal stromal tumor cell invasion. *Proceedings of the National Academy of Sciences* **2014,** *111* (2), 711-716.
159. Melo, S. A.; Luecke, L. B.; Kahlert, C.; Fernandez, A. F.; Gammon, S. T.; Kaye, J.; LeBleu, V. S.; Mittendorf, E. A.; Weitz, J.; Rahbari, N., Glypican-1 identifies cancer exosomes and detects early pancreatic cancer. *Nature* **2015,** *523* (7559), 177-182.
160. Zhang, P.; He, M.; Zeng, Y., Ultrasensitive microfluidic analysis of circulating exosomes using a nanostructured graphene oxide/polydopamine coating. *Lab on a Chip* **2016,** *16* (16), 3033-3042.
161. Squires, T. M.; Messinger, R. J.; Manalis, S. R., Making it stick: convection, reaction and diffusion in surface-based biosensors. *Nature biotechnology* **2008,** *26* (4), 417-426.
162. Stroock, A. D.; Dertinger, S. K.; Ajdari, A.; Mezić, I.; Stone, H. A.; Whitesides, G. M., Chaotic mixer for microchannels. *Science* **2002,** *295* (5555), 647-651.
163. Shang, Y.; Zeng, Y.; Zeng, Y., Integrated microfluidic lectin barcode platform for high-performance focused glycomic profiling. *Scientific reports* **2016,** *6* (1), 1-11.
164. Kelley, S. O.; Mirkin, C. A.; Walt, D. R.; Ismagilov, R. F.; Toner, M.; Sargent, E. H., Advancing the speed, sensitivity and accuracy of biomolecular detection using multi-length-scale engineering. *Nature nanotechnology* **2014,** *9* (12), 969.
165. Soleymani, L.; Fang, Z.; Sargent, E. H.; Kelley, S. O., Programming the detection limits of biosensors through controlled nanostructuring. *Nature nanotechnology* **2009,** *4* (12), 844.
166. Bin, X.; Sargent, E. H.; Kelley, S. O., Nanostructuring of sensors determines the efficiency of biomolecular capture. *Analytical chemistry* **2010,** *82* (14), 5928-5931.
167. Wang, S.; Wang, H.; Jiao, J.; Chen, K. J.; Owens, G. E.; Kamei, K. i.; Sun,

J.; Sherman, D. J.; Behrenbruch, C. P.; Wu, H., Three‐dimensional nanostructured substrates toward efficient capture of circulating tumor cells. *Angewandte Chemie International Edition* **2009,** *48* (47), 8970-8973.
168. Chen, G. D.; Fachin, F.; Fernandez‐Suarez, M.; Wardle, B. L.; Toner, M., Nanoporous elements in microfluidics for multiscale manipulation of bioparticles. *Small* **2011,** *7* (8), 1061-1067.
169. Chen, G. D.; Fachin, F.; Colombini, E.; Wardle, B. L.; Toner, M., Nanoporous micro-element arrays for particle interception in microfluidic cell separation. *Lab on a Chip* **2012,** *12* (17), 3159-3167.
170. Fachin, F.; Chen, G. D.; Toner, M.; Wardle, B. L., Integration of bulk nanoporous elements in microfluidic devices with application to biomedical diagnostics. *Journal of microelectromechanical systems* **2011,** *20* (6), 1428-1438.
171. Zeng, Y.; Harrison, D. J., Self-assembled colloidal arrays as three-dimensional nanofluidic sieves for separation of biomolecules on microchips. *Analytical chemistry* **2007,** *79* (6), 2289-2295.
172. Wang, S.; Liu, K.; Liu, J.; Yu, Z. T. F.; Xu, X.; Zhao, L.; Lee, T.; Lee, E. K.; Reiss, J.; Lee, Y. K., Highly efficient capture of circulating tumor cells by using nanostructured silicon substrates with integrated chaotic micromixers. *Angewandte Chemie International Edition* **2011,** *50* (13), 3084-3088.
173. Stott, S. L.; Hsu, C.-H.; Tsukrov, D. I.; Yu, M.; Miyamoto, D. T.; Waltman, B. A.; Rothenberg, S. M.; Shah, A. M.; Smas, M. E.; Korir, G. K., Isolation of circulating tumor cells using a microvortex-generating herringbone-chip. *Proceedings of the National Academy of Sciences* **2010,** *107* (43), 18392-18397.
174. Singh, G.; Pillai, S.; Arpanaei, A.; Kingshott, P., Multicomponent colloidal crystals that are tunable over large areas. *Soft Matter* **2011,** *7* (7), 3290-3294.
175. Nazemifard, N.; Wang, L.; Ye, W.; Bhattacharjee, S.; Masliyah, J. H.; Harrison, D. J., A systematic evaluation of the role of crystalline order in nanoporous materials on DNA separation. *Lab on a Chip* **2012,** *12* (1), 146-152.
176. Adams, A. A.; Okagbare, P. I.; Feng, J.; Hupert, M. L.; Patterson, D.; Göttert, J.; McCarley, R. L.; Nikitopoulos, D.; Murphy, M. C.; Soper, S. A., Highly efficient circulating tumor cell isolation from whole blood and label-free enumeration using polymer-based microfluidics with an integrated conductivity sensor. *Journal of the American Chemical Society* **2008,** *130* (27), 8633-8641.
177. Forbes, T. P.; Kralj, J. G., Engineering and analysis of surface interactions in a microfluidic herringbone micromixer. *Lab on a Chip* **2012,** *12* (15), 2634-2637.
178. Sheng, W.; Ogunwobi, O. O.; Chen, T.; Zhang, J.; George, T. J.; Liu, C.; Fan, Z. H., Capture, release and culture of circulating tumor cells from pancreatic cancer patients using an enhanced mixing chip. *Lab on a Chip* **2014,** *14* (1), 89-98.
179. Reátegui, E.; van der Vos, K. E.; Lai, C. P.; Zeinali, M.; Atai, N. A.; Aldikacti, B.; Floyd, F. P.; Khankhel, A. H.; Thapar, V.; Hochberg, F. H., Engineered nanointerfaces for microfluidic isolation and molecular profiling of tumor-specific extracellular vesicles. *Nature communications* **2018,** *9* (1), 1-11.
180. Domcke, S.; Sinha, R.; Levine, D. A.; Sander, C.; Schultz, N., Evaluating cell lines as tumour models by comparison of genomic profiles. *Nature communications* **2013,** *4* (1), 1-10.
181. Wan, Y.; Cheng, G.; Liu, X.; Hao, S.-J.; Nisic, M.; Zhu, C.-D.; Xia, Y.-Q.; Li, W.-Q.; Wang, Z.-G.; Zhang, W.-L., Rapid magnetic isolation of extracellular vesicles via lipid-based nanoprobes. *Nature biomedical engineering* **2017,** *1* (4), 1-11.
182. Davies, R. T.; Kim, J.; Jang, S. C.; Choi, E.-J.; Gho, Y. S.; Park, J.,

Microfluidic filtration system to isolate extracellular vesicles from blood. *Lab on a Chip* **2012,** *12* (24), 5202-5210.
183. Yang, J.; Choi, M. K.; Kim, D. H.; Hyeon, T., Designed assembly and integration of colloidal nanocrystals for device applications. *Advanced materials* **2016,** *28* (6), 1176-1207.
184. Kim, J.; Li, Z.; Park, I., Direct synthesis and integration of functional nanostructures in microfluidic devices. *Lab on a Chip* **2011,** *11* (11), 1946-1951.
185. Jeon, S.; Malyarchuk, V.; White, J. O.; Rogers, J. A., Optically fabricated three dimensional nanofluidic mixers for microfluidic devices. *Nano letters* **2005,** *5* (7), 1351-1356.
186. Park, S.-G.; Lee, S.-K.; Moon, J. H.; Yang, S.-M., Holographic fabrication of three-dimensional nanostructures for microfluidic passive mixing. *Lab on a Chip* **2009,** *9* (21), 3144-3150.
187. Hu, Y.; Lao, Z.; Cumming, B. P.; Wu, D.; Li, J.; Liang, H.; Chu, J.; Huang, W.; Gu, M., Laser printing hierarchical structures with the aid of controlled capillary-driven self-assembly. *Proceedings of the National Academy of Sciences* **2015,** *112* (22), 6876-6881.
188. Cederquist, K. B.; Kelley, S. O., Nanostructured biomolecular detectors: pushing performance at the nanoscale. *Current opinion in chemical biology* **2012,** *16* (3-4), 415-421.
189. Vogel, N.; Retsch, M.; Fustin, C.-A.; del Campo, A.; Jonas, U., Advances in colloidal assembly: the design of structure and hierarchy in two and three dimensions. *Chemical reviews* **2015,** *115* (13), 6265-6311.
190. Kuijk, A.; Van Blaaderen, A.; Imhof, A., Synthesis of monodisperse, rodlike silica colloids with tunable aspect ratio. *Journal of the American Chemical Society* **2011,** *133* (8), 2346-2349.
191. Brychta, N.; Krahn, T.; von Ahsen, O., Detection of KRAS mutations in circulating tumor DNA by digital PCR in early stages of pancreatic cancer. *Clinical chemistry* **2016,** *62* (11), 1482-1491.
192. Debrand, E.; Lykoudi, A.; Bradshaw, E.; Allen, S. K., A non-invasive droplet digital PCR (ddPCR) assay to detect paternal CFTR mutations in the cell-free fetal DNA (cffDNA) of three pregnancies at risk of cystic fibrosis via compound heterozygosity. *PloS one* **2015,** *10* (11), e0142729.
193. Del Re, M.; Tiseo, M.; Bordi, P.; D'Incecco, A.; Camerini, A.; Petrini, I.; Lucchesi, M.; Inno, A.; Spada, D.; Vasile, E., Contribution of KRAS mutations and c. 2369C> T (p. T790M) EGFR to acquired resistance to EGFR-TKIs in EGFR mutant NSCLC: a study on circulating tumor DNA. *Oncotarget* **2017,** *8* (8), 13611.
194. Malapelle, U.; de Luca, C.; Vigliar, E.; Ambrosio, F.; Rocco, D.; Pisapia, P.; Bellevicine, C.; Troncone, G., EGFR mutation detection on routine cytological smears of non-small cell lung cancer by digital PCR: a validation study. *Journal of clinical pathology* **2016,** *69* (5), 454-457.
195. Sanmamed, M. F.; Fernández-Landázuri, S.; Rodríguez, C.; Zárate, R.; Lozano, M. D.; Zubiri, L.; Perez-Gracia, J. L.; Martín-Algarra, S.; González, A., Quantitative cell-free circulating BRAFV600E mutation analysis by use of droplet digital PCR in the follow-up of patients with melanoma being treated with BRAF inhibitors. *Clinical chemistry* **2015,** *61* (1), 297-304.
196. Thierry, A. R.; Mouliere, F.; El Messaoudi, S.; Mollevi, C.; Lopez-Crapez, E.; Rolet, F.; Gillet, B.; Gongora, C.; Dechelotte, P.; Robert, B., Clinical validation of the detection of KRAS and BRAF mutations from circulating tumor DNA. *Nature medicine* **2014,** *20* (4), 430.

197. Thress, K. S.; Brant, R.; Carr, T. H.; Dearden, S.; Jenkins, S.; Brown, H.; Hammett, T.; Cantarini, M.; Barrett, J. C., EGFR mutation detection in ctDNA from NSCLC patient plasma: a cross-platform comparison of leading technologies to support the clinical development of AZD9291. *Lung cancer* **2015,** *90* (3), 509-515.
198. Dube, S.; Qin, J.; Ramakrishnan, R., Mathematical analysis of copy number variation in a DNA sample using digital PCR on a nanofluidic device. *PloS one* **2008,** *3* (8), e2876.
199. Dube, S.; Qin, J.; Ramakrishnan, R., Method and apparatus for determining copy number variation using digital PCR. Google Patents: 2016.
200. Whale, A. S.; Huggett, J. F.; Cowen, S.; Speirs, V.; Shaw, J.; Ellison, S.; Foy, C. A.; Scott, D. J., Comparison of microfluidic digital PCR and conventional quantitative PCR for measuring copy number variation. *Nucleic acids research* **2012,** *40* (11), e82-e82.
201. Devonshire, A. S.; Honeyborne, I.; Gutteridge, A.; Whale, A. S.; Nixon, G.; Wilson, P.; Jones, G.; McHugh, T. D.; Foy, C. A.; Huggett, J. F., Highly reproducible absolute quantification of Mycobacterium tuberculosis complex by digital PCR. *Analytical chemistry* **2015,** *87* (7), 3706-3713.
202. Zhao, Y.; Xia, Q.; Yin, Y.; Wang, Z., Comparison of droplet digital PCR and quantitative PCR assays for quantitative detection of Xanthomonas citri subsp. citri. *PloS one* **2016,** *11* (7), e0159004.
203. Brunetto, G. S.; Massoud, R.; Leibovitch, E. C.; Caruso, B.; Johnson, K.; Ohayon, J.; Fenton, K.; Cortese, I.; Jacobson, S., Digital droplet PCR (ddPCR) for the precise quantification of human T-lymphotropic virus 1 proviral loads in peripheral blood and cerebrospinal fluid of HAM/TSP patients and identification of viral mutations. *Journal of neurovirology* **2014,** *20* (4), 341-351.
204. Lui, Y. L. E.; Tan, E. L., Droplet digital PCR as a useful tool for the quantitative detection of Enterovirus 71. *Journal of virological methods* **2014,** *207*, 200-203.
205. Rutsaert, S.; Bosman, K.; Trypsteen, W.; Nijhuis, M.; Vandekerckhove, L., Digital PCR as a tool to measure HIV persistence. *Retrovirology* **2018,** *15* (1), 16.
206. Dobnik, D.; Štebih, D.; Blejec, A.; Morisset, D.; Žel, J., Multiplex quantification of four DNA targets in one reaction with Bio-Rad droplet digital PCR system for GMO detection. *Scientific reports* **2016,** *6*, 35451.
207. Gerdes, L.; Iwobi, A.; Busch, U.; Pecoraro, S., Optimization of digital droplet polymerase chain reaction for quantification of genetically modified organisms. *Biomolecular detection and quantification* **2016,** *7*, 9-20.
208. Morisset, D.; Štebih, D.; Milavec, M.; Gruden, K.; Žel, J., Quantitative analysis of food and feed samples with droplet digital PCR. *PloS one* **2013,** *8* (5), e62583.
209. Beer, N. R.; Hindson, B. J.; Wheeler, E. K.; Hall, S. B.; Rose, K. A.; Kennedy, I. M.; Colston, B. W., On-chip, real-time, single-copy polymerase chain reaction in picoliter droplets. *Analytical chemistry* **2007,** *79* (22), 8471-8475.
210. Guan, W.; Chen, L.; Rane, T. D.; Wang, T.-H., Droplet digital enzyme-linked oligonucleotide hybridization assay for absolute RNA quantification. *Scientific reports* **2015,** *5*, 13795.
211. Hindson, B. J.; Ness, K. D.; Masquelier, D. A.; Belgrader, P.; Heredia, N. J.; Makarewicz, A. J.; Bright, I. J.; Lucero, M. Y.; Hiddessen, A. L.; Legler, T. C., High-throughput droplet digital PCR system for absolute quantitation of DNA copy number. *Analytical chemistry* **2011,** *83* (22), 8604-8610.
212. Hindson, C. M.; Chevillet, J. R.; Briggs, H. A.; Gallichotte, E. N.; Ruf, I. K.; Hindson, B. J.; Vessella, R. L.; Tewari, M., Absolute quantification by droplet digital

PCR versus analog real-time PCR. *Nature methods* **2013,** *10* (10), 1003.
213. Link, D.; Anna, S. L.; Weitz, D.; Stone, H. A., Geometrically mediated breakup of drops in microfluidic devices. *Physical review letters* **2004,** *92* (5), 054503.
214. Mazutis, L.; Baret, J.-C.; Treacy, P.; Skhiri, Y.; Araghi, A. F.; Ryckelynck, M.; Taly, V.; Griffiths, A. D., Multi-step microfluidic droplet processing: kinetic analysis of an in vitro translated enzyme. *Lab on a Chip* **2009,** *9* (20), 2902-2908.
215. Strain, M. C.; Lada, S. M.; Luong, T.; Rought, S. E.; Gianella, S.; Terry, V. H.; Spina, C. A.; Woelk, C. H.; Richman, D. D., Highly precise measurement of HIV DNA by droplet digital PCR. *PloS one* **2013,** *8* (4), e55943.
216. Conte, D.; Verri, C.; Borzi, C.; Suatoni, P.; Pastorino, U.; Sozzi, G.; Fortunato, O., Novel method to detect microRNAs using chip-based QuantStudio 3D digital PCR. *BMC genomics* **2015,** *16* (1), 849.
217. Laig, M.; Ho, B.; Majumdar, N. S.; Lac, L. T.; Chan, F.; Sathiyaa, R.; Russel, I.; Cifuentes, P.; Straub, T.; Varma, K., TaqMan® rare mutation assays for QuantStudio® 3D digital PCR system. AACR: 2015.
218. Sefrioui, D.; Sarafan-Vasseur, N.; Beaussire, L.; Baretti, M.; Gangloff, A.; Blanchard, F.; Clatot, F.; Sabourin, J.-C.; Sesboüé, R.; Frebourg, T., Clinical value of chip-based digital-PCR platform for the detection of circulating DNA in metastatic colorectal cancer. *Digestive and Liver Disease* **2015,** *47* (10), 884-890.
219. Ottesen, E. A.; Hong, J. W.; Quake, S. R.; Leadbetter, J. R., Microfluidic digital PCR enables multigene analysis of individual environmental bacteria. *science* **2006,** *314* (5804), 1464-1467.
220. Ma, Y.-D.; Chang, W.-H.; Luo, K.; Wang, C.-H.; Liu, S.-Y.; Yen, W.-H.; Lee, G.-B., Digital quantification of DNA via isothermal amplification on a self-driven microfluidic chip featuring hydrophilic film-coated polydimethylsiloxane. *Biosensors and Bioelectronics* **2018,** *99*, 547-554.
221. Low, H.; Chan, S.-J.; Soo, G.-H.; Ling, B.; Tan, E.-L., Clarity™ digital PCR system: a novel platform for absolute quantification of nucleic acids. *Analytical and bioanalytical chemistry* **2017,** *409* (7), 1869-1875.
222. Pompano, R. R.; Liu, W.; Du, W.; Ismagilov, R. F., Microfluidics using spatially defined arrays of droplets in one, two, and three dimensions. *Annual Review of Analytical Chemistry* **2011,** *4*, 59-81.
223. Zhong, Q.; Bhattacharya, S.; Kotsopoulos, S.; Olson, J.; Taly, V.; Griffiths, A. D.; Link, D. R.; Larson, J. W., Multiplex digital PCR: breaking the one target per color barrier of quantitative PCR. *Lab on a Chip* **2011,** *11* (13), 2167-2174.
224. Yeh, E.-C.; Fu, C.-C.; Hu, L.; Thakur, R.; Feng, J.; Lee, L. P., Self-powered integrated microfluidic point-of-care low-cost enabling (SIMPLE) chip. *Science Advances* **2017,** *3* (3), e1501645.
225. Tian, Q.; Yu, B.; Mu, Y.; Xu, Y.; Ma, C.; Zhang, T.; Jin, W.; Jin, Q., An integrated temporary negative pressure assisted microfluidic chip for DNA isolation and digital PCR detection. *RSC Advances* **2015,** *5* (100), 81889-81896.
226. Zhu, Q.; Qiu, L.; Yu, B.; Xu, Y.; Gao, Y.; Pan, T.; Tian, Q.; Song, Q.; Jin, W.; Jin, Q.; Mu, Y., Digital PCR on an integrated self-priming compartmentalization chip. *Lab on a Chip* **2014,** *14* (6), 1176-1185.
227. Wang, Y.; Southard, K. M.; Zeng, Y., Digital PCR using micropatterned superporous absorbent array chips. *Analyst* **2016,** *141* (12), 3821-3831.
228. Cohen, D. E.; Schneider, T.; Wang, M.; Chiu, D. T., Self-digitization of sample volumes. *Analytical chemistry* **2010,** *82* (13), 5707-5717.
229. Schneider, T.; Yen, G. S.; Thompson, A. M.; Burnham, D. R.; Chiu, D. T., Self-digitization of samples into a high-density microfluidic bottom-well array.

Analytical chemistry **2013,** *85* (21), 10417-10423.
230. Gansen, A.; Herrick, A. M.; Dimov, I. K.; Lee, L. P.; Chiu, D. T., Digital LAMP in a sample self-digitization (SD) chip. *Lab on a Chip* **2012,** *12* (12), 2247-2254.
231. Zhu, Q.; Xu, Y.; Qiu, L.; Ma, C.; Yu, B.; Song, Q.; Jin, W.; Jin, Q.; Liu, J.; Mu, Y., A scalable self-priming fractal branching microchannel net chip for digital PCR. *Lab on a Chip* **2017,** *17* (9), 1655-1665.
232. Shang, Y.; Zeng, Y.; Zeng, Y., Integrated microfluidic lectin barcode platform for high-performance focused glycomic profiling. *Scientific reports* **2016,** *6*, 20297.
233. Xu, L.; Lee, H.; Jetta, D.; Oh, K. W., Vacuum-driven power-free microfluidics utilizing the gas solubility or permeability of polydimethylsiloxane (PDMS). *Lab on a Chip* **2015,** *15* (20), 3962-3979.
234. Zhu, Q.; Qiu, L.; Yu, B.; Xu, Y.; Gao, Y.; Pan, T.; Tian, Q.; Song, Q.; Jin, W.; Jin, Q., Digital PCR on an integrated self-priming compartmentalization chip. *Lab on a Chip* **2014,** *14* (6), 1176-1185.
235. Lee, S. H.; Song, J.; Cho, B.; Hong, S.; Hoxha, O.; Kang, T.; Kim, D.; Lee, L. P., Bubble-free rapid microfluidic PCR. *Biosensors and Bioelectronics* **2019,** *126*, 725-733.
236. Prakash, A. R.; Adamia, S.; Sieben, V.; Pilarski, P.; Pilarski, L.; Backhouse, C., Small volume PCR in PDMS biochips with integrated fluid control and vapour barrier. *Sensors and Actuators B: Chemical* **2006,** *113* (1), 398-409.
237. Heyries, K. A.; Tropini, C.; VanInsberghe, M.; Doolin, C.; Petriv, I.; Singhal, A.; Leung, K.; Hughesman, C. B.; Hansen, C. L., Megapixel digital PCR. *Nature methods* **2011,** *8* (8), 649.
238. Ning, Y.; Cui, X.; Yang, C.; Jing, F.; Bian, X.; Yi, L.; Li, G., A self-digitization chip integrated with hydration layer for low-cost and robust digital PCR. *Analytica chimica acta* **2019,** *1055*, 65-73.
239. Pinheiro, L. B.; Coleman, V. A.; Hindson, C. M.; Herrmann, J.; Hindson, B. J.; Bhat, S.; Emslie, K. R., Evaluation of a droplet digital polymerase chain reaction format for DNA copy number quantification. *Analytical chemistry* **2012,** *84* (2), 1003-1011.
240. Bobrie, A.; Théry, C., Exosomes and communication between tumours and the immune system: are all exosomes equal? Portland Press Ltd.: 2013.
241. Yokoi, A.; Yoshioka, Y.; Yamamoto, Y.; Ishikawa, M.; Ikeda, S.-i.; Kato, T.; Kiyono, T.; Takeshita, F.; Kajiyama, H.; Kikkawa, F., Malignant extracellular vesicles carrying MMP1 mRNA facilitate peritoneal dissemination in ovarian cancer. *Nature communications* **2017,** *8* (1), 1-15.
242. Otake, K.; Kamiguchi, H.; Hirozane, Y., Identification of biomarkers for amyotrophic lateral sclerosis by comprehensive analysis of exosomal mRNAs in human cerebrospinal fluid. *BMC medical genomics* **2019,** *12* (1), 7.
243. Gui, Y.; Liu, H.; Zhang, L.; Lv, W.; Hu, X., Altered microRNA profiles in cerebrospinal fluid exosome in Parkinson disease and Alzheimer disease. *Oncotarget* **2015,** *6* (35), 37043.
244. Nilsson, J.; Skog, J.; Nordstrand, A.; Baranov, V.; Mincheva-Nilsson, L.; Breakefield, X.; Widmark, A., Prostate cancer-derived urine exosomes: a novel approach to biomarkers for prostate cancer. *British journal of cancer* **2009,** *100* (10), 1603-1607.
245. Del Re, M.; Marconcini, R.; Pasquini, G.; Rofi, E.; Vivaldi, C.; Bloise, F.; Restante, G.; Arrigoni, E.; Caparello, C.; Bianco, M. G., PD-L1 mRNA expression in plasma-derived exosomes is associated with response to anti-PD-1 antibodies in melanoma and NSCLC. *British journal of cancer* **2018,** *118* (6), 820-824.

246. Kim, K. M.; Abdelmohsen, K.; Mustapic, M.; Kapogiannis, D.; Gorospe, M., RNA in extracellular vesicles. *Wiley Interdisciplinary Reviews: RNA* **2017,** *8* (4), e1413.
247. Wei, Z.; Batagov, A. O.; Schinelli, S.; Wang, J.; Wang, Y.; El Fatimy, R.; Rabinovsky, R.; Balaj, L.; Chen, C. C.; Hochberg, F., Coding and noncoding landscape of extracellular RNA released by human glioma stem cells. *Nature communications* **2017,** *8* (1), 1-15.
248. Yuan, T.; Huang, X.; Woodcock, M.; Du, M.; Dittmar, R.; Wang, Y.; Tsai, S.; Kohli, M.; Boardman, L.; Patel, T., Plasma extracellular RNA profiles in healthy and cancer patients. *Scientific reports* **2016,** *6*, 19413.
249. Meng, Y.; Eirin, A.; Zhu, X.-Y.; O'Brien, D. R.; Lerman, A.; van Wijnen, A. J.; Lerman, L. O., The metabolic syndrome modifies the mRNA expression profile of extracellular vesicles derived from porcine mesenchymal stem cells. *Diabetology & Metabolic Syndrome* **2018,** *10* (1), 58.
250. Chen, W. W.; Balaj, L.; Liau, L. M.; Samuels, M. L.; Kotsopoulos, S. K.; Maguire, C. A.; LoGuidice, L.; Soto, H.; Garrett, M.; Zhu, L. D., BEAMing and droplet digital PCR analysis of mutant IDH1 mRNA in glioma patient serum and cerebrospinal fluid extracellular vesicles. *Molecular Therapy-Nucleic Acids* **2013,** *2*, e109.
251. Chung, M. T.; Kurabayashi, K.; Cai, D., Single-cell RT-LAMP mRNA detection by integrated droplet sorting and merging. *Lab on a Chip* **2019,** *19* (14), 2425-2434.
252. Reinholt, S. J.; Behrent, A.; Greene, C.; Kalfe, A.; Baeumner, A. J., Isolation and amplification of mRNA within a simple microfluidic lab on a chip. *Analytical chemistry* **2014,** *86* (1), 849-856.
253. Zhou, X.; Ravichandran, G. C.; Zhang, P.; Yang, Y.; Zeng, Y., A microfluidic alternating-pull–push active digitization method for sample-loss-free digital PCR. *Lab on a Chip* **2019,** *19* (24), 4104-4116.
254. Tsugita, M.; Yamada, N.; Noguchi, S.; Yamada, K.; Moritake, H.; Shimizu, K.; Akao, Y.; Ohno, T., Ewing Sarcoma Cells Secrete EWS/Fli-1 Fusion mRNA via Microvesicles (E EWS/Fli-1 Fusion mRNA in Microvesicles). *PLOS ONE* **2013,** *8* (10), e77416.